Russian Original Vol. 49, No. 2, August, 1980

February, 1981

SATEAZ 49(2) 505-602 (1980)

SOVIET ATOMIC ENERGY

АТОМНАЯ ЭНЕРГИЯ
(ATOMNAYA ÉNERGIYA)

TRANSLATED FROM RUSSIAN

CONSULTANTS BUREAU, NEW YORK

SOVIET ATOMIC ENERGY

Soviet Atomic Energy is a translation of *Atomnaya Énergiya*, a publication of the Academy of Sciences of the USSR.

An agreement with the Copyright Agency of the USSR (VAAP) makes available both advance copies of the Russian journal and original glossy photographs and artwork. This serves to decrease the necessary time lag between publication of the original and publication of the translation and helps to improve the quality of the latter. The translation began with the first issue of the Russian journal.

Consultants Bureau journals appear about six months after the publication of the original Russian issue. For bibliographic accuracy, the English issue published by Consultants Bureau carries the same number and date as the original Russian from which it was translated. For example, a Russian issue published in December will appear in a Consultants Bureau English translation about the following June, but the translation issue will carry the December date. When ordering any volume or particular issue of a Consultants Bureau journal, please specify the date and, where applicable, the volume and issue numbers of the original Russian. The material you will receive will be a translation of that Russian volume or issue.

Subscription (2 volumes per year)
Vols. 48 & 49: $335 (domestic); $374 (foreign)
Vols. 50 & 51: $380 (domestic); $423 (foreign)

Single Issue: $50
Single Article: $7.50

Soviet Atomic Energy is abstracted or indexed in *Chemical Abstracts, Chemical Titles, Pollution Abstracts, Science Research Abstracts, Parts A and B, Safety Science Abstracts Journal, Current Contents, Energy Research Abstracts,* and *Engineering Index.*

CONSULTANTS BUREAU, NEW YORK AND LONDON

c/b
233 Spring Street
New York, New York 10013

Published monthly. Second-class postage paid at Jamaica, New York 11431.

SOVIET ATOMIC ENERGY

A translation of *Atomnaya Énergiya*

February, 1981

Volume 49, Number 2 August, 1980

CONTENTS

CONTENTS

(continued)

The Russian press date (podpisano k pechati) of this issue was 7/21/1980. Publication therefore did not occur prior to this date, but must be assumed to have taken place reasonably soon thereafter.

NUCLEAR POWER INSTALLATION AND MAIN LINES OF SCIENTIFIC AND TECHNICAL PROGRESS

M. Drahný and J. Svetlik*

UDC 621.039.003.2

A national nuclear power installation (NPI) is a complex entity of an interindustry nature, which incorporates, in addition to nuclear power engineering itself, an array of facilities which ensure and directly affect the development and operation of nuclear power.

The structure of the nuclear power installation has the following subsystems [1].

1. Atomic power plant subsystem (APPS) — a set of nuclear power plants and nuclear facilities that is a component part of the electric power system (EPS) and of systems of centralized heat supply (SCHS).

2. Nuclear fuel subsystem (NFS) — a set of units for extraction, processing, and enrichment of nuclear fuel, production of fuel elements, processing of these elements after irradiation, and transportation and storage of radioactive waste. The APPS and NFS are intimately linked and comprise the nuclear power engineering system (NPES) [2].

3. Nuclear power machinery subsystem (NPMS), incorporating the metallurgical, machine-building, and instrument-manufacture base of nuclear power.

4. Nuclear power construction subsystem (NPCS), incorporating facilities for construction of APPS and NFS.

5. A management system for ensuring proportional development and operation of NPI as a whole and coordinating its internal and external and interbranch and international linkages. It is intended for the development of nuclear power policy as a component of the energy, technological, and economic policy of a country, including international relations; for internal control of nuclear materials, nuclear safety, and protection of the environment and for creating rules for legal norms and information in the nuclear power field.

Figure 1 shows the system of material linkages of NPI, while Fig. 2 shows the system of information linkages.

Integrated Nuclear Power Installation

The nuclear power installation of a given country can be regarded as a subsystem of the integrated nuclear power installation (INPI) of the COMECON countries [3]. International cooperation, division of labor, specialization, joint construction or collaboration in capital investment within the framework of INPI facilitates effective solution of problems whose solution by one country would be difficult or impossible.

The aim of the INPI is to provide the COMECON member with power from nuclear resources (disregarding export to third countries). The material linkages are complex and interdependent in this case. Therefore, it is necessary to coordinate them effectively so as to manage the entire system with a view to long-term and short-term predictions.

The tasks of the nuclear power installation in the production and eocnomic sphere can be divided into two groups: material (technological) and socio-economic.

The first group includes construction and operation of nuclear power facilities, nuclear machinery and nuclear construction facilities (plants); construction, production, and delivery, including assembly; and import and export of nuclear power equipment, as well as construction of research facilities, laboratories, and experimental test sites.

The second group encompasses managerial activity, aimed primarily at the fulfillment of economic plans, and also bilaterial and multilateral collaboration. Multilateral collaboration in the production and economic sphere within the framework of COMECON is based on long-term programs and plans for the individiual agencies of COMECON — the Committee on

*Deceased.

Czechoslovak Commission on Atomic Energy. Translated from Atomnaya Énergiya, Vol. 49, No. 2, pp. 75-78, August, 1980. Original article submitted November 27, 1978; revision submitted November 12, 1979.

0038-531X/80/4902-0505$07.50

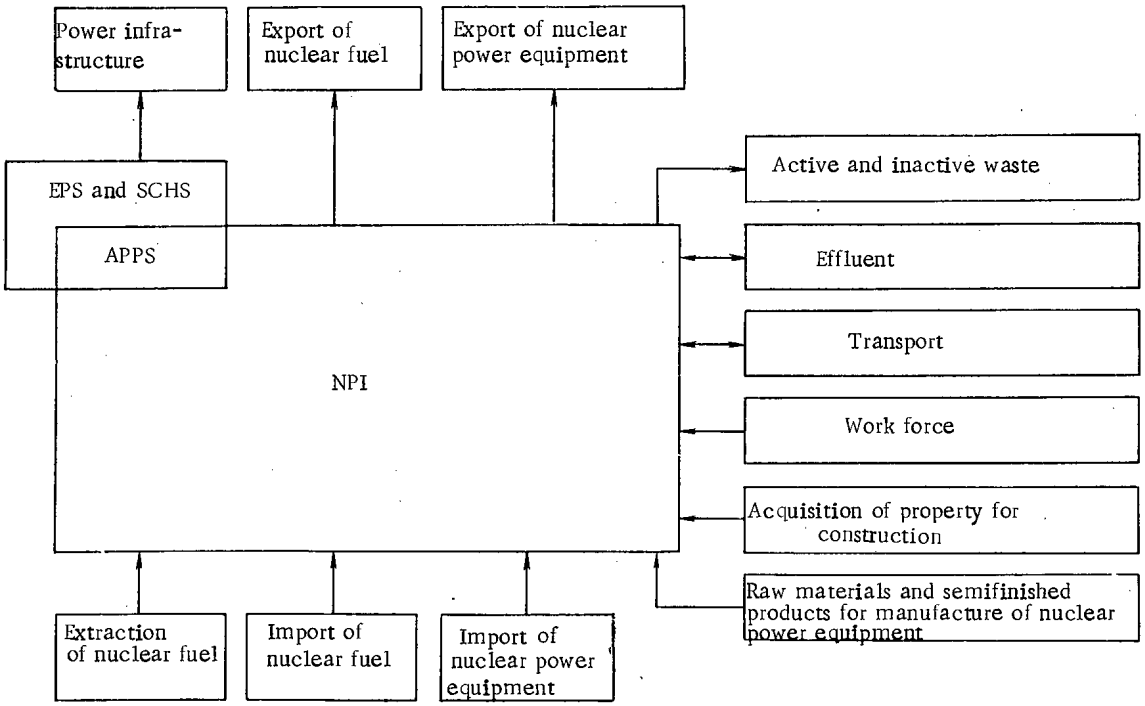

Fig. 1. External material linkages of NPI.

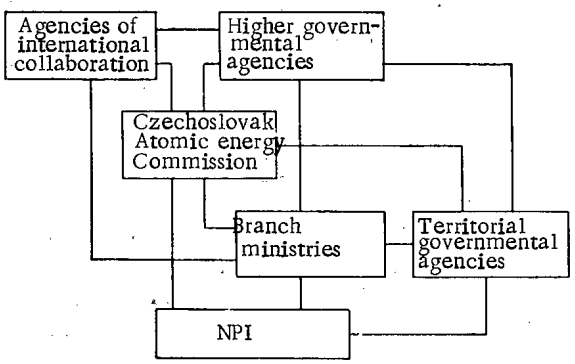

Fig. 2. External information linkages of NPI (using the Czechoslovak NPI as an example).

Collaboration in Planning, the Committee on Scientific and Technical Collaboration, the Permanent Commission on the Peaceful Use of Atomic Energy, the Permanent Commission on Electric Power, the Permanent Commission on Machine Building, and others. International agencies (Interatomenergo, Interatominstrument) have been created in some branches of industry for industrial and economic collaboration.

The problems of NPI in the fields of science and engineering include the conducting of research and preparation of design data for use in the production and economic sphere, specifically:

- basic data for the development of long-term and ordinary plants;
- data for design, construction, and operation of nuclear power facilities;
- information for construction of metallurgical, machine-building, and construction of metallurgical, machine-building, and construction capabilities, and also experimental and research installations.

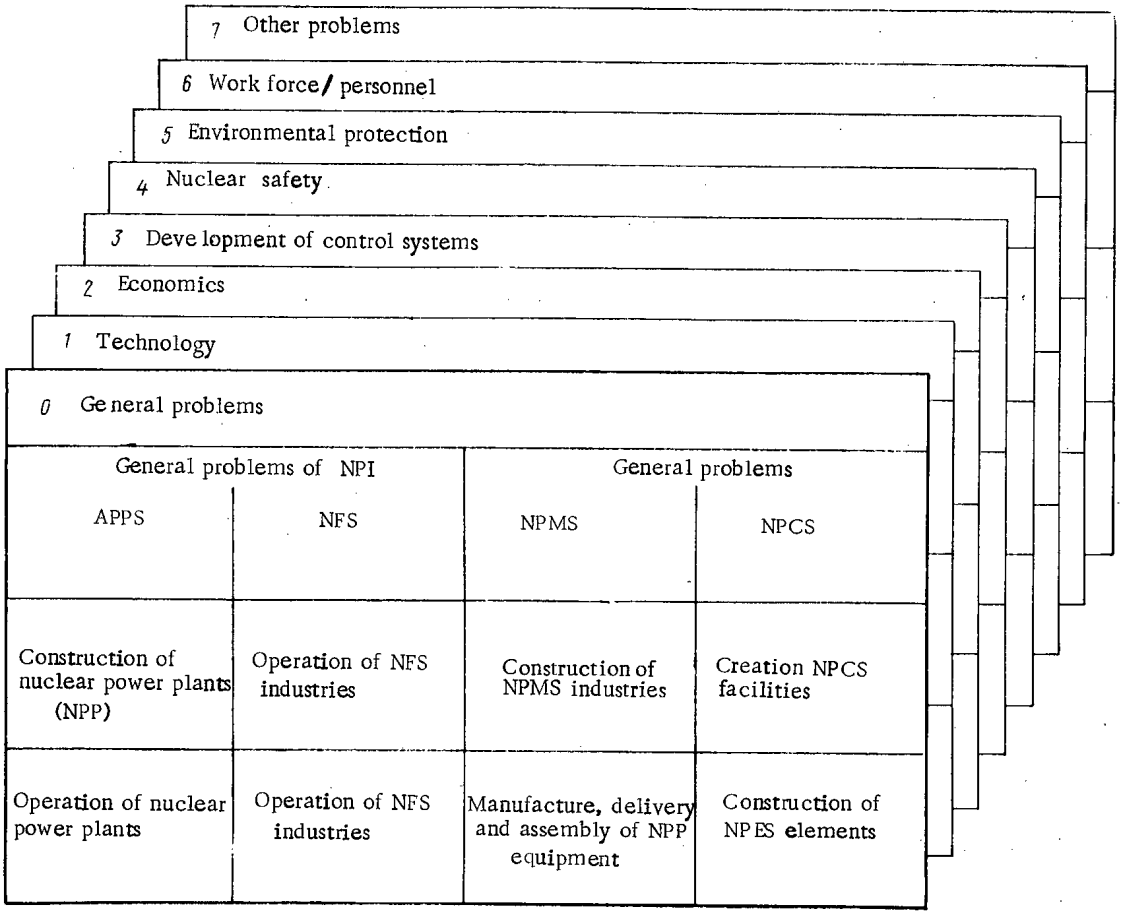

Fig. 3. Division of system of MLR into problems and tasks.

It is best to generate the spectrum of research topics by constructing a system of major lines of research (MLR). This system makes it possible to create and assure the following:

— coordination with respect to activities and time of scientific problems with problems with problems in the production and economic sector;

— similar coordination among scientific and technical problems on the national and international levels;

— the entire array of problems which must be solved in accordance with their degree of urgency or priority (elimination of so-called blank spots or "holes");

— coordinated use of all available capabilities, interaction among all concerned parties, and elimination of undesirable duplication;

— monitoring and evaluation of progress;

— effective utilization of achieved results.

It is best to divide the system of MLR into subsystems and hierarchical levels of NPI and into certain functional structures corresponding to the following specific areas (Fig. 3): general problems; technology; economics; development of control systems; nuclear safety; environmental protection; personnel; other problems. Of course, this division is not definitive, and can be supplemented or normalized as needed for appropriate control or orientation. It is necessary to point out that not all MLR have the same importance or scale.

With regard to problems of nuclear power installations and their subsystems, the aim of the main research lines is to develop a project for the program of development and operation of NPI. The project is the basis for the preparation of the five-year development plan for NPI in the production and economic sphere and in science and engineering, and also for preparation of a program of collaboration among COMECON member nations in the area of NPI for

for the development of a five-year plan for the agencies of COMECON and international economic entities.

This concerns primarily the development of predictions and structural and optimization solutions for the developmemt and operation of NPI, on the basis of the requirements of EPS and SCHs for power and energy production through nuclear sources. Naturally, these requirements are keyed to the capabilities of the national economies of the individual countries and to the capabilities and requirements of international collaboration, with appropriate observance of the conditions and restrictions on the part of the environment (territory, effluent water, transport, personnel, demographics, etc.).

The input information and data for free processing within the framework of the MLR can be obtained from the production and economic sphere of NPI, and also through solution of other specific problems, e.g., the part played by particular types of power reactors, economic impact and mathematical modeling, control systems (including ACS), systems issues of nuclear safety and protection of the environment, personnel problems, the expansion of the research and development base, etc.

The specific problems of MLR also include (to the appropriate extent in all subsystems), e.g., problems of choosing technical and economic parameters and operating figures for equipment for nuclear power plants which reactors of given types, problems of economics control systems, nuclear safety, protection of the environment, and personnel for power-generating and other nuclear installations.

Conclusions

Nuclear power installations in both their national and COMECON-integrated forms already exist and will develop rapidly in conformity with the energy requirements for the COMECON member-nations. The process of development and operation of the nuclear power installation is complex and intractable. It requires heretofore unimagined expenditures of material and intellectual effort and resources, and yet the capabilities for increasing these is limited. The problem is to better utilize them and to manage all processes with maximum efficiency. This requires that scientifically well-grounded and comprehensive data be systematically developed and made available.

In this paper we have stressed the general (systems) concept of an aggregate nuclear-power economy. The systems and organizational approach that we have described, however, makes it possible to take account of specific features and interrelationships by means of functional structures that can be defined where needed. The concept of nuclear power installation, with its subsystems, hierarchical levels, and functional structures, is sometimes regarded as inconsistent with the concept of so-called programmed-goal structures, whose effectiveness has been confirmed by practice.

A nuclear power installation is "all-encompassing," incorporating both the production and economic and the scientific and technical spheres, and, by means of the MLR system, it can be treated as a systems entity. Programmed-goal structures include only problems that must be solved to attain a certain goal. A nuclear power installation is "unique" but it passes through various phases of development. Programmed-goal structures are of a one-shot nature; there can be many of them (e.g., development of the VVÉR-1000 reactor, creation of atomic thermal power centers, the breeder reactor development program, creation of a training center for nuclear power plant personnel), and they differ quantitatively and qualitatively.

As a result of its complexity and large resource consumption, a nuclear power installation is inflexible and slow to respond. Programmed-goal structures do not contain "excesses" and lead to the goal in the shortest possible way. However, the simplest approach (i.e., programmed-goal structure) can be found only if there is a clear conception of the linkages and structure of the entire nuclear-power installation. Programmed-goal structures can be defined as some functional structure of NPI which makes it possible to evaluate how realistic the goal is, its interrelationship with other programmed-goal structures, and also to introduce order, preference, and proportionality.

Specific activity is carried out and local effects attained within the framework of programmed-goal structures. Within the framework of a nuclear power installation, the capability is created for implementing individual programmed-goal structures. Nuclear power

installations and programmed-goal structures are not mutually exclusive alternatives; they complement one another and form a coexisting unity.

LITERATURE CITED

1. M. Drahný, Yad. Energ., 24, No. 9, 327 (1978).
2. M. Drahný, Yad. Energ., 23, No. 11, 403 (1977).
3. M. Drahný and J. Svetlik, "Nuclear power engineering and the nuclear power installation of the COMECON member-nations," Conference of Specialists of COMECON Member-Nations on Criteria and Initial Data for Predicting the Development of Nuclear Power and Allowance for Heat Supply, Interaction with the Environment, and the Use of Mathematical Models, Moscow, Dec. 5-8, 1977.

SENSITIVITY OF CHARACTERISTICS OF HYBRID REACTOR TO SPECTRA OF SECONDARY NEUTRONS

D. V. Markovskii and G. E. Shatalov

UDC 621.039.51:539.125.52

The study of the relation between the errors of nuclear data and the results of calculations of the neutron-physical characteristics of various models is of considerable interest from the point of view of estimating the indeterminacy of the parameters of systems being designed and the strategy of nuclear data refinement. This problem was worked on intensively for fast reactors [1-3].

In order to estimate the error due to the nuclear data it is necessary to have the coefficients of the sensitivity of the functionals under consideration to the varied data as well as the matrix of the errors of those data. Information about the errors comes into being at the stage of estimation of the nuclear data. In order to obtain the sensitivity coefficients special calculations must be performed with a view to determining the types of systems, materials, and data.

The greatest error of neutron data in reactor blanket calculations correspond to the range 0.1-15 MeV, which has been investigated less than has the low-energy range so important for fission reactors. Not only a detailed description of the cross sections but also data on the scattering anisotropy, spectra, and yields of secondary neutrons from inelastic processes are essential here. In sensitivity calculations all of these parameters can, in principle, vary. The largest number of papers has been devoted to the study of sensitivity to cross sections [4-6].

The sensitivity to the spectra of secondary neutrons for the model of a "pure" thermonuclear reactor (without fissionable material) was considered in [6-8]. In the present paper we study the sensitivity of the fission rate, the fission source, and the tritium yield in the blanket of a hybrid reactor to the perturbations of the spectra of secondary neutrons from the reactions ^{238}U(n, 2n), ^{238}U(n, 3n), and Fe(n, 2n) as well as the spectra of inelastically scattered neutrons with excitation of a continuum of levels of ^{238}U(n, n') cont and Fe(n, n') cont. In the calculations we used estimated neutron data from the ENDL library [9] in the range 0.1-14.1 MeV and a 21-group system of constants [10] below 0.1 MeV.

Method of Calculation

Neutron Transport Equation. The space-energy distribution of the neutron flux in the problem with an external source satisfies the equation

$$\psi(x) = \hat{H}\psi(x) + S(x), \tag{1}$$

where $\hat{H}$ is the transport operator; $\psi(x)$, neutron flux at the phase coordinate $x = (r, E)$; and $S(x)$, flux of unscattered neutrons from the external source. Writing the solution as a series expansion in the generations of neutrons

Translated from Atomnaya Énergiya, Vol. 49, No. 2, pp. 79-83, August, 1980. Original article submitted June 4, 1979.

0038-531X/80/4902-0509$07.50

$$\psi(x) = \sum_i \psi_i(x) \tag{2}$$

and writing H as the sum of the operators $\hat{h}$ (describing the neutron transport) and $\hat{f}$ (describing the source of fission neutrons), we get

$$\psi(x) = \psi_1(x) + \sum_{i=2} \psi_i(x), \tag{3}$$

where

$$\psi_1(x) = \hat{h}\psi_1(x) + S(x); \tag{4}$$

$$\psi_i(x) = \hat{h}\psi_i(x) + \hat{f}\psi_{i-1}(x), \quad i > 1. \tag{5}$$

Equation (5) for fission neutrons can be solved quite exactly by the method of spherical harmonics in the P_1 approximation with 21-group constants [10]. In order to find the neutron flux ψ_1 from an external source in the high-energy range it is necessary to employ more exact approximations. In the present paper we use the Monte Carlo method with a detailed system of constants at high energies and the P_1 approximation below some limiting energy (E_{lim} = 0.1 MeV). Then

$$\psi_1(x) = \psi_1^{(1)}(x) + \psi_1^{(2)}(x);$$
$$\psi_1^{(1)}(x) = \hat{h}_1\psi_1^{(1)}(x) + S(x);$$
$$\psi_1^{(2)}(x) = \hat{h}_2\psi_1^{(2)}(x) + \hat{h}_{12}\psi_1^{(1)}(x),$$

where $\hat{h}_1$ and $\hat{h}_2$ are operators describing the neutron transport in the energy intervals (14.1 MeV, E_{lim}) and (E_{lim}, E_t) and $\hat{h}_{12}$ specifies the source of neutrons slowed down below and energy of E_{lim}.

For convenience we write

$$\varphi_1(x) = \psi_1^{(1)}(x);$$
$$\varphi_2(x) = \psi_1^{(2)} + \sum_{i=2} \psi_i(x),$$

and recast Eq. (1) in the form

$$\varphi_1(x) = \hat{h}_1\varphi_1(x) + S(x); \tag{6}$$

$$\varphi_2(x) = \hat{h}_2\varphi_2(x) + \hat{f}_1\varphi_1(x) + \hat{f}_2\varphi_2(x) + \hat{h}_{12}\varphi_1(x), \tag{7}$$

where the neutron fluxes $\varphi_1(x)$ and $\varphi_2(x)$ can be calculated in various approximations by using different libararies of nuclear data.

To find φ_1 in the energy range above E_{lim} we solved the exact equation of neutron transport by the Monte Carlo method. The constants for this energy range were prepared with the aid of the NEDAM program [11] from constants contained in the files of estimated data. Nuclei of scattering on elements are continuous functions of the scattering angle and the neutron energy before and after scattering while the probabilities of the processes are piecewise-continuous with respect to neutron energy up to collision. The neutron flux component φ_2 in Eq. (7) was found from the solution of the transport equation by the method of spherical harmonics in the P_1 approximation.

Calculation of the Sensitivity Coefficients. The neutron-physical characteristics of the model under study are usually linear functionals of the type of the reaction rates which, for integrals or sums over the entire phase space, can be written in the form of a scalar product $R(\Sigma_R, \varphi)$. The relative change in R corresponding to the relative change in some nuclear data σ_i,

$$S_{R,i} = (\sigma_i/R)(\delta R/\delta\sigma_i),$$

is called the sensitivity of R to the data σ_i.

TABLE 1. Composition of Blanket

No. of zone	Zone thickness, cm	Nuclear concns, 10^{-24}: ^{6}Li	^{7}Li	C	O	Fe	^{238}U
1	200	—	—	—	—	—	—
2	0,5	—	—	—	—	0,0848	—
3	1,1	—	—	—	—	0,0077	—
4	20	—	—	0,0163	—	0,0072	0,0163
5	1,3	—	—	—	—	0,0182	—
6	15	0,0188	0,0188	—	0,0141	0,0168	—
7	0,7	—	—	—	—	0,0121	—
8	35	—	—	0,0642	—	—	—
9	0,4	—	—	—	0,0212	—	—
10	10	0,0163	0,0163	—	0,0123	0,0165	—
11	0,8	—	—	—	—	0,0106	—

TABLE 2. Principal Functionals of Model

Flux	Energy range, MeV	$n, 2n$	$n, 3n$	Fission source	Absorption	Leakage	No. of fission	Titium yield
φ_1	0,1—14,1	0,267	0,092	1,296	0,761	0,014	0,325	0,276
φ_2	0—10,5	—	—	0,369	2,33	0,011	0,138	1,122
$\varphi_1+\varphi_2$	0—14,1	0,267	0,092	1,665	3,091	0,025	0,463	1,398

The value of δR was calculated by the correlated sampling method [12]. The calculations of the initial and perturbed systems were carried out according to one and the same set of neutron trajectories while the change in the properties of the scattering nucleus in the perturbed system was taken into account by introducing a weight.

The operator $\hat{h}_1$ In Eq. (6) is of the form

$$\hat{h} = \int K(x',\ x)\,dx';$$
$$K = C(\mathbf{E}',\ \mathbf{E},\ \mathbf{r})\,T(\mathbf{r},\ \mathbf{r},\ \mathbf{E}),$$

where C describes the change in the energy, angle, and number of particles during collisions and T describes the displacement of neutrons between collisions.

The solution of Eq. (6) can be written in the form of a Neumann series in collisions:

$$\varphi_1 = \sum_i \varphi_1^i(x);$$
$$\varphi_1^i(x) = \int \varphi_1^{i-1}(x')\,K(x,\ x')\,dx' =$$
$$= \int \ldots \int S(x_1)\,K(x_1, x_2)\ldots K(x_{i-1}, x)\,dx\ldots dx_{i-1}. \qquad (8)$$

The solution for the perturbed system is of the form

$$\varphi_1' = \sum_i \int \ldots \int S(x_1)\,K'(x_1,\ x_2)\ldots$$
$$\ldots K'(x_{i-1},\ x)\,dx_1\ldots dx_{i-1}.$$

Introducing the weight of the i-th collision

$$\omega_i = K'(x_{i-1},\ x_i)/K(x_{i-1},\ x_i),$$

we can represent the perturbed flux by

$$\varphi_1' = \sum_i \int \dots \int S(x_1)\,\omega_1 K(x_1, x_2) \dots \\ \dots \omega_{i-1} K(x_{i-1}, x)\,dx_1 \dots dx_{i-1}. \quad (9)$$

Comparison of Eqs. (8) and (9) reveals that the estimate φ_1' can be made on the same series of trajectories as φ_1, but at each collision the estimator should be multiplied by

$$W_i = \prod_{h=1}^{i-1} \omega_h.$$

Since the estimates φ_1 and φ_1' in this case are highly correlated, the error in the calculation of the deviation δR_1 of the functional may be appreciably smaller than the statistical error of R_1.

Along with an estimate δR we can find the perturbation of the source, which is used to calculate φ_2:

$$\delta S_{12} = (\hat{f}_1 + \hat{h}_{12})\,|\varphi_1'(x) - \varphi_1(x)|.$$

The variation of R can finally be written as

$$\delta R = \delta(\Sigma_R, \varphi) = (\delta\Sigma_{R_1}, \varphi_1) + (\Sigma_{R_1}, \delta\varphi_1) + \\ + (\delta\Sigma_{R_2}, \varphi_2) + (\Sigma_{R_2}, \delta\varphi_2).$$

The first and second terms of this equation are determined in the correlation calculation, the third is zero, and the last is calculated in the P_1 approximation with the source perturbation δS_{12}.

Inclusion of Perturbations. The calculations were carried out according to a modified BLANK program [13] which realizes the above methods of solving the neutron transport equation and correlated estimation. The constants for calculations in the range 0.1-14.1 MeV were prepared according to the NEDAM program [11] from the estimated data files of the ENDL library. In the working constants we used library spectra of secondary neutrons, converted to the argument $x = E/E_i'$ and referred to ranges bounded by neighboring values E_i', where E_i' are discrete values of the initial energy. The perturbed neutron spectrum p'(x) was obtained by compressing the initial spectrum p(x) according to the relation

$$p'(x) = \begin{cases} cp(cx), & x \leqslant a/c; \\ 0, & x > a/c, \end{cases}$$

where a is the upper limit of the initial spectrum and c is the compression coefficient. This approach makes it possible to deform the distribution of any form. In this case $\bar{x}' = (1/c)\,\bar{x}$ or, for a spectrum of temperature T, we have $T' = (1/c)\,T$ and the relative change in the data, i.e., the "hardness" of the spectrum is

$$f = \frac{\delta\bar{x}}{\bar{x}} = \frac{\delta T}{T} = \frac{1-c}{c}.$$

In all the calculations we set c = 1.2, which corresponds to a "softening" of the spectrum. To study the dependence of the sensitivity on the neutron energy up to collision the weight of the neutrons was varied only in the range from the given threshold E'_{min} to 14.1 MeV. The sensitivity $S(E'_{min})$ to such a change in the spectra will henceforth be described as integrated. The differential sensitivity s(E') is related to the integrated sensitivity by

$$s(E') = -\partial S(E'_{min})/\partial E'_{min}.$$

Results of Calculations

For our calculations we chose the variant of hybrid blanket [14] in which the ^{238}U carbide is used as fissionable material and lithium oxide is employed to produce tritium (Table 1). In the working system of constants for Monte Carlo calculations the range 0.1-14.1 MeV was divided into 18 groups for the probability of processes and 8 groups in the description of the anisotropy of elastic scattering. The secondary neutron spectra of each reaction were described by assigning 36 equiprobable values of the secondary energy for each range of primary energies indicated in the estimated data files.

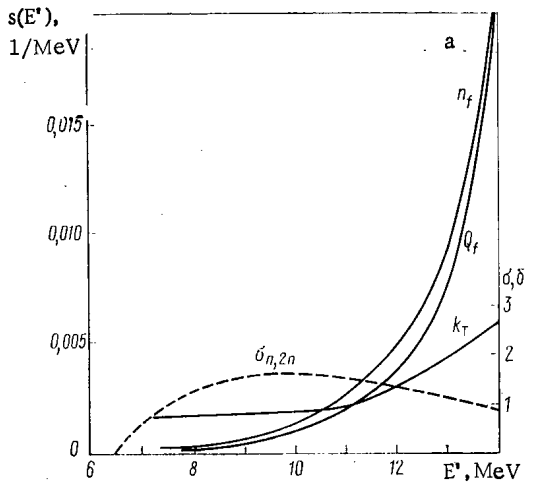

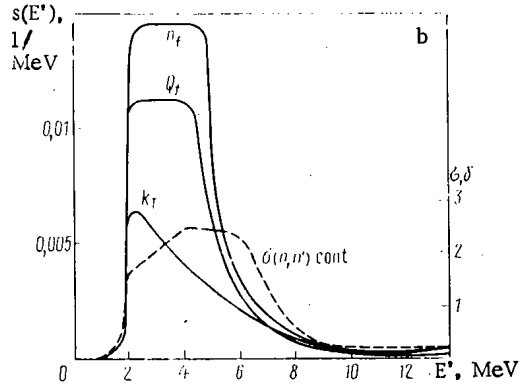

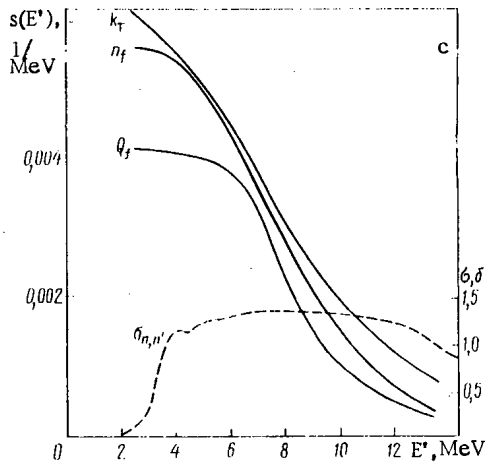

Fig. 1. Differential sensitivity to neutron spectra of reactions: a) ^{238}U(n, 2n), b) ^{238}U(n, n') cont, c) Fe(n, n') cont.

All of the calculations were carried out for 10,000 histories. The principal functionals of the unperturbed model with normalization to one source neutron in the plasma are given in Table 2. The integrated sensitivity coefficients for the fission rate n_f, the fission neutron source Q_f, and the tritium yield k_T are given in Tables 3 and 4 as a function of E'_{min}. The statistical errors of the functionals and the deviations of their correlated values were estimated directly during calculations by the Monte Carlo method and amounted to ∿1% for and, depending on the effect, from 10 to 60% for the deviations.

As follows from Tables 3 and 4 the greatest influence on the principal functionals of the hybrid reactor is exerted by the spectra of secondary neutrons from the reactions ^{238}U(n, 2n), ^{238}U(n, n') cont, and Fe(n, n') cont, for which the contribution to the rate of fission in ^{238}U may be considerable. The total sensitivity with respect to these reactions is 0.22 for the fission rate, 0.19 for the source, and 0.13 for the tritium yield, with a spread of 15-20% in the mean energy of the secondary neutron electrons in various estimated data files [8] this corresponds to an indeterminacy of 3-4.5% for the fission rate and the source and 2-2.5% for the tritium yield. The sensitivity of the functional to the spectra of the reactions ^{238}U(n, 3n) and Fe(n, 2n) is substantially lower because of the smaller cross sections for these reactions and lower secondary neutron energy.

Figure 1 gives the curves of the differential sensitivity to the spectra of the reactions ^{238}U(n, 2n), ^{238}U(n, n') cont, and Fe(n, n') cont in the range from the threshold to 14.0 MeV, obtained by differentiating smooth curves drawn according to the data of Tables 3 and 4.

The differential sensitivity of the fission rate and the source to the neutron spectrum of the reaction ^{238}U(n, 2n) rises sharply above 11 MeV, which corresponds to the shape of the neutron spectrum in the uranium zone, shown in Fig. 2. As follows from Table 3,

TABLE 3. Integrated Sensitivities to ^{238}U Spectra

Parameter	^{238}U $(n, 2n)$					^{238}U (n, n') cont							^{238}U $(n, 3n)$
	E'_{min}, MeV												
	6,5	10	12	13	14	1	2	3	5	6	8	14	14
n_f	0,1098	0,1086	0,1028	0,0962	0,0817	0,0581	0,0578	0,0438	0,0148	0,0122	0,0073	0,0066	0,0118
Q_f	0,092	0,0910	0,087	0,0816	0,0694	0,0458	0,0457	0,0359	0,0142	0,0121	0,0080	0,0079	0,0084
k_T	0,051	0,0445	0,0404	0,0361	0,0311	0,0142	0,0155	0,00523	0,00376	0,00176	−0,00524	−0,0069	0,0258

TABLE 4. Integrated Sensitivities to Fe Spectra

Parameter	Fe (n, n') cont					Fe $(n, 2n)$
	E'_{min}, MeV					
	2	4	8	12	14	14
n_f	0,0504	0,0413	0,0217	0,0162	0,0174	0,00162
Q_f	0,0474	0,0408	0,0255	0,0209	0,0205	0,00103
k_T	0,0558	0,0438	0,0251	0,021	0,0145	0,0127

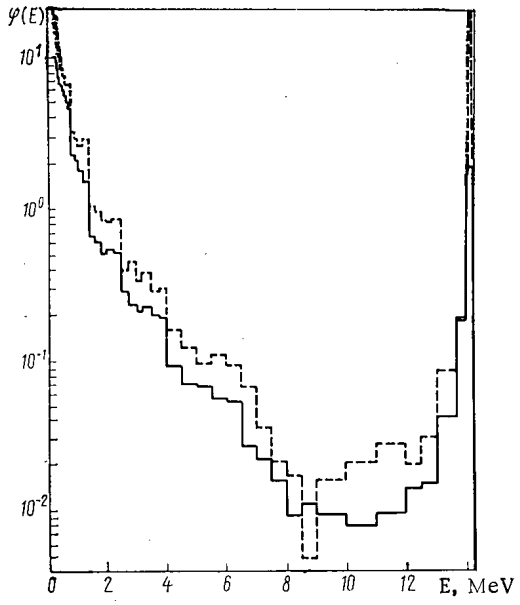

Fig. 2. Spectra of neutrons in blanket: - - -) first wall; ———) uranium zone.

neutrons with an energy above 14 MeV account for 75% of the integrated sensitivity of the fission rate and ∿60% of the sensitivity of the tritium yield.

Neutrons from inelastic scattering with excitation of a continuum of levels in ^{238}U make the greatest contribution to the functionals at an energy in the range 2-6 MeV prior to collision while only 15-20% of the contribution corresponds to an energy above 14 MeV. This is in accord with the position of the maximum of the cross section of the reaction and the increase in the neutron flux at an energy below 6 MeV (see Fig. 2).

Approximately one-third of the sensitivity to the spectra of neutrons from the reaction Fe(n, n') cont is accounted for by the interaction between source neutrons with an energy of 14.1 MeV and the first wall. At a lower energy the sensitivity increases with a decrease in the energy, judging by the spectrum of neutrons in the uranium zone.

Conclusion. In cases when the neutron transport equation is solved by the Monte Carlo method, the application of the correlation sampling technique to the calculation of the sensitivity coefficients makes it possible by means of a straightforward change in the algorithm to attain an accuracy of calculation of differential effects that is sufficient for estimations. This method is most convenient when the difference in the kernels of the integral equations corresponding to the ground-state and perturbed problem can be taken into account by introducing a weight function and the region of definition of the kernels. This

corresponds to the cases of perturbation of the secondary neutrons, their spectra, or absorption cross section.

The calculated sensitivity coefficients show that in a hybrid reactor the greatest influence on the principal functionals is exerted by the secondary neutron spectra of the reactions $^{238}U(n, 2n)$, $^{238}U(n, n')$ cont, and Fe(n, n') cont, for which the contribution to the fission rate in ^{238}U and, therefore, in neutron multiplication per source neutron, may be considerable. The indeterminacy of the functionals, owing to the 15-20% inaccuracy of the spectra, is estimated for the hybrid reactor model studied to be 3-4.5% for the fission rate and 2-2.5% for the tritium yield.

LITERATURE CITED

1. L. Usachev, J. Nucl. Eng., A/B, 18, 371 (1964).
2. L. N. Usachev and Yu. G. Bobkov, in: Proc. Conf. "Neutron Physics" [in Russian], Part I, Naukova Dumka, Kiev (1972), p. 47.
3. Yu. G. Bobkov et al., in: Proc. Conf. "Neutron Physics" [in Russian], Part I, Izd. TsNIIatominform, Moscow (1976), p. 76.
4. R. Conn and W. Stacey, Nucl. Fusion, 13, 185 (1973).
5. S. Gerstl, D. Dudziak, and D. Muir, Nucl. Sci. Eng., 62(1), 137 (1977).
6. D. Steiner and M. Tobias, Nucl. Fusion, 14, 153 (1974).
7. S. Gerstl, in: Proc. Fifth Int. Conf. on Reactor Shielding, Knoxville, Tenn., April 18-22 (1976).
8. V. V. Kotov et al., Preprint IAÉ-2817, Moscow (1977).
9. R. Howerton et al., UCRL-50400 (1971), Vol. 4.
10. S. M. Zakharova, B. N. Sivak, and G. N. Toshinskii, Information Bulletin of Nuclear Data Center. No. 3. Appendix 1. Nuclear-physical Constants for Reactor Calculations [in Russian], Atomizdat, Moscow (1967).
11. L. N. Zakharov et al., Preprint IAÉ-2994, Moscow (1978).
12. V. G. Zolotukhin and D. A. Usikov, Estimation of Reactor Parameters by the Monte Carlo Method [in Russian], Atomizdat, Moscow (1979).
13. S. V. Marin, D. V. Markovskii, and G. E. Shatalov, Preprint IAÉ-2832, Moscow (1977).
14. V. Kotov and G. Shatalov, in: Proc. of US–USSR Symp. on Fusion–Fission Reactors, Livermore, July 13-16 (1976), p. 129.

CHARACTERISTICS OF FLOW RATE-LIMITING INSERTS IN MODELING EMERGENCY LOSS OF INTEGRITY OF A REACTOR LOOP

L. K. Tikhonenko, É. K. Karasev,
S. Z. Lutovinov, B. A. Gabarev,
and E. I. Trubkin

UDC 621.039.587

The problem of limiting the flow of heat-transfer agent under conditions of emergency loss of integrity is an extremely pressing one. The patent literature proposes several solutions for this problem [1, 2]. As a rule, these solutions involve either safety devices which automatically seal off a section of piping at the instant that emergency loss of integrity occurs, or Venturi-type nozzles that do not seal off but only restrict the flow of heat-transfer agent. The latter are more promising from the standpoint of realiability, since they do not contain moving parts. At the same time, it should always be borne in mind that, under rated operating conditions, such nozzles are "parasitic" resistances, and therefore in choosing the geometry of the flow part of the nozzle it is necessary not only to ensure efficient limiting the flowrate of heat-transfer agent under emergency conditions, but also to guarantee low hydraulic resistance under normal operating conditions.

The design of limiting nozzles requires appropriate data on the flow of heat-transfer agent under emergency and normal reactor operating conditions. The large number of factors that determine the flow in these cases makes theoretical investigation difficult, so that such investigations have chiefly employed approximate models [3, 4]: equilibrium homogenous flow; flow with phase slippage; flow of a metastable fluid, and so forth. Such models are in agreement with experiments only in narrow parameter ranges. The available information on experimental studies (see Table 1) indicates that the ranges of operating and geometrical parameters have been studied are diverse. None of the studies mentioned in the table offers a systematic account of the relationship between the critical flowrate and the geometrical parameters. Paper [6] is something of an exception; this paper considered a nozzle with a cylindrical section 120 mm in diameter and a minimum cross-sectional diameter of 19.0 mm. This study was conducted, however, only for saturated water ($\Delta t_{no} = 0$). At the same time, for channel reactors of type RBNK the parameter range of practical interest is $\Delta t_{no} = 0$–30°C, $p_o = 0.1$–9 MPa and $d_{th} \leqslant 150$ mm. As Table 1 indicates, this range has hardly been studied at all. Extrapolation of the available empirical data to this region is evidently not legitimate.

In this paper we offer some experimental results relating to the critical flowrate characteristics of Venturi-type nozzles as a function of geometrical factors (diameter and length of the cylindrical throat of the nozzle, aperture angle of conical diffuser) and of the operating parameters (pressure and underheating of water at nozzle inlet). The experiments were conducted using axisymmetric nozzles consisting of three elements: a narrowing input section with rounding in the form of a quarter-arc of a circumference (R = 30 mm), a cylindrical section (d_{th} = 10–30 mm, l_{th} = 0–160 mm, and an expanding diffuser α = 3°, 6° and 180°). The nozzle geometry is given in Fig. 1 and Table 2. Experiments were conducted under conditions of steady-state outflow for $p_o = 0.1$–9 MPa and Δt_{no} = 0–100°C. The measurement error did not exceed ±2% for the pressure, ±1.4°C for the temperature, and ±4% for the mass flow rate. The experimental setup and procedure were borrowed from [11].

The measurement results indicate that p_o and Δt_{no} exert a substantial influence on the critical mass velocity, referred to the minimum cross section of the flow part of the nozzle. It follows from Figs. 2 and 3 that the critical mass velocity increases with p_o and Δt_{no}. It should be pointed out that the results corresponding to $\Delta t_{no} = 0$, were obtained by interpolation of the graphs plotted in $(\rho w)_{cr} - (\Delta i/r)_o$ coordinates. In the case under consideration, this step results from the technical difficulties associated with obtaining exact values of the saturation parameters at the inlet to the nozzle.

Translated from Atomnaya Énergiya, Vol. 49, No. 2, pp. 83–86, August, 1980. Original article submitted October 22, 1979.

 0038-531X/80/4902-0516$07.50

TABLE 1. Data of Experimental Studies

Initial parameters		Inlet section		Throat		Diffuser		Literature
p_0, bar	Δt_{n0}, °C	profile	l_{in}, mm	d_{th}, mm	l_{th}, mm	profile	F_{cr}/F_0	
6	5—6	Lemniscate	40	3	1	Cone 3—7°	12—45	[5]
20—100	0	Arc with R = = 10 mm	10	3,84	18	Cone 3°	3,8	[6]
		Cone with R = = 180 mm	114	19,0	65—120	Cone 3—6°	2,17—2,50	
8—90	0—140	Cone	—	6,4	0	Cone 24°	21,6—40,9	[7]
5—20	1—70	Cone	103	10,0	0	Cone 3,6°	12,0	[8]
			93	5,0	7	Cone 3,9°	13,9	
1,1—20	0—10	Plane nozzle						[9]
5—20	0—60	The same						[10]

TABLE 2. Geometry of Nozzles Investigated

Nozzle No.	Inlet section		Throat		Diffuser		
	R, mm	l_{in}, mm	d_{th}, mm	l_{th}, mm	α, deg	l_{dif}, mm	d_{co}, mm
1	30	30,5	20,04	0	6	180,3	38,95
2	30	30,5	20,04	41,3	6	180,3	38,95
3	30	30,5	20,04	81,1	6	180,3	38,95
4	30	30,5	20,04	160,7	6	180,3	38,95
5	30	30,5	20,04	161,3	Without diffuser		
6	30	30,5	20,04	160,7	3	180,4	29,45
7	30	29,0	30,0	165,5	6°35	90	40,4
8	30	31,03	19,98	26,0	5°42	193	38,85
9	30	34,4	10,03	156,4	Without diffuser		

Of the geometrical factors investigated, it is the length l_{th} of the cylindrical throat that exerts the greatest influence on $(\rho w)_{cr}$. Obviously, the critical mass velocity depends not on the length of the cylindrical section but on a somewhat larger effective value that represents the sum of the length of the cylindrical section and of the length of part of the input section. The latter is reckoned from the cross-section where the fluid begins to boil. It can be seen from Fig. 4 that, over the entire range of p_0 investigated, an increase in l_{th} leads to a decrease in the critical mass velocity of the outflow of both saturated and underheated water. The effect of l_{th} on $(\rho w)_{cr}$ attenuates more rapidly, the greater the unjerheating of water at the nozzle inlet. For example, for Δt_{n0} = 10°C increasing l_{th} from 0 to 160 mm results in a 47% drop in $(\rho w)_{cr}$, whereas for Δt_{n0} = 30°C variation of l_{th} within the same limits reduces $(\rho w)_{cr}$ by only around 13% in all.

Of considerable practical interest is the probable effect of the diameter of the nozzle throat on the critical mass velocity of outflow of underheated and saturated water. In the present study, experiments were conducted using nozzles with throat diameters of 10, 20, and 30 mm. Figure 5 indicates that there is some stratification with respect to d_{th} of the curves that describe $(\rho w)_{cr}$ as a function of the relative underheating $(\Delta i/r)_0$ for various values of the water pressure at the nozzle inlet. It follows from the figure that for d_{th} = 30 mm the values of $(\rho w)_{cr}$ are 5-8% higher than for d_{th} = 10 mm. Of course, the problem of the effect of throat diameter requires further experimental study, since the observed stratification of the $(\rho w)_{cr} = f(\Delta i/r)_0$ curves with respect to d_{th} is commensurable with the possible error in measurement of $(\rho w)_{cr}$ (which amounts to ±4%).

In this study we also investigated the effect of the aperture angle α of the conical diffuser in the range from 3 to 180°. As the experimental data show (Fig. 6), the effect of α on $(\rho w)_{cr}$ is negligible, at least in the range under consideration and for nozzles of sufficient extension.

Conclusions

We have experimentally investigated the relationship between the critical mass velocity of hot water on a number of operating and geometrical parameters. The greatest effect on

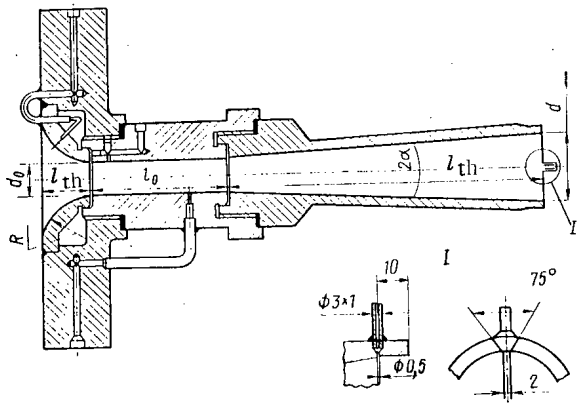

Fig. 1. Typical working section.

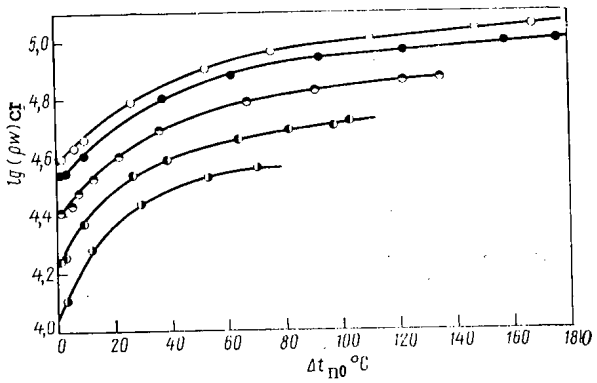

Fig. 2. Effect of intake under heating on critical mass velocity (nozzle No. 9) for p_o = 9.0 (○); 7.0 (●); 4.0 (◓); 2.0 (◐); 1.0 (◑) MPa.

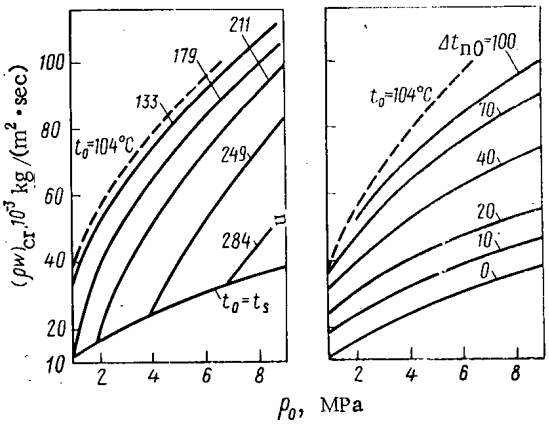

Fig. 3. Effect of pressure at inlet to nozzle on critical mass velocity (nozzle No. 9).

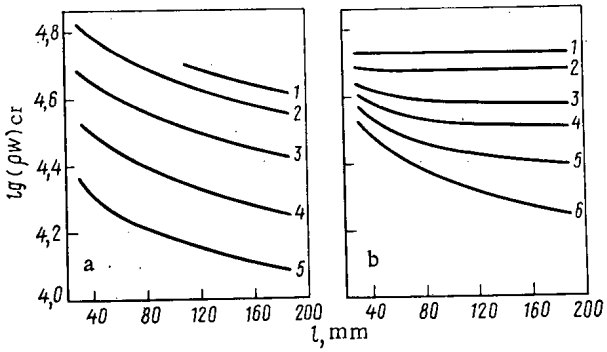

Fig. 4. Effect of length on critical mass velocity (nozzle with throat 20 mm in diameter): a) saturated water, p_o = 9.0 (1); 7.0 (2); 4.0 (3); 2.0 (4); 1.0 MPa (5); b) underheated water, Δt_{no} = 100 (1) 60 (2); 30 (3); 20 (4); 10 (5); 0° (6).

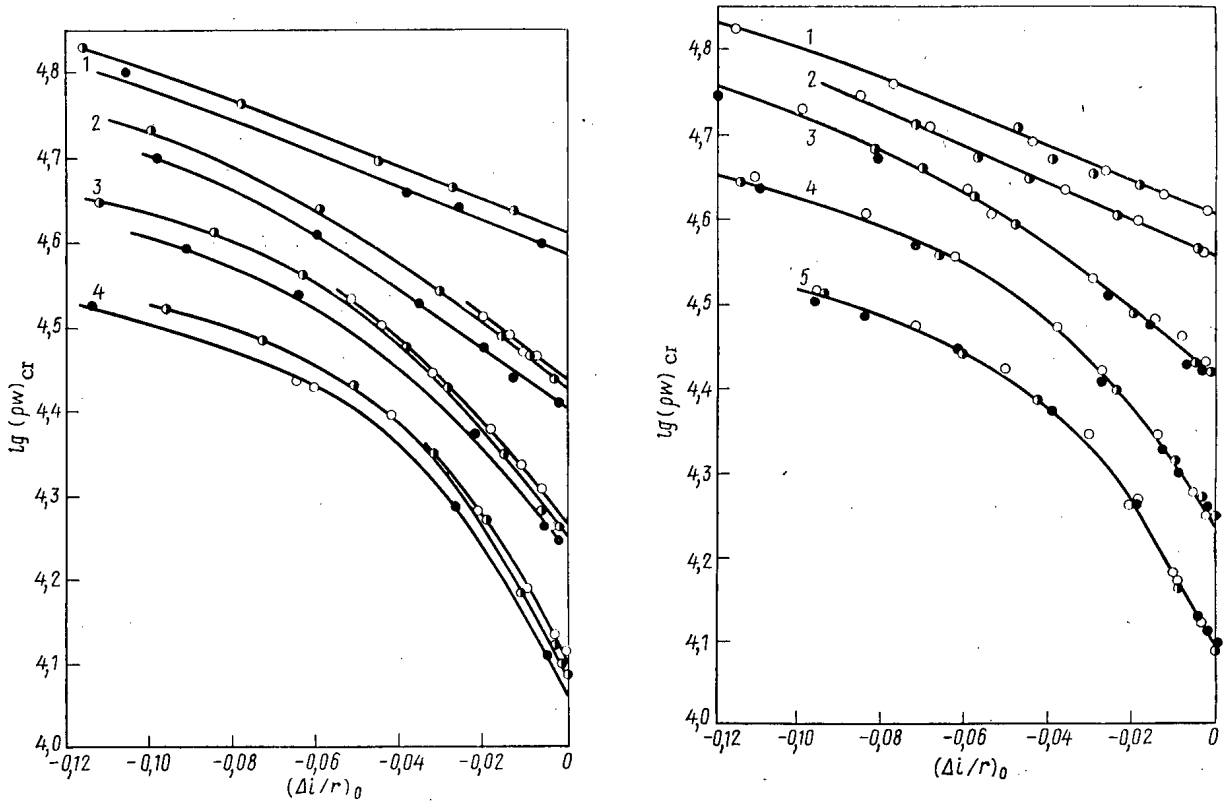

Fig. 5. Effect of throat diameter on critical mass velocity (nozzles Nos. 4-7, 9 with throat length 160 mm) for p_o = 9.0 (1), 4.0 (2), 2.0 (3), 1.0 MPa (4) and d_{th} = 10.03 (●), 20.04 (◑) and 30.0 (○) mm.

Fig. 6. Critical mass velocity as a function of underheating at inlet for various aperture angles of the output section (nozzles Nos. 4-6 with cylindrical throat 160 mm long and 20 mm in diameter) for p_o = 9.0 (1), 7.0 (2), 4.0 (3), 2.0 (4), 1.0 MPa (5) and α = 180 (●), 6 (◑), 3° (○).

$(\rho w)_{cr}$ is exerted by the pressure and underheating of the water at the nozzle inlet. For example, increasing p_o from 2 to 9 MPa for Δt_{no} = 20°C results in an increase in $(\rho w)_{cr}$ from 30 to $55 \cdot 10^3$ kg/(m²·sec), while a change in Δt_{no} from 0 to 60°C for p_o = 7 MPa increases $(\rho w)_{cr}$ from 35 to $74 \cdot 10^3$ kg/(m²·sec).

The critical mass velocity of outflow of underheated or saturated water also depends on the length of the cylindrical throat of the nozzle. It has been established that $(\rho w)_{cr}$ decreases as l_{th} increases. However, this effect gradually attenuates as l_{th} increases. The greater the underheating of the water at the nozzle inlet, the sooner the effect of l_{th} attenuates. Investigation of the effect of throat diameter revealed that increasing d_{th} from 10 to 30 mm resulted in roughly a 5-8% increase in $(\rho w)_{cr}$. The effect of the aperture angle of the diffuser turned out to be negligible, at least for $3 \leq \alpha \leq 180°$ and $l_{th}/d_{th} \geq 1.5$.

Notation

P_o, water pressure at the nozzle inlet, MPa, Δt_{no}, underheating of the water at the nozzle inlet, °C; $(\rho w)_{cr}$, critical mass velocity, referred to the narrow cross section, kg/(m²·sec), $(\Delta i/r)_o$, dimensionless value of the underheating at the nozzle inlet, l_{th} and d_{th}, length and diameter of the cylindrical throat of the nozzle, mm, α, aperture angle of the conical diffuser, deg.

LITERATURE CITED

1. R. Stroehlen, FRG patent No. 1155649, class 47g 49/02 (1964).
2. J. Piston, US patent No. 3172819, class 176-31 (1965).
3. V. A. Zysin et al., Boiling Adiabatic Flows [in Russian], Atomizdat, Moscow (1976).

4. G. V. Tsiklauri, V. S. Danilin, and L. I. Seleznev, Two-Phase Adiabatic Flows [in Russian], Atomizdat, Moscow (1973).
5. T. N. Parfenova, Candidate's Dissertation, Leningrad (1971).
6. É. K. Karasev et al., At. Energ., 42, No. 6, 478 (1977).
7. W. Schrock, E. Starkman, and R. Braun, Teploperedacha, 99, No. 2, 113 (1977).
8. M. A. Koronkevich, Preprint, Institute of Technical Physics, Siberian Branch, Academy of Sciences of the USSR, Novosibirsk (1977), pp. 55-77.
9. G. A. Mukhachev, B. M. Pavlov, and V. G. Tonkonog, in: Proceedings of Kazan Aviation Institute, No. 158 (1973).
10. V. G. Tonkonog, Author's Abstract of Candidate's Dissertation, Kazan Aviation Inst. (1975).
11. L. R. Kevorkov, S. Z. Lutovinov, and L. K. Tikhonenko, Teploenergitika, No. 7, 72 (1977).

DETERMINATION OF SOME CHARACTERISTICS OF SPENT FUEL OF BOILING-WATER REACTORS USING α AND γ SPECTROMETRY

A. G. Zelenkov, S. V. Pirozhkov, Yu. F. Rodionov, and I. K. Shvetsov

UDC 621.09.54:539.128.4.144:539.166.3

The international system of guarantees regarding the nonproliferation of nuclear weaponry places considerable emphasis on supervision of special nuclear materials (SNM), using methods of physical protection (protective measures) and nondestructive methods of recording nuclear emissions.

An important element in supervision at spent-fuel reprocessing plants is the identification of SNM in all phases of the technological process, from delivery to the plant until storage of the product and localization of radioactive waste. The problem reduces to checking the correspondence between the product and the certification data for fuel assemblies: initial enrichment, average burn depth ($\bar{B}$), and unloading time from reactor (holding time) [1]. The solution of this problem is one of the tasks of the "Minimum Isotope Inventory Safeguard Technique" (MIST), whose authors, however, confined themselves to only linear isotope correlations and mass-spectrometric measurement techniques [2].

We will confine ourselves to the problem of identifying SNM for the purpose of detecting their possible illegal inclusion into the technological process. For this it is extremely useful to determine the relative content of the maximum number of nuclides of the actinoid elements, including nuclides of the transplutonium elements. The relative spectral line intensities resulting from emission of not one but several nuclides can also be employed.

It is desirable to employ nonlinear isotope correlations because of the possibility of predicting the relative content of nuclides for a batch of reprocessed fuel, primarily for assemblies with known $\bar{B}$, and also because of the achievable accuracy in determining the above certification data. To solve the problem, it is desirable to employ relatively simple methods, characterized by moderate equipment costs and speed and ease of analysis. Current mass-spectrometric techniques can meet these requirements only with difficulty.

It appears promising to employ α-spectrometry (with semiconductor detectors) in combination with γ spectrometry for this purpose: both types of measurements can be made using one device equipped with two kinds of detectors, the methods are easily accessible, relatively simple, fast, and insensitive to chemical admixtures. Alpha spectrometry is relatively insensitive to the presence of radioactive fission products as well, but requires the preparation of uniform thin-layer targets (around 10 $\mu g/cm^2$).

Translated from Atomnaya Énergiya, Vol. 49, No. 2, pp. 86-91, August, 1980. Original article submitted August 6, 1979.

 0038-531X/80/4902-0520$07.50

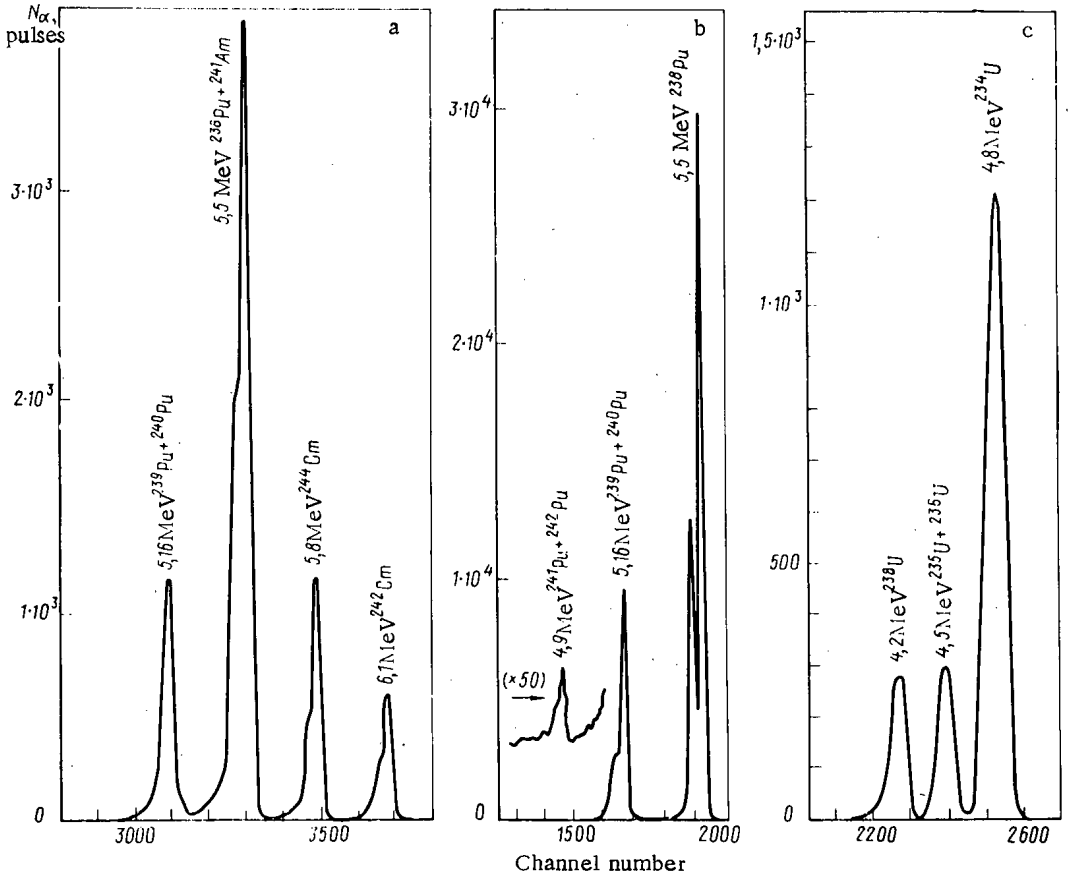

Fig. 1. Alpha spectrum of spent fuel of VVÉR-440 reactor (a) and of Pu (b) and U (c) extracted from it.

As an example, Fig. 1 shows the α spectra of a sample of solution of VVÉR-440 fuel (from the Novovoronezh nuclear power plant) with a burn-up of 32 kg/ton, initial enrichment of 3.6%, and holding time of 2.6 years, and also for plutonium and uranium extracted from the same fuel sample. Measurements were made using a semiconductor silicon detector.

For purposes of considering the degree of informativeness of the measured relationships, we give the absolute (Fig. 2a) and relative (Fig. 2b-d) group intensities in the α spectrum of VVÉR fuel as a function of the burn depth. The figure also gives the ratios of the α decay rates of ^{238}Pu, ^{239}Pu, and ^{241}Pu, and also of ^{235}U and ^{238}U, as measured by γ spectrometry. Figures 2b and c show that the α spectrum of the fuel sample can be used to check the extent to which the relative intensity of $^{244}Cm[^{244}Cm/(^{239}Pu + ^{240}Pu)]$ corresponds to the burn-depth data, and the extent to which the relative intensity of $^{242}Cm \times [^{242}Cm/(^{239}Pu + ^{240}Pu)]$ (for given $\bar{B}$) corresponds to the known holding time. In view of the fact that the dependence of the yield of these isotopes on the burn-up is very steep, and in view of the rapid decay of ^{242}Cm ($T_{1/2}$ = 163 days), there is no need for a high degree of precision in determining their relative content.

For large holding times, we can also employ the relative intensity of the 5.5 MeV line $[(^{238}Pu + ^{241}Am)/(^{239}Pu + ^{240}Pu)]$, which reflects the accumulation of ^{241}Am from ^{241}Pu (see Fig. 2c). We can also employ γ-spectrum data, which enable us to determine the relative content of ^{106}Ru, ^{134}Cs, ^{137}Cs, ^{144}Ce, ^{154}Eu and ^{95}Zr. As we know, they make it possible to evaluate the burn-up (on the basis of ^{134}Cs, ^{137}Cs, ^{154}Eu), the contribution of plutonium fission products (on the basis of ^{106}Ru), and the holding time (on the basis of ^{144}Ce, ^{95}Zr).

Information on spent-fuel composition can be greatly expanded through α- and γ-spectrometric analysis of the plutonium and uranium it contains. The chromatographic method can be employed to separate small amounts of uranium from plutonium and to achieve the purification depth required for γ spectrometry (sorption of uranium and plutonium from hydrochloric acid solution on an anionite and subsequent washing with hydrochloric and hydrobromic acid [6]).

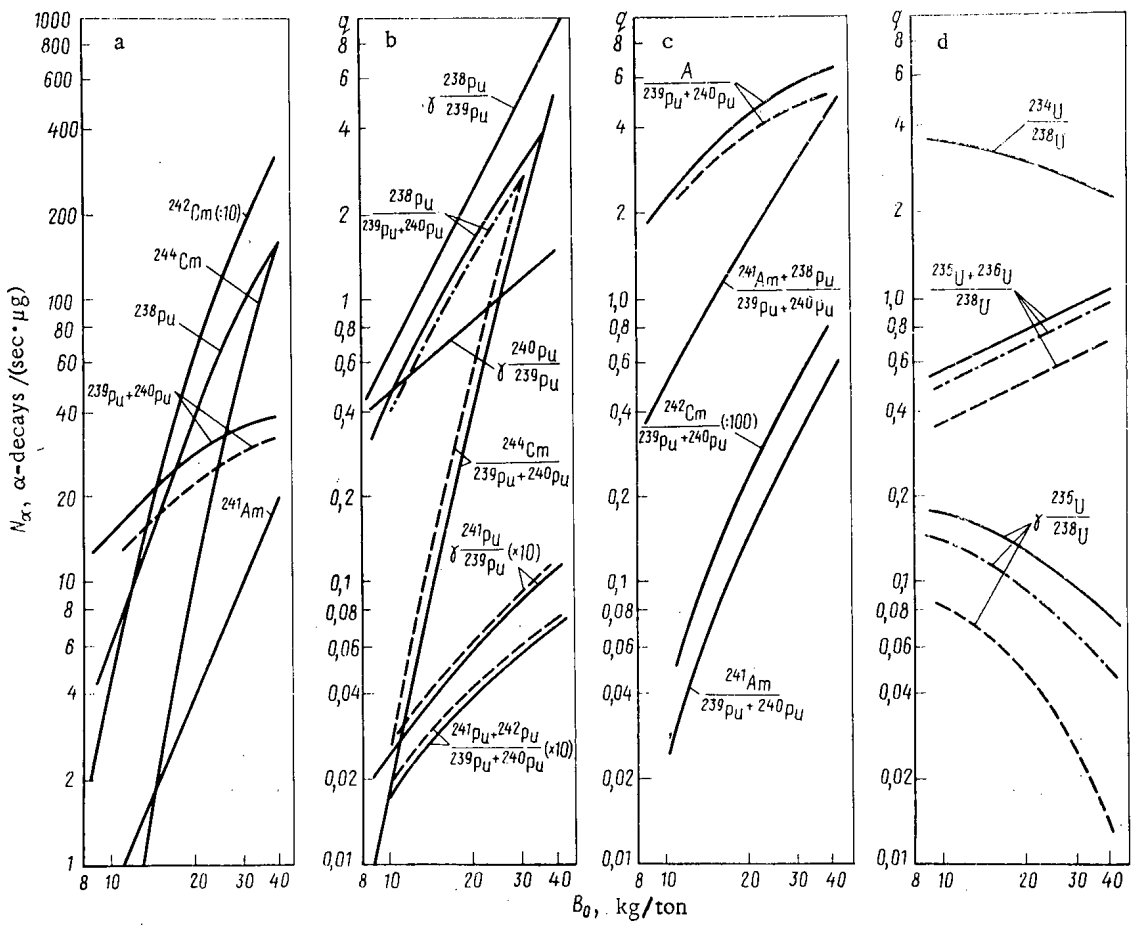

Fig. 2. Absolute α-emission intensity (N_α) and ratio of α-decay rates of nuclides, obtained from α or γ spectra (q) as a function of the burn depth B; solid line: experimental data for Yankee nuclear power plant [3]; dashed line and dot–dash line: data for first [4] and second [5] units of Novovoronezh nuclear power plant, initial ^{235}U enrichment 3.4, 2, and 3% respectively (A is the radioactivity of ^{241}Am corresponding to the content of ^{241}Pu).

The α spectrum of plutonium (see Fig. 1b) can be used to determine the relative content of ^{238}Pu, and hence of ^{241}Am, and to additionally check the burn-up and holding time. Here we can also isolate the weak 4.9 MeV emission line of ^{241}Pu and ^{242}Pu. The γ spectrum of plutonium can be used to determine the relative content of ^{238}Pu, ^{239}Pu, ^{240}Pu and ^{241}Pu. These data can be used (see Fig. 2b) to additionally check the burn-up and, possibly, the initial enrichment. The lines of ^{241}Am will also be present in the γ spectra of stored purified plutonium taken from storage. The mass ratio of ^{241}Am and ^{241}Pu makes it possible to determine the time elapsed from the moment of plutonium extraction.

The isotope composition of uranium is unambiguously related to its origin. In the α spectrum, the relationship between the emission lines of ^{234}U, ^{238}U and the combined emission line of (^{235}U + ^{236}U) and ^{238}U (see Fig. 1c) can be used to determine the initial uranium enrichment and the burn depth (see Fig. 2d). Measurements of the γ spectrum make it possible to determine the ratio of ^{235}U and ^{238}U.

The accompanying table gives the principal lines of the α and γ spectra of spent boiling-water reactor fuel, their origin, and information on fuel characteristics obtained via α and γ spectroscopy. Thus, measurements of the α and γ spectra of a sample of spent fuel makes it possible to estimate the burn depth and the holding time [1]. The nature of the plutonium spectra is determined by the burn-up and storage time of the fuel. By analyzing uranium emission, it is possible to determine the initial and final enrichments and the burn-up.

TABLE 1. Principal Lines in α and γ Spectra of Spent Boiling-Water Reactor Fuel and of Uranium and Plutonium Extracted from It

Source of emission	α-emission			γ-emission		
	nuclide	E_α, MeV	characteristic determined	nuclide	E_γ,* MeV	characteristic determined
Initial fuel mixture	$^{239}Pu + ^{240}Pu$	5,16	Baseline	^{137}Cs	0,662	Baseline
	$^{238}Pu + ^{241}Am$	5,5	Burn-up and holding time	^{134}Cs	0,604	Burn-up
					0,796	
	^{244}Cm	5,8	Burn-up	^{154}Eu	1,004	»
	^{242}Cm	6,1	Holding time		1,274	
				$^{144}Ce(^{144}Pr)$	0,696	Holding time
					1,489	
				$^{95}Zr(^{95}Nb)$	0,724	» »
					0,766	
				$^{106}Ru(^{106}Rh)$	0,622	Contribution of plutonium fission to fission products
Uranium	^{238}U	4,2	Baseline	$^{238}U(^{234m}Pa)$	1,001	Baseline
	$^{235}U + ^{236}U$	4,5	Burn-up and initial enrichment	^{235}U	0,186	Final enrichment
	^{234}U	4,8				
	$^{239}Pu + ^{240}Pu$	5,16	Baseline	^{239}Pu	0,129	Baseline
					0,414	
Plutonium	$^{238}Pu + ^{241}Am$	5,5	Burn-up and storage time after extraction	^{240}Pu	0,160	Burn-up
				^{238}Pu	0,153	»
				$^{241}Pu(^{237}U)$	0,149	»
	$^{241}Pu + ^{242}Pu$	4,9	Burn-up		0,208	
				^{241}Am	0,060	Storage time after extraction

*Most intense lines.

It should be pointed out that the curves in Fig. 2 correspond to local burn-up and cannot be employed directly to determine the content of nuclides in fuel assemblies. To solve this problem we need to know how the burn-depth values are distributed over the mass of the fuel; this can be determined from the burn-up distribution over the cross section of the assembly and the length of the elements [7-9]. Figure 3 shows the distribution of the burn depth over the fuel mass computed in this fashion, for the assemblies of the VVÉR reactor. The abscissa axis gives the relative burn depth ($B/\bar{B}$), while the ordinate axis gives the relative content of fuel with the given burn-up. The "tail" of the distribution in the direction of low burn-up results from the lower burn-up at the ends of the elements (down to 0.3 $\bar{B}$), while the drop-off in the region of relatively large burn-ups results from increased burn-up of peripheral elements of the assemblies. Analysis of the data indicates that the histogram (see Fig. 3) gives a fairly good account of the distribution of burn-up for most assemblies of boiling-water reactors with differing average burn-up and initial enrichment, and can be used for estimating the production of nuclides of transuranium elements.

The curves in Figs. 2 and 3 were used to compute the intensity of some lines in the α spectra of a sample of initial fuel mixture from the assemblies of the VVÉR-2 reactor and of uranium and plutonium extracted from the sample for average burn-ups of 15, 20, and 30 kg/ton; it turned out that the expected differences in the relative line intensities in the alpha spectra of samples taken from the assembly mixture and of samples corresponding to local burn-up result in errors in determining the burn depth not greater than 10%, i.e., they are within the limits of accuracy in determining the calculated burn-up.

The accuracy in estimating the burn-up can be improved, of course, if we employ experimental data obtained in measuring the nuclide content in dissolved fuel assemblies of a given type with differing burn-up. Here we can also take account of the effect of distortion of the neutron spectrum at the edges of the assemblies. The achievevable accuracy in estimating the average burn-up will be determined by the variations in the measured ratios of the nuclide content in response to the conditions of irradiation of the assemblies in the reactor. In using the proposed procedure it is desirable that fuel with the same initial enrichment and maximally similar burn-up be combined into one batch in the radiochemical plant [9]. Evidently there are also economic reasons for doing this. Consequently, α and γ spectrometry of fuel at the radiochemical plant enables us to determine with the necessary degree of pre-

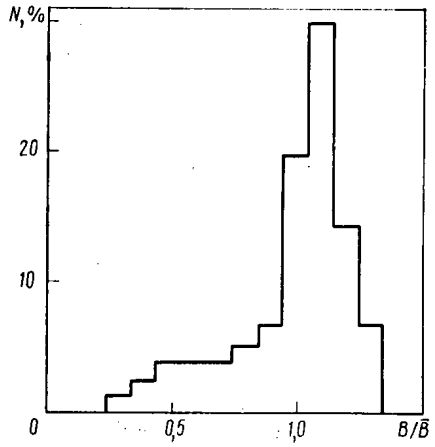

Fig. 3. Distribution of degree of burn-up over fuel mass.

cision the extent to which the nuclide composition of the product (both the initial mixture and the purified uranium and plutonium) corresponds to the certification data. As for the basic problem of meeting the guarantees (monitoring illegal incorporation of extraneous SNM into the technological process), it is natural to assume that this fuel has a different origin and different initial composition, and was irradiated in a reactor of a different type. The nuclide composition of transuranium elements in spent fuel differs greatly for reactors of different types [10]. In view of the fact that the relative content of 18 nuclides can be determined using α and γ spectrometry (see Table 1), we can anticipate that our method will be highly sensitive to illegal incorporation of appreciable amounts of foreign products.

Yet another interesting possibility should be pointed out. In view of the high degree of sensitivity of the yield of heavy nuclides formed as a result of multiple neutron capture to the irradiation conditions for the assemblies in the reactor, we can assert that each batch of SNM obtained as a result of reprocessing of a batch of assemblies will have an individual nonduplicable nuclide composition, or "dactyloscopic signature." Indeed, α and γ spectrometry can be used to measure the ratio of four isotopes of uranium and five isotopes of plutonium. The necessary accuracy in measuring the relative spectral intensity is evidently around 1%, a figure that is quite achievable experimentally.

Thus, it becomes possible to employ "dactyloscopy" of a batch of SNM over the entire course of fuel reprocessing until it is used in new fuel elements. The problem can be simplified by artificial tagging of nuclear materials by small amounts of ^{244}Cm, ^{234}U, or ^{233}U. In our opinion, a combination of α and γ spectrometry provides a good method for this kind of "dactyloscopy" of SNM.

In concluding, we wish to thank V. A. Pchelin, V. P. Tarasevich, and V. S. Shiryaev for their assistance with the paper, and A. N. Novikov, O. A. Miller, and V. D. Sidorenko for discussion of the results.

LITERATURE CITED

1. W. Häfele and D. Nentwich, in: Proc. IAEA Symp. Safeguards Techniques, Karlsruhe, 6-10 July 1970, p. 1.
2. D. Christiansen. ibid., p. 563.
3. R. Matsen, Nucl. Technol., 15, 343 (1972).
4. V. Ya. Gabeskiriya et al., Preprint, NIIAR, No. 88, Dmitrovgrad (1976).
5. V. Ya. Gabeskiriya et al., At. Energ., 44, No. 5, 446 (1978).
6. O. A. Miller, S. V. Pirozhkov, and Yu. F. Rodionov, in: Proc. IAEA Symp. Nuclear Safefuards Technology 1978. IAEA-SM-231/142. Vienna, 2, 797 (1979).
7. D. I. Kamyshin and A. I. Novikov, in: Proc. IAEA Symp. Reactor Burn-Up Physics, Vienna (1973), p. 125.
8. G. Ya. Andrianov et al., Kernenergie, 20, No. 10, 309 (1977).
9. L. V. Kochanovskaja, ibid., p. 307.
10. A. K. Kruglov and A. P. Rudik, Artificial Isotopes and Methods of Calculating Their Formation in Nuclear Reactors [in Russian], Atomizdat, Moscow (1977).

DETERMINATIN OF LOW CONTENTS OF ELEMENTS FROM VANADIUM TO MOLYBDENUM BY AN X-RAY FLUORESCENT METHOD USING A NEW VARIANT OF STANDARDIZATION

A. G. Belov, V. Ya. Vyropaev
N. Sodnom, B. Dalkhsurén,
Sh. Gérbish, P. Zuzaan,
and S. Davaa

UDC 543.422.8

X-ray spectral analysis is widely used in the determination of the content of elements in ores, soils, materials of biological orgin, and in samples collected for environmental monitoring [1-2]. A peculiarity of the analysis of such objects is the monitoring of low contents of a group of elements, whereas in most cases there are no standards available. As a result of this, the development and investigation of methods of x-ray spectral analysis based on the use of a minimum of standards are promising. In this work we present the results of the development of a new method of x-ray spectral fluorescent analysis, based on the use of one reference element as the standard for a group of elements from vanadium to molybdenum. It is expedient to use this method in the determination chiefly of low concentrations of the elements, ($\leq 0.5\%$).

Theoretical Substantiation of the Method

Quantitative x-ray spectral analysis is a variant of the internal standard method [3], based on the use of the relative specific intensity R_l^j of the analytical lines of the elements to be determined. The value of R_l^j is determined calculated for 1%:

$$R_l^j = (I_j/I_l)(C_l/C_j), \tag{1}$$

where I_l, I_j and C_l, C_j are the intensities of the analytical lines and the concentrations of the elements l and j, respectively, for the sample under consideration (in this case the element is the reference element — internal standard).

Let us assume that in the sample under consideration the content of the group of elements does not exceed $\sim$0.5%. Let this be, e.g., elements from ^{23}V to ^{42}Mo. Using ^{109}Cd to excite the x-ray fluorescence, we can simultaneously investigate the K-spectra of these elements. In a calculation of the fluorescence intensity excited in the sample under consideration by a ^{109}Cd source, the primary spectrum can be considered monochromatic with acceptable accuracy, since the contribution of the hard component with energy 88 keV will be negligible. In view of the fact that the entire absorption edge of elements with $23 \leq Z \leq 42$ lies on the long-wave side of AgK — the spectrum of the source — All the calculations can be made for the AgK_α line [4]. In this case we can neglect the contribution of the effect of selective excitation to the fluorescence intensities. Then the following formula will be correct:

$$I_l = kW_k^l P_i^l \frac{S_k^l - I}{S_k^l} \mu_{ml}^l \frac{C_l}{\mu_{ml}^{samp} + n\mu_{mi}^{samp}} \tag{2}$$

where k is a coefficient of proportionality; n = sin φ/sin ψ, angles of incidence of the primary fluorescent radiation on the sample and of collection of fluorescent radiation; W_k^l, fluorescence yield of the element l; P_i^l, probability of transition of the atom l with emission of the line i; S_k^l, jump in the absorption of the k-level; μ_{ml}^l, μ_{ml}^{samp}, and μ_{mi}^{samp}, mass coefficients of absorption of the primary radiation by element l and the sample, as well as the fluorescent radiation of the element l and the sample.

USSR. Mongolia. Translated from Atomnaya Énergiya, Vol. 49, No. 2, pp. 91-94, August, 1980.

0038-531X/80/4902-0525$07.50

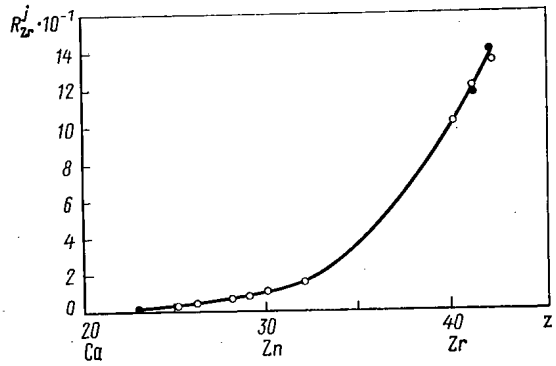

Fig. 1. Dependence of the relative specific intensity on the atomic number: •) calculation; o) experiment.

If now we introduce the notation

$$\eta_j = W_k^j P_i^j \frac{S_k^j - I}{S_k^j} \mu_{mI}^j, \tag{3}$$

then for R_l^j we obtain the following expression

$$R_l^j = \frac{\eta_j}{\eta_l} \frac{\mu_{mI}^{samp} + n\mu_{mil}^{samp}}{\mu_{mI}^{samp} + n\mu_{mij}^{samp}}. \tag{4}$$

Figure 1 shows the dependence of the relative specific intensity R_l^j for elements from ^{23}V to ^{42}Mo on the atomic number Z. The curve was constructed according to the results of a theoretical estimate. We selected ^{40}Zr ($R_l^{Zr} = 1$) As the reference standard. All the necessary parameters were taken from the tables of [5, 6]. The mass coefficients of absorption were calculated according to the formula

$$\mu_m^j = C_j \lambda^{\alpha j}, \tag{5}$$

where λ is the wavelength of the radiation, while the parameters C_j and α_j were calculated for each element. A value of n equal to 0.707 corresponds to angles $\varphi = 45°$ and $\psi = 90°$.

It is not difficult to show that the dependence shown in Fig. 1 is constant when the chemical composition is varied within broad limits, if there are no absorption edges of the elements with a larger concentration (> 0.4-1.0%) in the range of wavelengths between λ (primary radiation) and $\lambda_{i\ max}$ (maximum wavelength of radiation of the analytical line, in the case under consideration VK_α). Actually, in the case the mass coefficient of absorption of the sample will be a continuous function within the wavelength ($\lambda_I - \lambda_{i\ max}$). Then, in accordance with formula (5)

$$\mu_{mI}^{samp} = \left(\frac{\lambda_I}{\lambda_i^j}\right)^{\alpha} \mu_{mij}^{samp}, \tag{6}$$

and the expression for R_l^j can be transformed into:

$$R_l^j = \frac{\eta_j}{\eta_l} \frac{I + n(\lambda_i^l/\lambda_I)^{\alpha}}{I + n(\lambda_l^j/\lambda_I)^{\alpha}}. \tag{7}$$

From this it is evident that the parameter R_l^j does not depend on the chemical composition of the samples. Thus, the mutual influences of the elements are considered with the aid of the relative specific intensity for the type of samples under consideration.

According to formula (3) we find that at small n, the value of R_l^j is entirely determined by the ratio η_j/η_l. For large n, when μ_{mI} can be neglected, formula (3) takes the form

$$R_l^j = \frac{\eta_j}{\eta_l} \frac{\mu_{mil}^{samp}}{\mu_{mj}^{samp}} \tag{8}$$

In this case the mass coefficient of absorption of the radiation of the analytical line of an element with atomic number Z is always greater than for an element with (Z + 1), etc.

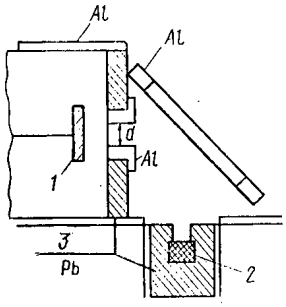

Fig. 2

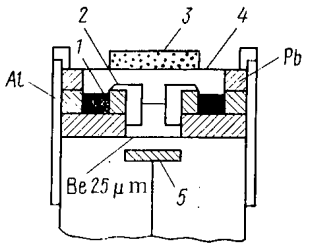

Fig. 3

Fig. 2. Sample holder for a point source. 1) Detector; 2) source; 3) shield.

Fig. 3. Sample holder for a ring-shaped source: 1) source; 2) aluminator collimator; 3) sample; 4) mylar; 5) detector.

As of a result of this, when n is increased, the value of R_l^j will always increase for elements with large Z. Analysis according to the proposed method is performed as follows.

1. For a group of elements the dependence of the relative specific intensity on Z is determined.

2. For samples one finds an element that can serve as a standard. Such an element should not be present in the samples, or its concentration should be less than a definite level.

3. A definite amount of material containing the standard element is added to the sample to be analyzed. Such material may be, for example, boric acid, since strong tablets are produced when it is introduced into the sample.

4. The intensity of the analytical lines is measured for the samples to be analyzed under set conditions of analysis.

5. The results of the measurements are treated (finding the areas of the peaks, intensities of the background, intensities of the analytical lines of I_j).

6. The concentration of the elements to be determined is calculated according to the formula

$$C_j = \frac{I_j}{I_l} \frac{I}{R_l^j} \frac{C_l}{I - C_b}, \qquad (9)$$

where C_b is the boric acid concentration in the emitter.

Experimental Verification of the Method

The effectiveness of the proposed variant of the internal standard method was verified on an ORTEC x-ray spectrometer. In the investigation we used an ORTEC Mode 7016 Si(Li) detector (ϕ10 mm, resolution $\sim$ 200 eV for the emission of the MnK_α line, beryllium window 25 μm thick) and a ring-shaped radioactive ^{109}Cd source from Amersham with activity 20 mCi (inner diameter of source 26.5 mm, outer diameter 34.25 mm). Figures 2 and 3 present the scheme of arrangement of the sample holder, exciting source, collimator, and detector. The instrument is supplemented by a set of mixed collimators of aluminum 13 mm high with diameter of opening 4, 6, 8, 10, and 14 mm. The possibility of varying the source–sample distance is also provided.

A ring-shaped excitation source has divergent beams. For example, at a distance from the source to the sample of 15 mm and a diameter of the collimator 6 mm, the minimum value of φ is equal to 34°, the maximum 83°, while the angle ψ varies in this case from 65 to 90°. The value of n correspondingly increases from 0.62 to 1.09. In an estimate of the influence of variation of this parameter on the shape of the curve (Fig. 1), it was found that the relative specific intensity R_{Zr}^{Ni} decreases from 0.04 to 0.05. Since the maximum contribution

TABLE 1. Theoretical and Experimental Values

z	Element	R^j_{Zr} theor.	R^j_{Zr} exp.	R^j_{Zr} exp./R^j_{Zr} theor, %
23	V	0,0058	0,00695±0,0003	+2,6
25	Mn	0,0144	0,0136±0,0003	—5,6
26	Fe	0,0219	0,0220±0,0002	+0,5
28	Ni	0,0469	0,0469±0,0010	0,0
29	Cu	0,0664	0,0685±0,0010	+3,2
30	Zn	0,0894	0,0863±0,0010	—3,5
32	Ge	0,159	0,142±0,0020	—10,7
40	Zr	1,0	1,0	—
41	Nb	1,185	1,207±0,007	+1,9
42	Mo	1,395	1,36±0,003	—1,5

TABLE 2. Results of X-Ray Fluorescent Determination of the Content of Elements in Standard and Copper–Molybdenum Ore Samples

z	Element	TS		TB		GM	
		certified	exp.	certified	exp.	certified	exp.
26	Fe	5,21±0,07	—	1,41±0,02	1,24	4,84±0,028	5,59
29	Cu	493±102	473	12,8±1,4	—	51±5,5	—
30	Zn	—	—	39,1±8,4	—	93±8,5	82,0
37	Rb	222±22,8	226	253±20	263	177±15	193,0
38	Sr	93,3±27	114	133±11	129	150±13	166,0
39	Y	—	174	26,3±5,3	33	39,3±3,1	52,0
40	Zr	279±28,9	Standard	148±17	Standard	178±15	Standard
41	Nb	—	—	17±7	22	—	—
42	Mo	132±29,3	155	—	—	—	—

to the intensity recorded by the detector is made by the central part of the sample, the following values of the angles were selected for further calculations: $\varphi = 45°$ and $\psi = 90°$, which corresponds to n = 0.707.

Table 1 compares the values of the relative specific intensities R^j_z for the theoretical estimates and the experimental measurements. The experimental data for vanadium were corrected considering differences in detector efficiency. Evidently, the discrepancy of the theoretical and experimental data does not exceed 11% (see R^j_z for Ge). The coefficient of variation, characterizing the discrepancy of the theoretical and experimental values, R^j_z was 4.4%.

The correctness of function (7) was verified on samples with a content of the elements to be determined, Ni, Zn, Zr, and Nb, equal to 0.4% each, a filler of SiO_2 (78.4%) and boric acid (20%). It was found that replacement of the SiO_2 filler by Fe_2O_3 did not lead to any significant change in the relative specific intensities of the K_α lines of the elements under consideration. The experimental values R^{Zn}_{Zr} and R^{Nb}_{Zr} proved equal to 0.089, 0.090, and 1.20, 1.212 for fillers of SiO_2 and Fe_2O_3, respectively. The rate of count of the analytical lines ZnK_α, ZrK_α, and NbK_α changed approximately five fold when the filler was replaced. Analogous results were obtained when 20% of the SiO_2 was replaced in the sample by SnO_2.

When the concentration of any element from the range under consideration (from ^{23}V to ^{42}Mo) is increased substantially, the values of R^j_z for certain elements also are changed.

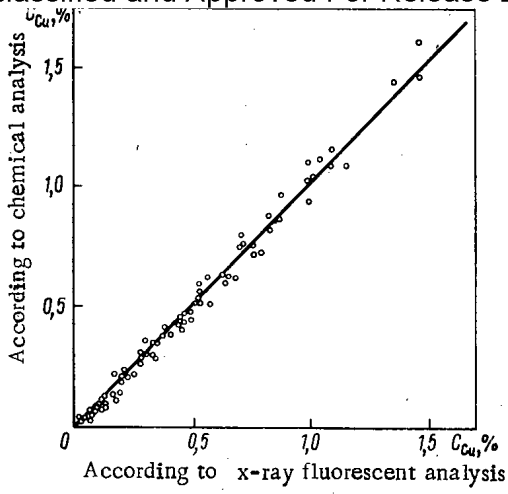

Fig. 4. Comparison of the results of x-ray fluorescent and chemical analyses.

For example, when the nickel content is increased from 0.1 to 10%, the value of R_{Zr}^{Ni} increases by 30%. The quantities R_{Zr}^{Cu}, R_{Zr}^{Co}, R_{Zr}^{Fe}, etc. change analogously (for elements from vanadium to copper, λ_R^{Ni} lies within the range from λ_1 and λ_i). The value of R_{Zr}^{j} for elements with $Z \geq 30$ is practically unchanged in this case, since function (6) is undisturbed. Consequently, when samples containing increased concentrations of individual elements ($\sim$ 0.5%) are analyzed according to the proposed method, it is necessary to consider the change in R_l^j (the level of concentration of such elements is determined by the accuracy of the analysis).

An x-ray spectral analysis of a number of artificial samples was made according to the proposed procedure. The calculated values were used as the parameters R_l^j. The error of the analysis did not exceed the discrepancies between the thoeretical and experimental R_l^j. Thus, for these elements it was not necessary to perform any measurements at the preliminary stage of the experiment.

For a verification of the method, we detected the content of a number of elements in standard samples TS, TB, and GM. Zirconium, present in sufficient amounts in all three standards, was selected as the reference elements, and Fe, Cu, Zn, Rb, Sr, Y, Nb, and Mo were also determined. The superposition of $K_{\beta 1}$ lines of Rb, Sr, Y, and Zr upon the analytical K_α lines of Y, Zr, Nb, and Mo, respectively, was taken into consideration. For the copper K_α line, a correction was introduced for the background content of copper in the collimator in front of the detector (sample TS). As a result of the fact that this correction proved comparatively large ($\sim$ 500 g/ton), the copper content in sample TB was not determined. For a determination of iron we considered the change in R_l^{Fe} with increasing Fe concentration ($C_{Fe} \geq$ 0.5%). From the results obtained, cited in Table 2, we can see the satisfactory coincidence of the certified values of the content and the data of x-ray spectral analysis. Samples of copper and molybdenum ore were also analyzed. The results were compared with chemical analysis of more than 300 samples in the determination of copper according to the proposed procedure (Fig. 4). The reliability of this method was estimated by the method of variation statistics. The method of analysis developed is used in finding a number of elements in samples of plant materials and soils.

The authors would like to express sincere gratidude to Academician G. N. Flerov for constant support and interest in the work, as well as to Candidate of Physicomathematical Sciences of Zhdanov Irkutsk State University, A. G. Revenko, for participation in the experiment and in the discussion of the results of the work.

LITERATURE CITED

1. I. F. Losev, A. I. Smagunova, A. G. Revenko, et al., Zavod. Lab., 43, No. 2, 160 (1977).
2. L. Birks and J. Gilfrich, Anal. Chem., 48, No. 48, 273R (1976).
3. I. I. Losev, Quantitative X-Ray Spectral Fluorescent Analysis [in Russian], Nauka, Moscow (1969), p. 336.

4. Yu. I. Velichko and A. G. Revenko, in: Investigations in the Field of Solid-State Physics [in Russian], No. 2, Irkutsk State Univ. (1974), p. 204.
5. M. A. Blokhin, Physics of X-Rays [in Russian], Gostekhizdat, Moscow (1957), p. 518.
6. R. Fink et al., Rev. Mod. Phys., 38, No. 3, 513 (1966).

SPECTROPHOTOMETRIC STUDY OF THE EQUILIBRIUM OF THE REACTION $Pu^{4+} + Cl^- \rightleftarrows Pu^{3+} + 1/2Cl_2$ IN MOLTEN NaCl–2CsCl

S. K. Vavilov, G. N. Kazantsev and V. V. Gushchin

UDC 546.799.4:143.543.42

The equilibrium of the reaction

$$Pu^{4+} + Cl^- \rightleftarrows Pu^{3+} + 1/2Cl_2$$

in molten NaCl–2CsCl was studied by a spectrophotometric method in the near IR region for the temperature interval 550–750°C.

The arbitrary equilibrium constant of the reaction studied is described by the empirical equation:

$$\lg K^* = 2.52 - \frac{2570}{T} \pm 0.05.$$

The values of the thermodynamic reaction parameters are equal to:

$$\Delta H^* = (49 \pm 2) \text{ kJ/mole};$$
$$\Delta S^* = (48 \pm 2) \text{ J/(mole} \cdot \text{deg K)}.$$

The temperature dependence of the arbitrary formal redox potential of the couple Pu^{4+}/Pu^{3+} relative to a chloride reference electrode takes the form

$$E_{Pu^{4+}/Pu^{3+}} = -0.51 + 5.0 \cdot 10^{-4} T \pm 0.01 .$$

The results of an investigation of the equilibrium of the reaction

$$Pu^{4+} + Cl^- \rightleftarrows Pu^{3+} + 1/2Cl_2 \qquad (1)$$

by a spectrophotometric method in molten LiCl–KCl [1] and LiCl–CsCL [2] are evidence of the low stability of tetravalent plutonium in chloride melts, which can be judged according to the closeness to zero of the arbitrary formal redox potential of the couple Pu^{4+}/Pu^{3+} relative to a chloride reference electrode.

It is interesting to continue an investigation of the equilibrium of reaction (1) according to a whole series of molten chlorides of the alkaline metals and their mixtures, for a more complete idea of the chemical behavior of oxygen-free reduced forms of plutonium in salt systems. We might expect an increase in the stability of the tetravalent state of plutonium in the series from lithium chloride to cesium chloride, as has been established for other metals [3]. This work presents the results of a study of the thermal dynamics of reaction (1) in molten NaCl–2CsCl by the method of spectrophotometric measurements of the equilibrium concentrations of tri- and tetravalent plutonium at various values of the partial pressure of chlorine in the gas phase.

Experimental

The equilibrium concentrations of tri- and tetravalent plutonium at various values of the partial pressure of chlorine were measured on an IKS-14A spectrophotometer, equipped for work with molten salts [4]. The solvent was a NaCl–2CsCl eutectic (T_m = 495°C), prepared by fusing the individual cp grade salts and freed of traces of moisture and oxygen by treating the melt with hydrogen chloride and chlorine. The density of the melt was calculated according to the equation [5]

Translated from Atomnaya Énergiya, Vol. 49, No. 2, pp. 94–98, August, 1980. Original article submitted July 3, 1979.

 0038-531X/80/4902-0530$07.50

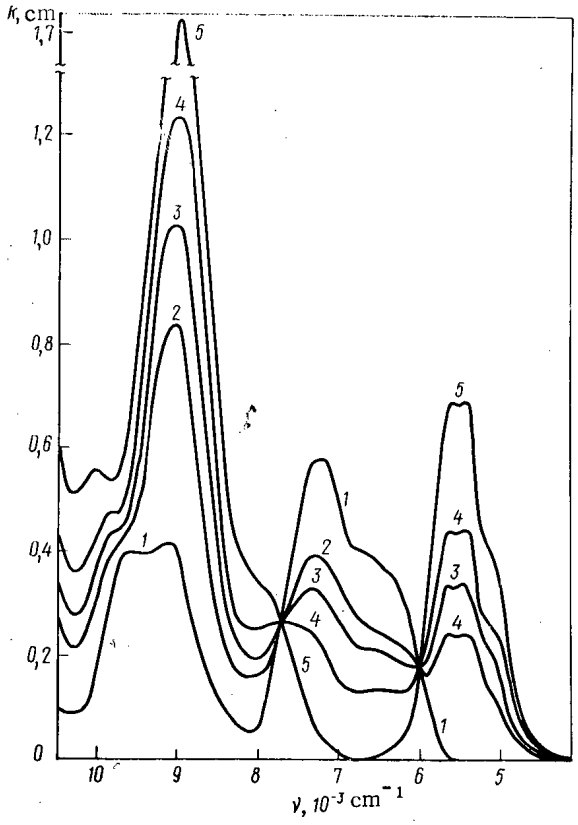

Fig. 1. Spectrum of molten NaCl–2CsCl, containing equilibrium concentrations of tri- and tetravalent plutonium at C_{Pu} = 0.130 M; T = 650°C: 1) $P_{Cl_2} = 0$, 2) $P_{Cl_2} = 0.08 \times 10^5$ Pa; 3) $P_{Cl_2} = 0.16 \times 10^5$ Pa; 4) $P_{Cl_2} = 1.0 \cdot 10^5$ Pa; 5) spectrum of Pu(IV) calculated according to Eq. (19).

$$d = 3.175 - 10.01 \cdot 10^{-4} T. \quad (2)$$

Plutonium was introduced into the melt in the form of the trichloride, which was synthesized according to the reaction between plutonium dioxide with a purity of 99.5-99.7% by mass and vapors of carbon tetrachloride at 600°C.

The reaction vessel was a spectrophotometric quartz cuvette (l = 1 cm), equipped with a hermetic teflon plug with a loading device and central inlet for the gas pipe. The temperature of the melt in the cuvette was maintained with ±2°C. The gas mixtures of chlorine and hydrogen chloride was produced in a steel gas holder. The partial pressure of chlorine in them was varied from $2 \cdot 10^3$ to $1 \cdot 10^5$ Pa with an accuracy no lower than ±3%.

The experimental procedure consisted of the following. Plutonium trichloride, in an amount such that the summary plutonium concentration was $(1.0\text{-}1.4) \cdot 10^{-1}$ M, was introduced into the melt through the loading device. Then a gas mixture of chlorine and hydrogen chloride of a definite composition was bubbled through the melt along the gas pipe. The absorption spectrum of the melt was periodically recorded in the range from 12,000 to 4000 cm^{-1}. treatment of the melt with the gas mixture was continued until a stable spectrum was obtained, which was evidence of the reaching of equilibrium in the system.

Results and Discussion

Figure 1 presents the absorption spectra of molten NaCl–2CsCl, containing equilibrium concentrations of tri- and tetravalent plutonium, obtained at various values of the partial pressure of chlorine in the gas mixture. When the partial pressure of chlorine is lowered the intensity of the absorption band with maximum at 7200 cm^{-1}, belonging to trivalent plutonium [6, 7], increases, while the intensity of the absorption band with maximum at 5300 cm^{-1}, assigned to the spectrum of tetravalent plutonium [6, 7], decreases, i.e., there is a

TABLE 1. Values of the Molar Extinction Coefficients of Trivalent ε_3 and Tetravalent ε_4 Plutonium in Molten NaCl-2CsCl

, liters/(mole·sec)	T, °C				
	550	600	650	700	750
ε_3 (ν = 7200 cm^{-1})	4,3±0,1	4,4±0,1	4,5±0,2	4,6±0,1	4,8±0,1
ε_4 (ν = 5300 cm^{-1})	4,7±0,3	4,9±0,3	5,2±0,4	5,4±0,5	5,7±0,5

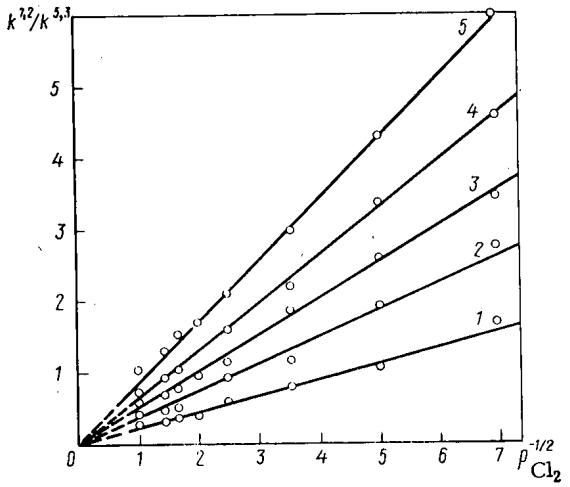

Fig. 2. Graphical verification of Eq. (8) for 550 (1), 600 (2), 650 (3), 700 (4), 750°C (5).

reduction of tetravalent plutonium to the trivalent state. The presence of isobestic points at 6000 and 7700 cm^{-1} is evidence of the presence in the melt of only two spectrally different forms of plutonium. It is evident that the absorption band at 5300 cm^{-1} is practically free of the interference of other bands and can be used for analytical purposes. However, it does not seem possible to determine the molar extinction coefficient for it directly, since melts containing only tetravalent plutonium cannot be obtained on account of its insufficient stability.

We established that in melts containing only trivalent plutonium, for the absorption band at 7200 cm^{-1} the Beer–Lambert law is fulfilled at optical densities from 0 to 1.2. The dependence of the change in the molar extinction coefficient on the temperature for the absorption band of trivalent plutonium at 7200 cm^{-1} (ε_3) is cited in Table 1. For melts containing equilibrium mixtures of tri- and tetravalent plutonium, the contribution of the latter to the absorption at 7200 cm^{-1} is unknown.

The indices of absorption of a melt containing equilibrium concentrations of tri- and tetravalent plutonium at 7200 and 5300 cm^{-1}, respectively, are equal to

$$k^{7.2} = \varepsilon_3 C_{Pu(III)} + \varepsilon'_4 C_{Pu(IV)}; \quad (3)$$

$$k^{5.3} = \varepsilon_4 C_{Pu(IV)}, \quad (4)$$

where $k^{7\cdot2}$ and $k^{5\cdot3}$ are the indices of absorption of the melt at 7200 and 5300 cm^{-1}, respectively, cm^{-1}, $C_{Pu(III)}$ and $C_{Pu(IV)}$, equilibrium concentration of tri- and tetravalent plutonium, M, ε_3 and ε'_4, molar extinction coefficients of tri- and tetravalent plutonium at 7200 cm^{-1}, liters/(mole·cm), ε_4, molar extinction coefficient of tetravalent plutonium at 5300 cm^{-1}, liters/(mole·sec).

Dividing Eq. (3) by Eq. (4), we obtain

$$k^{7.2}/k^{5.3} = \varepsilon'_4/\varepsilon_4 + \varepsilon_3 C_{Pu(III)}/\varepsilon_4 C_{Pu(IV)}. \quad (5)$$

TABLE 2. Dependence of the Ratio of the Equilibrium Concentrations of Tri- and Tetravalent Plutonium on the Relative Partial Pressure of Chlorine at Various Temperatures in Molten NaCl–2CsCl

$\lg P_{Cl_2}$	550° C			600° C			650° C			700° C			750° C		
	n	$\frac{C_3}{C_4}$	$\lg \frac{C_3}{C_4}$	n	$\frac{C_3}{C_4}$	$\lg \frac{C_3}{C_4}$	n	$\frac{C_3}{C_4}$	$\lg \frac{C_3}{C_4}$	n	$\frac{C_3}{C_4}$	$\lg \frac{C_3}{C_4}$	n	$\frac{C_3}{C_4}$	$\lg \frac{C_3}{C_4}$
−1,698	3	1,74	0,24	2	2,46	0,39	3	3,88	0,59	2	5,25	0,72	3	7,58	0,88
−1,397	4	1,07	0,03	3	1,55	0,19	4	2,46	0,39	3	3,31	0,52	4	5,02	0,70
−1,096	4	0,72	−0,14	3	1,15	0,06	4	1,78	0,25	3	2,51	0,40	4	3,47	0,54
−0,795	3	0,54	−0,27	2	0,81	−0,09	3	1,26	0,10	2	1,70	0,23	3	2,57	0,41
−0,602	2	0,49	−0,31	—	—	—	2	0,95	−0,02	—	—	—	2	2,00	0,30
−0,444	2	0,36	−0,45	2	0,54	−0,27	2	0,79	−0,10	2	1,20	0,08	2	1,70	0,23
−0,310	2	0,34	−0,47	2	0,45	−0,35	2	0,76	−0,12	2	0,94	−0,04	2	1,41	0,15
0,000	2	0,25	−0,60	2	0,35	−0,45	2	0,56	−0,25	2	0,74	−0,13	2	1,10	0,04

Note. $C_3 = C_{Pu(III)}$, $C_4 = C_{Pu(IV)}$, n is the number of experimental points.

TABLE 3. Values of the Arbitrary Equilibrium Constant and the Arbitrary Standard Gibbs Energy of the Reaction $Pu^4 + Cl^- \rightleftarrows Pu^{3+} + 1/2\ Cl^2$ in Molten NaCl–2CsCl

T, °C	n*	Exponent of P_{Cl_2}	$\lg K$*	K*	ΔG*, kJ/mole
550	22	0,50±0,02	−0,64±0,06	0,23±0,03	+10,0±0,9
600	16	0,52±0,02	−0,39±0,06	0,41±0,05	+6,5±1,0
650	22	0,51±0,01	−0,24±0,05	0,58±0,07	+4,2±0,9
700	16	0,51±0,01	−0,12±0,05	0,79±0,09	+2,2±0,9
750	22	0,50±0,01	0,00±0,05	1,00±0,12	0±1

*n is the number of experimental points.

From the function for the arbitrary equilibrium constant of reaction (1)

$$K^* = \frac{C_{Pu(III)}}{C_{Pu(IV)}} P_{Cl_2}^{1/2} \tag{6}$$

we find the ratio of the equilibrium concentrations of tri- and tetravalent plutonium:

$$\frac{C_{Pu(III)}}{C_{Pu(IV)}} = K^* P_{Cl_2}^{-1/2}, \tag{7}$$

where K* is the arbitrary equilibrium constant of reaction (1); P_{Cl_2} represents the relative partial pressure of chlorine in the gas phase (related to standard pressure $1.01 \cdot 10^5$ Pa).

Substituting function (7) into Eq. (5), we arrive at the expression

$$k^{7.2}/k^{5.3} = \varepsilon_4'/\varepsilon_4 + \varepsilon_3/\varepsilon_4 K^* P_{Cl_2}^{-1/2}, \tag{8}$$

which permits a determination of the ratio of the molar extinction coefficients of tetravalent plutonium at 7200 and 5300 cm^{-1} as the segment intercepted on the y axis by a straight line constructed in a plot of $k^{7.2}/k^{5.3}$ versus $P_{Cl_2}^{-1/2}$.

Graphical verification of Eq. (8) showed (Fig. 2) that the ratio $k^{7.2}/k^{5.3}$ is proportional to the quantity $P_{Cl_2}^{-1/2}$, while the ratio $\varepsilon'_4/\varepsilon_4$ is equal to zero. Consequently, the contribution of tetravalent plutonium to the absorption of the melt at 7200 cm^{-1} can be neglected.

The summary plutonium concentration in the melt C_{Pu} as a sum of the equilibrium concentrations of tri- and tetravalent plutonium can be expressed by the equation

$$C_{Pu} = k^{7.2}/\varepsilon_3 + k^{5.3}/\varepsilon_4, \tag{9}$$

TABLE 4. Values of the Arbitrary Formal Redox Potential of the Couple Pu^{4+}/Pu^{3+} (relative to a chloride reference electrode)

Solvent	$(E_{Pu^{4+}/Pu^{3+}} - E_{Cl_2/Cl^-})$,				
	550° C	600° C	650° C	700° C	750° C
LiCl – KCl (40 mole %) *	0,023	0,046	0,072	0,096	0,120
LiCl – CsCl (55 mole %) †	–0,090	–0,060	–0,024	0,010	0,042
NaCl – CsCl (66 mole %) ‡	–0,110	–0,084	–0,056	–0,028	0,000

*Calculation according to the data of [1].
†Calculation according to the data of [2].
‡The present work.

from which

$$\varepsilon_4 = k^{5.3}/(C_{Pu} - k^{7.2}/\varepsilon_3). \tag{10}$$

The values of ε_4 (see Table 1), calculated according to Eq. (10), as well as the values of ε_3, were used to find the equilibrium concentrations of tri- and tetravalent plutonium in the study of the equilibrium of reaction (1).

The arbitrary equilibrium constant of reaction (1) was calculated from the expression obtained after taking the logarithm of Eq. (7):

$$\lg \frac{C_{Pu(III)}}{C_{Pu(IV)}} = \lg K^* - 1/2 \lg P_{Cl_2}. \tag{11}$$

Table 2 presents the experimental values of $C_{Pu(III)}/C_{Pu(IV)}$ as a function of the relative partial pressure of chlorine and the temperature, while Table 3 presents the values of the exponent of P_{Cl_2} and the arbitrary equilibrium constant of reaction (1), calculated by the method of least squares according to Eq. (11) and the data of Table 2. From Table 3 it is evident that the relative partial pressure of chlorine in the gas phase enters into the expression for the arbitrary equilibrium constant of reaction (1) to the exponent 0.5.

The temperature dependence of the arbitrary equilibrium constant of reaction (1) is satisfactorily described by the equation

$$\lg K^* = 2.52 - 2570T^{-1} \pm 0.05. \tag{12}$$

Using Eq. (12) we calculated the arbitrary formal redox potential of the couple Pu^{4+}/Pu^{3+} relative to a chloride reference electrode:

$$E^*_{Pu^{4+}/Pu^{3+}} = \frac{2.3RT}{nF} \lg K^* = -0.51 + 5.0 \cdot 10^{-4}T \pm 0.01 \text{ V} \tag{13}$$

and the change in the arbitrary standard Gibbs energy (ΔG^*_1) for reaction (1) in molten NaCl–2CsCl:

$$\Delta G^*_1 = -2.3RT \lg K^* = 49 - 4.8 \cdot 10^{-2}T \pm 1, \text{ kJ/mole.} \tag{14}$$

From Eq. (14) we found the changes in the entropy and thermal effect of reaction (1)

$$\Delta S^* = 48 \pm 2 \text{ J/mole} \cdot \text{deg K};$$
$$\Delta H^* = 49 \pm 2, \text{ kJ/mole.}$$

Earlier [8] the emf method was used to find ΔG^* in the formation of dilute solutions of trivalent plutonium, which for molten NaCl–2CsCl is equal to

$$\Delta G^*_{PuCl_3} = -1.09 + 3.11 \cdot 10^{-4}T, \text{ MJ/mole.} \tag{15}$$

Therefore we can calculate ΔG^* in the formation of dilute solutions of tetravalent plutonium. It is made up of ΔG_{PuCl_3} and ΔG^*_1 of reaction (1), taken with the opposite sign, i.e.,

$$\Delta G^*_{PuCl_4} = \Delta G^*_{PuCl_3} + (-\Delta G^*) = -1.14 + 3.6 \cdot 10^{-4}T, \text{ MJ/mole.} \tag{16}$$

Using the expression cited in the work of Benz [9] for the change in the standard Gibbs energy in the formation of liquid plutonium tetrachloride from the elements

$$\Delta G^0_{PuCl_4} = -0.89 + 2.1 \cdot 10^{-4} T, \text{ MJ/mole,} \quad (17)$$

and Eq. (16), we calculated the energy of mixing of liquid plutonium tetrachloride with molten NaCl–2CsCl:

$$\Delta G_{mix} = \Delta G^*_{PuCl_4} - \Delta G^0_{PuCl_4} = -0.25 + 1.5 \cdot 10^{-4} T \text{ MJ/mole.} \quad (18)$$

From the results cited it follows that the stability of the tetravalent state of plutonium in molten NaCl–2CsCl, just as in molten LiCl–KCl [1] and LiCl–CsCl [2], decreases with increasing temperature, since the equilibrium constant of reaction (1) increases. In the series of solvents LiC – KCl, LiCl – CsCl and NaCl – 2CsCl, the arbitrary formal redox potential of the couple Pu^{4+}/Pu^{3+} in the interval 550-750°C is displaced in the negative direction (Table 4), which is evidence of an increase in the stability of tetravalent plutonium in this solvent series.

The mixing of liquid plutonium tetrachloride with molten NaCl–2CsCl is an exothermic process, evidently due to the formation of chloride complexes of tetravalent plutonium of the $PuCl_6^{2-}$ type in the melt [10].

APPENDIX

The contour of the spectrum of tetravalent plutonium was calculated according to the equation

$$k^{\nu i}_{Pu(IV)} = \frac{k^{\nu i} - k^{7,2}\varepsilon_3^{\nu i}\varepsilon_3^{-1}}{C_{Pu} - k^{7,2}\varepsilon_3^{-1}} C_{Pu}, \quad (19)$$

which was obtained in simultaneous solution of the following functions:

$$k^{\nu i} = \varepsilon_3^{\nu i} C_{Pu(III)} + \varepsilon_4^{\nu i} C_{Pu(IV)}; \quad (20)$$

$$C_{Pu} = C_{Pu(III)} + C_{Pu(IV)}; \quad (21)$$

$$C_{Pu(III)} = k^{7,2}\varepsilon_3^{-1}; \quad (22)$$

$$k^{\nu i}_{Pu(IV)} = \varepsilon_4^{\nu i} C_{Pu}, \quad (23)$$

where $k^{\nu i}$ is the index of absorption of a melt containing equilibrium concentrations of tri- and tetravalent plutonium at a set partial pressure of chlorine in the gas phase at the i-th wave number, cm^{-1}, $\varepsilon_3^{\nu i}$, $\varepsilon_4^{\nu i}$, molar extinction coefficients of tri- and tetravalent plutonium at the i-th wave number, liters/(mole·cm), C_{Pu}, $C_{Pu(III)}$, $C_{Pu(IV)}$, summary and equilibrium concentrations of tri and tetravalent plutonium in the melt, M, $k^{\nu i}_{Pu(IV)}$, index of absorption of a melt containing only tetravalent plutonium with concentration C_{Pu}.

LITERATURE CITED

1. G. Landresse and G. Duyckaerts, Inorg. Nucl. Chem. Lett., 10, No. 8, 675 (1974).
2. G. Landresse and G. Duyckaerts, ibid., No. 11, 1051.
3. M. V. Smirnov, Electrode Potentials in Molten Chlorides [in Russian], Nauka, Moscow (1973).
4. V. V. Gushchin and V. M. Barinov, Prib. Tekh. Eksp., 3, 279 (1972).
5. M. V. Smirnov, V. P. Stepanov, and T. Mukatov, in: Transactions of the Institute of Electrochemistry [in Russian], Vol. 16, Izd. UNTs Akad. Nauk SSSR, Sverdlovsk (1972), p. 16.
6. Y. Swanson, J. Phys. Chem., 68, 438 (1964).
7. S. K. Vavilov et al., in: Summaries of Reports at the Fifth All-Union Conference on Physical Chemistry and Electrochemistry of Molten Salts [in Russian], Part 1, Izd. UNTs Akad. Nauk SSSR, Sverdlovsk (1973), p. 67.
8. V. M. Silin and O. V. Skiba, Preprint of the V. I. Lenin Scientific-Research Institute of Atomic Reactors P-118 (1971).

9. R. Benz, J. Inorg. Nucl. Chem., 24, 1191 (1962).
10. Yu. A. Barbanel' and V. R. Klokman, Radiokhimiya, 18, No. 5, 699 (1976).

DETERMINATION OF THE COEFFICIENTS OF SEPARATION OF BORON ISOTOPES IN THE DISTILLATION OF BCl_3 IN THE TEMPERATURE RANGE 278-438°K

A. S. Aloev, V. A. Kaminskii,
A. G. Kudziev, and R. Sh. Metreveli

UDC 621.039.33

The production of boron isotopes is an important scientific and technical problem, therefore, it is necessary to select the most economically efficient method of separation of these isotopes. Among the methods suitable for this purpose, researchers have always been attracted by the distillation of BCl_3, thanks to the cheap and readily available initial raw material and the simple technological formulation of the process. The deciding factor in the question of the use of the above-mentioned method is the value of the coefficient of separation and its temperature dependence. Despite a number of investigations [1-4], this problem has not received a final resolution, especially for the region of increased temperature. In view of this, in the present work an investigation was made of the temperature dependence of the coefficient of enrichment of two mutually supplementing and controlling methods. One of them permitted direct measurement of the difference of the saturated vapor pressures of isotopically substituted varieties of BCl_3, while the other permitted direct estimation of the separation achieved on the column in the process of fractionation of BCl_3, all the way up to a temperature close to the critical point.

Determination of the Coefficient of Enrichment by a Differential Method. For a measurement of the coefficient of enrichment we used the setup whose scheme is presented in Fig. 1. A copper block 60 mm in diameter and 70 mm high with two working chambers with volumes of 10 cm^3 each was placed in a vessel with a boiling temperature-controlling liquid, the vapors of which were condensed in a condenser. The boiling point of the temperature-controlling liquid was determined by the air pressure in the cylinder. On account of the rather large volume of the cylinder and the constant conditions of boiling, the pressure in the thermostat system and the boiling point of the temperature controlling liqiud were preserved with high accuracy in the process of the experiment. The pressure difference was measured with the aid of a brass mercury differential manometer and a KM-6 cathetometer. The use of mercury, despite its great density, was due to the necessity of minimizing the solubility of the gas in the manometric liquid, especially in the high-pressure region.

The differential manometer was placed in a warming jacket together with the tubes in order to exclude condensation of BCl_3 vapors in them. Up to 300°K the absolute pressure was measured with mercury manometers, above it, the pressure was determined according to the curve of the dependence of the saturated vapor pressure of BCl_3 on the temperature, considering the temperature of the copper block of the thermostat. The accuracy of the measurement of the latter was ensured by the duplicate measurements of the temperature and pressure of the boiling temperature-controlling liquid.

The boron trichloride used in this work (both enriched with ^{10}B to 86.5% and of the natural isotopic composition) was produced from BF_3 according to the reaction

$$BF_3 + AlCl_3 - BCl_3 + AlF_3.$$

Its purification was achieved by several vacuum redistillations at 190 and 210°C, followed by distillation of BCl_3 on a packed glass column 15 mm in diameter and 1 mm long at the normal boiling point. The temperature dependence of the saturated vapor pressure of purified BCl_3 of the natural isotopic composition coincided highly accurately with the published data, which was a criterion of the absence of impurities that might have influenced the results of the measurements.

Translated from Atomnaya Énergiya, Vol. 49, No. 2, pp. 98-101, August, 1980. Original article submitted June 26, 1979, revision submitted January 24, 1980.

 0038-531X/80/4902-0536$07.50

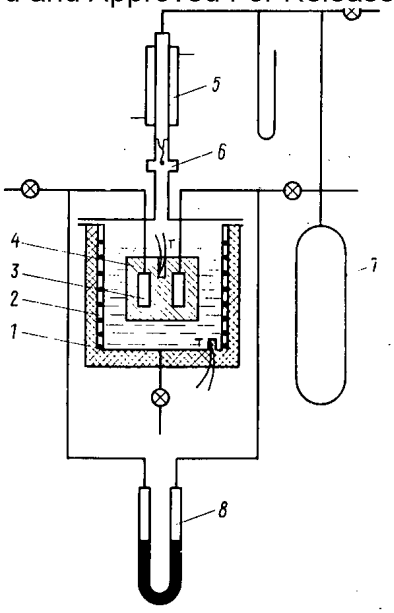

Fig. 1. Scheme of thermostat: 1) thermal insulation; 2) casing with heater) 3) working chambers; 4) copper block; 5) condenser; 6) viewing window; 7) cylinder of manostat; 8) differential manometer.

TABLE 1. Values of the Coefficient of Enrichment at Various Temperatures, Determined by a Differential Method

Temp., °K	p_2, 10^{-5} Pa	Δp, Pa	ε	Rel. error, %
278	0,758	188,9	0,0036	4,3
285	0,971	203,5	0,0030	4,0
300	1,714	255,4	0,0021	3,3
313	2,527	268,2	0,0014	4,8
338	4,852	295,3	0,0008	3,7
350	6,469	305,9	0,0006	3,4
393	16,072	325,8	0,0002	2,9

To ascertain equality of the temperatures of the two working chambers, control experiments were conducted at 285 and 393°K, in which both chambers were loaded with boron trichloride of the natural isotopic composition. In this case, with an accuracy within 0.01 mm, no difference was noted in the levels of mercury in the differential manometer.

The results of the experiments are presented in Table 1. The pressure difference Δp was determined according to a large number of measurements, in the process of which the samples in the chambers changed places. The standard deviation in the values of Δp was 3.1 Pa.

When nonmonoisotopic samples are used, according to [5, 6], the coefficient of enrichment is expressed by the formula

$$\varepsilon = \frac{\Delta p}{p_2^0 (C_{enr} - C_n)} \left(1 + \frac{Bp_1^0}{RT}\right), \quad (1)$$

obtained with the assumption of ideality of the liquid phase and equality of the second virial coefficients of isotopically substituted molecules, which is fulfilled in practice for all the isotopes, with the exception of hydrogen and helium isotopes. Here p_1^0 and p_2^0 are the saturated vapor pressures of the pure components, C_{enr} and C_n are the concentrations of enriched and normal samples, B is the second virial coefficient. The unknown quantities p_1^0 and p_2^0 entering into this formula for BCl_3 can be replaced by the corresponding values of the absolute pressure of samples of the enriched and natural compositions with an accuracy within 0.06%, after which the formula for calculation of ε takes the following final form:

$$\varepsilon = \frac{\Delta p}{p_2 (C_{enr} - C_n)} \left(1 + \frac{Bp_1}{RT}\right). \quad (2)$$

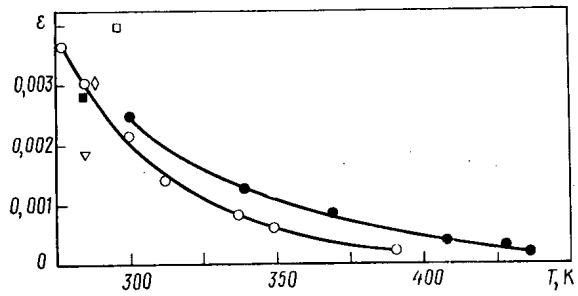

Fig. 2. Dependence of the coefficient of enrichment on the temperature: ○) differential method, ●) method of fractionation; ▽, ◇, □, ■) data of [1-4], respectively.

In the calculation of the second virial coefficient we used the force constants of interaction for the Lennard-Jones potential, cited in [7]. Within the investigated temperature region the value of B remains negative, so that the correction for nonideality of the gas phase led to a decrease in the coefficients of enrichment. Within the entire investigated temperature region, the compound $^{11}BCl_3$ proved more volatile. As can be seen from Table 1, the coefficient of separation decreases separation with increasing temperature. It should be noted that the increase in the relative error in the transition to the temperature 313°K is caused by a change in the method of determining the absolute pressure.

Determination of the Coefficient of Enrichment on a Column. For the determination of the coefficient of separation of boron isotopes in the fractionation of BCl_3 at 300-438°K, we used a column with inner diameter 15 mm and length of the packed portion 1.5 m, filled with packing of segments of a triangular wire spiral 2.2 × 2 mm. The column had an evaporator with a 500-cm^2 capacity with an inner electric heater. Together with the evaporator, it was surrounded by a vacuum jacket with a compensating electric heating element situated above it. The condenser was cooled with flowing water, its upper part was connected to a cylinder in which a set pressure of argon, determining the temperature of the process, was maintained. On the column there was a device for measuring the irrigation flux. The column was made of stainless steel, while the tubes of the level gauge and flow meter were made of thick-walled glass, which permitted work up to the critical pressure $3.87 \cdot 10^6$ Pa.

The small values of the separation factor and their substantial decrease with increasing temperature excluded the possibility of use of methods of determination of ε according to an analysis of the dependence of the concentration on the collection and according to the kinetics of the change in the composition in the period of a nonsteady-state process. Therefore, all the experiments were conducted with complete irrigation and a fixed evaporator power of 33 W.

For a determination of the temperature dependence of the coefficient of enrichment according to the values of the equilibrium separation factor obtained as a result of the experiments, we used the values of the height of an equivalent theoretical plate (HETT), calculated by the method of [8, 9]. In view of the small column diameter and the large values of the irrigation density, the number of zones of complete statis λ can be assumed equal to zero, and the following formula can be used for the determination of the HETT:

$$\text{HETT} = i\left[\frac{q_r}{6\pi D_g}\left(1-\frac{r_0^2}{R^2}\right)+\frac{q_c}{4\pi D_g}\left(1-\frac{1}{2}\frac{r_0^2}{R^2}\right)+\frac{11}{40}\frac{\Gamma m}{D_l}\right], \qquad (3)$$

which in the region of the loads used leads to an error of no more than 10%. For packing of segments of a triangular spiral 2.2 × 2.0 mm, the number of elements in a unit volume N = 100, equivalent radius of the channel R = 0.7 mm, and the average value of the sine of the angle of inclination of the elements of the packing i = 0.9. The remaining quantities in this formula are: the volume flows of gas in the ring and central regions of the channel q_r and q_c, the radius of the central region r_0, the liquid flow rate Γ, and the film thickness m, depend on the load and the working conditions (temperature and pressure in the column) [10]. The formulas for their calculation and the sequence of operations were described in detail in [8], the diffusion coefficients D_g and D_l were calculated according to the formulas of [11].

The results of a calculation of the HETT and the experimental values of the equilibrium separation factor are presented in Table 2. It should be noted that work at a fixed power of the evaporator led to an increase in the load with increasing temperature on account of a

TABLE 2. Experimental Values of the Equilibrium Separation Factor and Calculated Values of the HETT for Various Temperatures

Temp., °K	Pressure in coln. 10^{-5} Pa	Irrigation density, (kg/(m^2·sec)	Calc. value of HETT, cm	No. of stages in column	Equilibrium separation factor, q_0
300	1,71	0,94	1,90	79	1,215
340	5,05	1,00	1,94	77	1,105
370	10,10	1,13	2,0	75	1,065
410	20,77	1,46	2,2	68	1,032
430	28,3	1,88	2,3	60	1,019
438	31,8	1,96	2,7	56	1,013

decrease in the heat of vaporization. In this case, the increase in irrigation density determined a more rapid increase in the HETT than the competing influence of the actual temperature of the process on the HETT.

The dependence of the coefficient of enrichment on the temperature obtained on the column is presented in Fig. 2. Since ε is determined by the expression ε is determined by the expression $\varepsilon = h \ln q_0/H$ (where h = HETT, while H is the height of the column), the absolute error of Δε was calculated according to the formula

$$\Delta\varepsilon = \frac{\ln q_0}{H}\Delta h + \frac{h \ln q_0}{H^2}\Delta H + \frac{h}{H q_0}\Delta q_0. \quad (4)$$

In the entire region of measurements, Δε did not exceed ±0.0005.

DISCUSSION OF RESULTS

As can be seen from Fig. 2, the results of the two methods are in rather good agreement. Moreover, in the region of the normal boiling point of BCl_3, the two methods gave results close to the data of other authors, which also indicates correctness of the methods used, including the new method of estimation of ε according to the calculated value of the HETT. However, even if we refrain from estimating ε, the dependence of the equilibrium separation factor obtained on the column unambiguously indicates a deterioration of the separation with increasing temperature and a virtual disappearance of the separating effect at a temperature close to the critical value. This conclusion is correct despite the large negative error in the region close to the critical temperature.

The temperature dependence of the coefficient of enrichment obtained is evidence of the inadvisability of using the method of fraction of BCl_3 for the production of boron isotopes.

LITERATURE CITED

1. M. Green and G. Martin, Trans. Faraday Soc., 48, No. 353, 416 (1952).
2. F. Muhlenpfordt et al., in: Proc. Int. Symp. Isotope Separation, Amsterdam (1958), p. 408.
3. M. Ya. Kats, G. M. Kukavadze, and R. L. Serdyuk, Zh. Teor. Fiz., 26, No. 12, 2744 (1956).
4. N. N. Sevryugova, O. V. Uvarov, and N. M. Zhavoronkov, At. Energ., No. 4, 113 (1956).
5. A. M. Rozen, Theory of the Separation of Isotopes in Columns [in Russian], Atomizdat, Moscow (1960).
6. A. V. Borisov, Candidate's Dissertation, Moscow State Univ., Moscow (1966).
7. I. F. Golubev and N. E. Gnezdilov, Viscosity of Gas Mixtures [in Russian], Goskomiteta Standartov, Moscow (1971).
8. V. A. Kaminskii and N. A. Giorgadze, Isotopenpraxis, 9, No. 1, 1 (1973).
9. V. A. Kaminskii and N. A. Giorgadze, ibid., 14, No. 9, 321 (1978).
10. V. A. Kaminskii and N. A. Giorgadze, Zh. Prikl. Khim., 51, No. 10, 2266 (1978).
11. J. O. Hirschfelder et al., Molecular Theory of Gases and Liquids, Wiley (1964).

POSSIBILITIES OF PROTON-ACTIVATION ANALYSIS FOR DETERMINING THE CONTENT OF ELEMENTS FROM SHORT-LIVED RADIONUCLIDES

V. A. Muminov, S. Mukhammedov, and A. Vasidov

UDC 543.53

The proton-activation method of analysis used when determining trace elements in materials from their nuclear properties is not suitable for instrumental neutron-activation analysis [1-3] or for investigating the elementary composition of the various parts of samples [4]. For multielement analysis, we mainly use relatively long-lived radionuclides [5-7]. We can develop highly sensitive and rapid methods of activation analysis using charged particles on the basis of nuclear reactions that form radionuclides with halflives $T_{1/2} <$ 1000 sec. However, few articles have so far been published on methods of determining elements from short-lived radionuclides.

Reference [8] indicates the possibilities of determining eight elements with $Z \geq 34$ in 13 matrices by the active products of reactions with $1 \leq T_{1/2} \leq 60$ sec. To determine elements with concentrations $10^{-7} - 10^{-10}$ g/g, we must often use radionuclides with $T_{1/2} >$ 1 min [9]. Rapid methods of determining nitrogen [10-12], carbon, magnesium, silicon [13], and sulfur [14-15] have been developed. Nevertheless, there have been very few articles published up to the present that investigate the possibilities of determining elements by the use of radionuclides with $T_{1/2}$ = 10-1000 sec that arise out of reactions based on protons. In a previous article [16], we estimated the sensitivity of determining sulfur, chromium, nickel, copper, zinc, and molybdenum by the proton-activation method, which proved to be comparable with the sensitivity of other nuclear-physical methods. In the present article, we assess the possibilities of determining 20 elements by measuring the emission of γ quanta after activation by protons with energies E_p = 12 MeV, and we also give the results of investigations of nondestructive, rapid, and selective methods of analysis.

In the nuclide that is most widely distributed in nature, the reaction has a large section, and in this instance a radionuclide with $T_{1/2} >$ 1000 sec is induced. In this case, we are not considering nuclides with a natural occurrence of less than 1%, radionuclides with relative intensities of γ quanta of less than 1%, or elements which in their reactions with protons do not form radionuclides with $T_{1/2}$ = 10-1000 sec. Determining these elements by proton-activation methods of analysis is of particular interest, since it is especially difficult to determine them by any other means, in view of the unsuitable activation characteristics of the reaction. We therefore, in the present article, compare the analytical parameters of the various nuclear methods of analysis.

Experimental Technique. In our experiment, we used a 150-cm cyclotron of the Institute of Nuclear Physics of the Academy of Sciences of the Uzbek SSR accelerating protons up to an energy of 18 MeV. The samples were irradiated with the aid of a semiautomatic installation equipped with a pneumatic rabbit (Fig. 1). The sample, held in a Duralumin target holder, is fed to the position of irradiation along a polyethylene tube by the action of compressed air. The target holder is stopped in a small chamber partitioned off from the main chamber by a thin nickel foil ($\sim$ 20 μm). The center of the cylindrical target holder coincides with that of a 10-mm collimator. The former is pushed against a rubber seal and limit switch by the action of the compressed air. The limit switch then cuts off the supply of compressed air. The beam is first conducted to a refrigerated "Shutter" which, after receiving the target holder, is opened by an electromagnet on the command of the limit switch to start the irradiation of the sample. The exposure time is set with the aid of a relay. The small chamber is insulated from the large chamber by Teflon. The target holder is served by a Faraday cylinder. After irradiation of the samples, the shutter closes and the target holder is transported by compressed air to the position at which the radioactivity is measured. The

Translated from Atomnaya Énergiya, Vol. 49, No. 2, pp. 101-105, August, 1980. Original article submitted September 28, 1979.

 0038-531X/80/4902-0540$07.50

TABLE 1. Emissions of γ Quanta Y_γ [10^6 quanta (sec· μA)] and Sensitivity in Determining Elements at E_p = 10 MeV [10^{-9} g/(g·μA^{-1})]

Determined element and product of reaction	Energy and intensity of quanta	Y_γ at E_p, MeV							Sensitivity of analysis*
		6	7	8	9	10	11	12	
$^{10}B \rightarrow {}^{10}C$	0,718(100)			1,6	3,3	6,3	9,8	15,2	2600
$^{13}C \rightarrow {}^{13}N$	0,510(200)	150	270	340	400	430	470	500	3,70
$^{14}N \rightarrow {}^{11}C$	0,510(200)	480	720	1760	2560	3400	4160	5000	0,5
$^{14}N \rightarrow {}^{14}O$	2,312(99)			197	410	650	950	1144	2,5
$^{16}O \rightarrow {}^{13}N$	0,510(200)		480	960	1400	1800	2200	2600	0,9
$^{23}Na \rightarrow {}^{23}Mg$	0,439(9,1)	11	30	42	64	100	130	174	160
$^{52}Cr \rightarrow {}^{52m}Mn$	1,434(98)			910	2100	3480	5200	7120	0,5
$^{60}Ni \rightarrow {}^{60}Cu$	1,332(88)		42	92	183	325	570	935	5,1
$^{64}Zn \rightarrow {}^{64}Ga$	0,991(43)					21	40	65	79
$^{80}Se \rightarrow {}^{80}Br$	0,612(7)	91	136	176	214	250	280	308	6,6
$^{79}Br \rightarrow {}^{79m}Kr$	0,127(30)	5,5	15	28	44	66	97	134	250
$^{81}Br \rightarrow {}^{81m}Kr$	0,190(65)		6	21	46	78	110	147	200
$^{89}Y \rightarrow {}^{89m}Zr$	0,578(100)			80	180	300	440	595	5,5
$^{90}Zr \rightarrow {}^{90m}Nb$	0,1225(71)				16	38	68		420
$^{92}Mo \rightarrow {}^{92}Tc$	0,773(97)					0,6	30	68	760
$^{112}Cd \rightarrow {}^{112}In$	0,6174(27,6)			39,6	88	139	198	260	12
$^{116}Sn \rightarrow {}^{116}Sb$	1,293(88)	4,0	9,5	16,8	25	35	41	59	47
$^{118}Sn \rightarrow {}^{118}Sb$	1,230(100)			9,8	14	18,6	24	29,0	89
$^{120}Sn \rightarrow {}^{120}Sb$	1,171(2)			6,8	10,8	14,4	17,4	21,5	110
$^{134}Ba \rightarrow {}^{134}La$	0,6049(100)			0,1	0,3	0,6	1,2	2,1	2600
$^{136}Ba \rightarrow {}^{136}La$	0,8185(2,5)			0,1	0,3	0,5	1,1	2,1	3200
$^{139}La \rightarrow {}^{139m}Ce$	0,754(93)			9,2	22	43	78	128	370
$^{141}Pr \rightarrow {}^{141m}Nd$	0,755(92)				0,2	18	25	75	89
$^{142}Nd \rightarrow {}^{142}Pm$	1,575(3,3)			0,1	0,3	0,6	1,2	2,0	2600
$^{180}W \rightarrow {}^{180}Re$	0,902(99,4)					0,6	2,0	4,8	2670

*The sensitivity is expressed as the quantity of the element being determined per 1 g of the material at which irradiation forms a radionuclide with an activity of 1000 γ quanta/min ($T_{1/2} \leq 1$ min) and 100 γ quanta/min ($T_{1/2} > 1$ min).

time needed to transport the samples to the measurement station, a distance of 15 mm, is 1-5 sec. Behind the shutter on the same side as the sample there is a drum with twelve holes for selecting absorbers. The drum can be rotated by a motor. The energy of the protons is reduced with the aid of aluminum absorbers. In view of the fact that at proton energies > 12 MeV a large number of interfering reactions of the (p, 2n), (p, 3n), (p, pn), (p, d), etc. types take place, this energy was chosen as optimum. The charge on the Faraday cylinder was measured by a current integrator.

Various compounds of the experimental elements type CLDA served as target, being glued to the surface of the foil by a sticky suspension of polystyrene dissolved in dichlorethane [9]. This film was subjected to irradiation by a 0.01-0.3 μA beam of protons for 5-20 sec.

The activity of the radionuclides was measured with the aid of a semiconductor Ge(Li) detector with a working volume of 90 cm^3 connected to a multichannel AI-4096 analyzer. The energy resolution of the detector was not lower than 9 keV for the 1330 keV ^{60}Co line. The memory of the analyzer was divided into 16 groups of 256 channels, the information in the last group being accumulated to the extent that the first group is filled. We were thus able to measure the activity of 16 targets which facilitated our work with short-lived radionuclides. The detector was energy calibrated and the relative efficiency was measured with the aid of precision sources of γ quanta.

Discussing the Results. Depending upon the halflife of the nuclide, the films were irradiated either separately as one sample or as several samples by combining them in a stack. The emission of quanta from the thin targets can be found by employing the expression

$$Y_\gamma[E_p] = St_{rad}e^{\lambda t_{ref}}/[t_m f\varepsilon q\Delta x(1-e^{-\lambda t_{rad}})\times \times(1-e^{-\lambda t_m})]\ [\gamma\ \text{quanta}\cdot\text{cm}^2/(\text{sec}\cdot\mu\text{A}\cdot\text{mg})], \quad (1)$$

where S is the area of the photopeak in pulses, t_{rad}, t_m, t_{ref}, irradiation, measurement of radioactivity, and sample refrigeration times, respectivel, sec, ε, efficiency of the detector, f, proportion of the element being studied present in the target by weight, Δx, thickness of the target, mg/cm^2, q, accumulated charge, μC, λ, decay constant, sec^{-1}, the emissions of the thin targets are summated over an interval of thickness, the differences of the

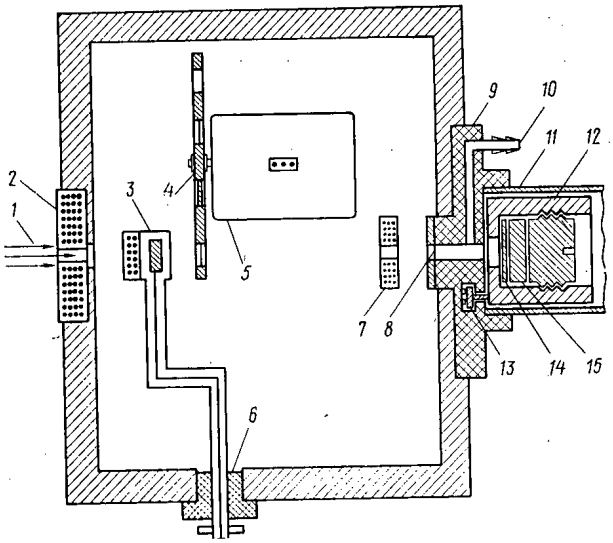

Fig. 1. Diagram of equipment with pneumatic rabbit for irradiating samples in a cyclotron: 1) beam of protons, 2, 7) graphite collinators; 3) refrigerated shutter; 4) drum with absorbers; 5) motor; 6) insulating ring; 8) nickel foil; 9) flange; 10) tube for feeding compressed air; 11) polyethylene tube and penumatic rabbit; 12) target holder; 13) limit switch; 14) monitor; 15) sample.

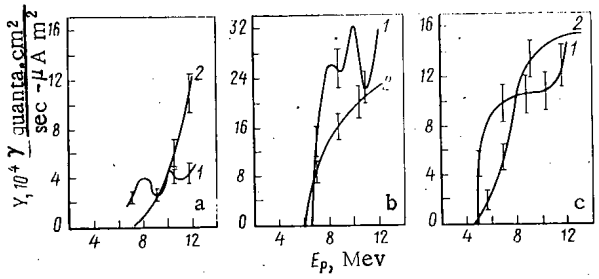

Fig. 2. Emissions from thin targets of certain radionuclides formed by the reactions (p, n); a) 1(×4): $^{10}Be \rightarrow {}^{10}C$, 2 (× 0.2): $^{124}Ba \rightarrow {}^{124}La$, b) 1: $^{14}N \rightarrow {}^{14}O$, 2: $^{25}Cr \rightarrow {}^{52m}Mn$, c) 1: $^{23}Na \rightarrow {}^{23}Mg$, 2: $^{112}Cd \rightarrow {}^{112}In$.

ranges corresponding to the initial energy of the protons and the range of the reaction, gives us the emission of γ quanta for a thick target:

$$Y_\gamma = \sum^{R} Y_\gamma [E_p] \Delta x \, [\gamma\text{- quanta}/(\text{sec} \cdot \mu\text{A})], \tag{2}$$

where R is the range of the particle, mg/cm². The relationship of Y_γ to proton energy is built up by using a "range–energy" table [17].

Figure 2 shows the emissions of γ quanta from the thin targets. Table 1 gives the emission of the more intense γ quanta from thick targets for the proton energy range 6-12 MeV. Table 1 also shows the sensitivity in determining elements at E_p = 10 MeV.

TABLE 2. Comparison of the Emissions of Radionuclides Formed by Activation of Elements by Various Nuclear Particles

Activation by protons*		Activation by fast neutrons†		Activation by slow neutrons ‡		Activation by γ quanta‡‡	
nuclide	Y, 10^6 decays. $sec^{-1} \cdot g^{-1}$	nuclide	Y, 10^6 decays. $sec^{-1} \cdot g^{-1}$	nuclide	Y, 10^6 decays. $sec^{-1} \cdot g^{-1}$	nuclide	Y, 10^6 decays. $sec^{-1} \cdot g^{-1}$
$^{10}B \rightarrow {}^{10}C$	57,3	$^{11}B \rightarrow {}^{11}Be$	14,6				
$^{14}N \rightarrow {}^{14}O$	6074,7	$^{14}N \rightarrow {}^{13}N$	6,3			$^{14}N \rightarrow {}^{13}N$	70
$^{23}Na \rightarrow {}^{23}Mg$	8459,1	$^{23}Na \rightarrow {}^{23}Ne$	1099	$^{23}Na \rightarrow {}^{24}Na$	6640	$^{23}Na \rightarrow {}^{22}Na$	0,0009
$^{52}Cr \rightarrow {}^{52m}Mn$	7102	$^{52}Cr \rightarrow {}^{52}V$	59,1	$^{50}Cr \rightarrow {}^{51}Cr$	82,4	$^{50}Cr \rightarrow {}^{49}Cr$	2
$^{60}Ni \rightarrow {}^{60}Cu$	2306,2	$^{58}Ni \rightarrow {}^{58}Co$	0,007	$^{64}Ni \rightarrow {}^{65}Ni$	428	$^{58}Ni \rightarrow {}^{57}Ni$	0,3
$^{64}Zn \rightarrow {}^{64}Ga$	287	$^{64}Zn \rightarrow {}^{64}Cu$	0,5	$^{68}Zn \rightarrow {}^{69m}Zn$	75,4	$^{64}Zn \rightarrow {}^{63}Zn$	50
$^{80}Se \rightarrow {}^{80}Br$	1316	$^{78}Se \rightarrow {}^{77m}Se$	150,7	$^{80}Se \rightarrow {}^{81}Se$	16900		
$^{79}Br \rightarrow {}^{79m}Kr$	1158	$^{79}Br \rightarrow {}^{78}Br$	134,8	$^{79}Br \rightarrow {}^{80}Br$	293000	$^{79}Br \rightarrow {}^{78}Br$	500
$^{81}Br \rightarrow {}^{81m}Kr$	639,5						
$^{89}Y \rightarrow {}^{89m}Zr$	1579	$^{89}Y \rightarrow {}^{89m}Y$	270,6	$^{89}Y \rightarrow {}^{90}Y$	932	$^{89}Y \rightarrow {}^{88}Y$	0,04
$^{90}Zr \rightarrow {}^{90m}Nb$	281,6	$^{94}Zr \rightarrow {}^{94}Y$	0,18	$^{96}Zr \rightarrow {}^{97}Zr$	3,7	$^{90}Zr \rightarrow {}^{89}Zr$	0,7
$^{92}Mo \rightarrow {}^{92}Tc$	3,21	$^{92}Mo \rightarrow {}^{91}Mo$	4,98	$^{100}Mo \rightarrow {}^{101}Mo$	11,3	$^{92}Mo \rightarrow {}^{91}Mo$	20
$^{112}Cd \rightarrow {}^{112}In$	2451,4	$^{111}Cd \rightarrow {}^{111m}Cd$	0,79	$^{110}Cd \rightarrow {}^{111m}Cd$	3,81	$^{114}Cd \rightarrow {}^{113}Ag$	0,1
$^{116}Sn \rightarrow {}^{116}Sb$	180,4						
$^{118}Sn \rightarrow {}^{118}Sb$	80,8						
$^{120}Sn \rightarrow {}^{120}Sb$	3130,4	$^{124}Sn \rightarrow {}^{123}Sn$	2,4	$^{124}Sn \rightarrow {}^{125}Sn$	0,037	$^{112}Sn \rightarrow {}^{111}Sn$	3
$^{134}Ba \rightarrow {}^{134}La$	2,8	$^{138}Ba \rightarrow {}^{137m}Ba$	289,2	$^{138}Ba \rightarrow {}^{139}Ba$	42,6		
$^{136}Ba \rightarrow {}^{136}La$	88,3						
$^{139}La \rightarrow {}^{139m}Ce$	200,9			$^{139}La \rightarrow {}^{140}La$	6450		
$^{141}Pr \rightarrow {}^{141m}Nd$	84,8	$^{141}Pr \rightarrow {}^{140}Pr$	574,1	$^{141}Pr \rightarrow {}^{142}Pr$	15400	$^{141}Pr \rightarrow {}^{140}Pr$	1000
$^{142}Nd \rightarrow {}^{142}Pm$	79,2			$^{150}Nd \rightarrow {}^{151}Nd$	3200	$^{142}Nd \rightarrow {}^{141}Nd$	20
$^{180}W \rightarrow {}^{180}Re$	3,4	$^{186}W \rightarrow {}^{185m}W$	43,6	$^{186}W \rightarrow {}^{187}W$	9790	$^{186}W \rightarrow {}^{185}W$	0,05

*Proton current 1 μA/cm².
†Neutron current density 10^9 $cm^{-2} \cdot sec^{-1}$, energy 14 MeV, t_{rad} = 5 min [18].
‡Neutron current density 10^{13} $cm^{-2} \cdot sec^{-1}$, t_{rad} = 1 h [18].
‡‡Electron current 100 μA, energy E_γ = 25 MeV, t_{rad} = 10 min [19].

The quanta were emitted from various nuclides at a level of 10^7-10^{10} quanta/(sec·μA). A sensitivity of determination of $(2670-0.5) \cdot 10^{-9}$ g/(g· μA^{-1}) is achieved with the samples irradiated up to saturation by a 1-μA proton beam current in cases where the protons of the matrix (Li, Be, B, Al, Mn, Co, Eu, Ta, Bi, etc.) are not activated or where radionuclides with short halflives are not formed and where the concentration of other traces is below 10^{-7} g/g (which means that they do not have any marked influence on the analysis). In all other cases, the sensitivity of nondestructive testing by activation analysis varies over the range 10^{-3}-10^{-7} g/(g· μA^{-1}) depending on the emission of radionuclides from the base and trace impurities. The sensitivity in determining chromium, nitrogen, nickel, selenium, yttrium, cadmium, and promethium is $5 \cdot 10^{-10}$ to $4 \cdot 10^{-7}$ g/(g· μA^{-1}), while that for other elements is no worse than $2 \cdot 10^{-5}$ g/(g· μA^{-1}).

As regards the specific use of various nuclear methods in elementary analysis, it is of interest to compare the emissions of radionuclides arising during activation of the elements by protons, thermal and fast neutrons, and high-energy γ quanta. Table 2 lists the radionuclides that have the highest emission when activated by penetrating radiation. As we can see from Table 1 the emissions of radionuclides arising following activation of the sample by protons is always 10-10^8 times the emission of active products of reactions based on fast neutrons. Furthermore, it is mainly long-lived radionuclides that are formed when elements are activated by slow neutrons, and the emissions of these are close to the emission by protons. Sodium, selenium, bromide, barium, neodymium, and tungsten all have high emissions. If we use γ quanta during the activation, then the emissions of the products of photonuclear reactions with Mo, Br, and Pr are 2-10 times as great, and in all the remaining cases lower by factors of 10-1000 than the emission of the radionuclides formed by nuclear reactions with protons.

We can see from what has been said so far that irradiation of samples for short periods with high intensity beams of protons is a way of determining the majority of the groups of elements studied, with a limit of observation of 10^{-5}-10^{-6} %.

We have, therefore, shown that proton activation analysis by means of short-lived products of nuclear reaction has the following advantages over other methods of analysis:

The sensitivity of determining elements is $(2670-0.5)\cdot10^{-9}$ g/(g·μA^{-1}), which in the majority of instances is 10-1000 times the sensitivity of other methods. When large proton fluxes are used (> 1 μA), this limit will be lower.

The methods are nondestructive and rapid in use and the cost of determining one element is less than the cost of analysis by means of long-lived radionuclides, since the time needed to irradiate the sample is markedly lower.

The nondestructive analysis of matrices having large activation sections for thermal and fast neutrons and γ quanta is possible.

The content of elements can be determined, which would be impossible using other methods, due to interference.

The method can be used for multicyclic and automated analysis.

The method has certain drawbacks, however, connected with difficulties in suppressing the background due to the more long-lived radionuclides (particularly when the number of these is large) and the Compton distribution arising out of annihilated quanta with constant, high levels of intensity, since almost all the radionuclides decay by radiating β^+ particles.

LITERATURE CITED

1. P. Benaben, I. Barrandon, and J. Debrun, Anal. Chim. Acta., 78, 129 (1975).
2. J. Debrun et al., Anal. Chem., 47, 637 (1975).
3. N. Krasnov, Ju. Sevasthyanov, I. Konstantinov, J. Radioanal. Chem., 16, 395 (1973).
4. V. A. Muminov, C. Mukhammedov, and R. A. Khaidarov, Zavod. Lab., 1, 40 (1977).
5. B. V. Zatolokin, I. O. Konstantinov, and N. N. Krasnov, At. Energ., 42, No. 4, 311 (1977).
6. J. Barrandon et al., Nucl. Instrum. Methods, 127, 269 (1975).
7. J. Debrun, J. Barrandon, and P. Beneben, Anal. Chem., 48, 167 (1976).
8. J. Debrun, D. Riddle, and E. Schweikert, Anal. Chem., 44, 1386 (1977).
9. V. A. Muminov et al., Nuclear Methods of Analysis and Checking Manufacturing Processes [in Russian], Fan, Tashkent (1976), p. 50.
10. B. Sultanov, Authors Abstract of Candidate's Dissertation, Institute of Nuclear Physics, Academy of Sciences of the Uzbek SSR, Tashkent (1977).
11. S. Bankert, S. Bloom, and G. Sauter, Anal. Chem., 45, 692 (1973).
12. I. V. Kozachevskii, V. D. Knozorov, and V. V. Sokol'skii, in: Applied Nuclear Physics, Book 2 [in Russian], Fan, Tashkent (1973), p. 123.
13. I. McGinly and E. Schweikert, Anal. Chem., 47, 2403 (1975).
14. T. Burton, D. Swindle, and E. Schweikert, Radiochem. Radioanal. Lett., 9, 155 (1972).
15. I. Thomas and E. Schweikert, Nucl. Instrum. Methods., 9, 461 (1972).
16. V. A. Muminov, S. Mukhammedov, and R. A. Khaidarov, Izotopy SSSR, 49, 11 (1977).
17. C. Williamson, I. Boujot, and I. Picard, Rep. CEA-3042 (1966).
18. I. A. Maslov and V. A. Lukinitskii, Handbook of Neutron Activation Analysis [in Russian], Nauka, Lenningrad (1971).
19. G. Lutz, Anal. Chem., 41, 424 (1969).

SPATIAL DISTRIBUTION AND BALANCE OF ^{3}H and ^{137}Cs IN THE BLACK SEA IN 1977

S. M. Vakulovskii, I. Yu. Katrich,
Yu. V. Krasnopevtsev, A. I. Nikitin,
V. B. Chumichev, and V. N. Shkuro

UDC 551.464.6.02

Studies of the behavior of radioactive impurities in the sea are aimed primarily at human radiation safety and at preservation of the natural resources of the ocean. Particular attention should be paid to radioactive contamination of seas with restricted water exchange, including, in particular, the Black Sea, since this type is the most sensitive to contamination of technological origin.

At present the ^{90}Sr content of the Black Sea has been fairly well studied [1-5]. The reserve of ^{137}Cs, however, has been estimated on the basis of limited experimental data [2, 3]. There is no published information on the content of ^{137}Cs in bottom sediments of the Black Sea or on the reserve and constituents of the tritium balance.

To obtain more detailed data on radioactive contamination of the Black Sea, samples of seawater and bottom sediments were taken on board the research ship Mgla during September and October 1977. Water samples were taken by a stainless-steel bathometer, while bottom sediments were sampled using a Okean-0.25 bottom scoop. The sample volume was 2 liters for determining ^{3}H, and 100 liters for ^{137}Cs. The ^{3}H radiometry in the water samples was conducted using the liquid of Mark-II and SL-30 scintillation spectrometers after preliminary enrichment by the method of electrolysis [6]. The error in measuring the minimum activity did not exceed 35%. In determining the ^{137}Cs, water samples were passed through a column with selective sorbent [7] on board the ship. The degree of cesium extraction was 80%. Samples were measured using a low-background γ-ray spectrometer (detector with well). The minimum detectable ^{137}Cs content for a 100-liter sample was 0.05 pCi/liter (1 Ci = $3.7 \cdot 10^{10}$ dis/sec) for a measurement time of 10 h and a relative error of 50%. The ^{137}Cs content in bottom sediments was determined from measurements of dried samples of the bottom using a DGDK-80 detector.

The mean ^{3}H concentration for surface water (Fig. 1) in the eastern part (the boundary between the parts being the 36° meridian) was (60 ± 6) tu, in the western and northwestern part it was (48 ± 10) tu. In the western part there is a distinct shore region (from the Bosphorus to the mouth of the Danube) with a mean ^{3}H concentration of (35 ± 3) tu.

One possible reason for this distribution of ^{3}H over the water area is differences in its intake with atmospheric precipitation. The mean annual precipitation increases from 400-600 mm/y in the west to 1700-5000 mm/y in the east in the Sukhumi-Batumi region [8]. The concentration of ^{3}H in atmospheric precipitation over the entire water area is the same, while the amount of precipitation in the various regions of the sea and the adjacent shore areas is similar. The tritium concentration in surface water in 1977, as averaged over the entire water area, was (51 ± 3) tu, while in the layer from 0 to 100 m it was 36 tu, or around 40% lower than in 1973 [9].

The distribution of ^{137}Cs in surface water is more uniform than that of ^{3}H. The average concentration for the entire water area is 0.53 ± 0.03 pCi/liter, except for the northwestern part, where the mean ^{137}Cs concentration is lower than in the remaining area, by approximately a factor of 1.3. This is evidently to be explained by the influx into this region of river water with a low ^{137}Cs concentration [10].

Measurements of ^{3}H and ^{137}Cs concentration at various levels revealed that the distribution depth of these radionuclides is the same as in the eastern and central parts. This made it possible to obtain averaged concentration profiles for these regions (Fig. 2), which

Translated from Atomnaya Énergiya, Vol. 49, No. 2, pp. 105-108, August, 1980. Original article submitted September 28, 1979.

0038-531X/80/4902-0545$07.50

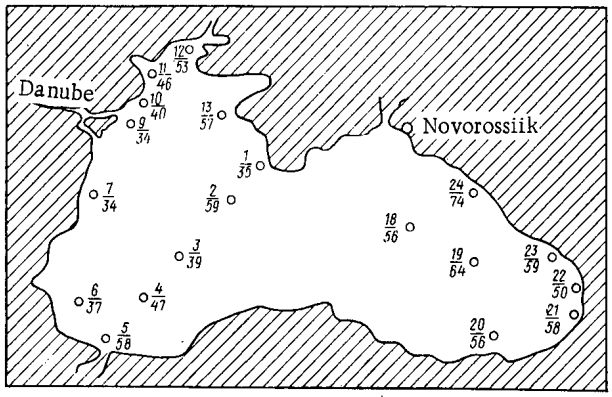

Fig. 1. Concentration of tritium at various sampling points on voyage of research ship Mgla in September-October 1977 (the numerator represents the number of the points, the denominator the tritium concentration in tu).

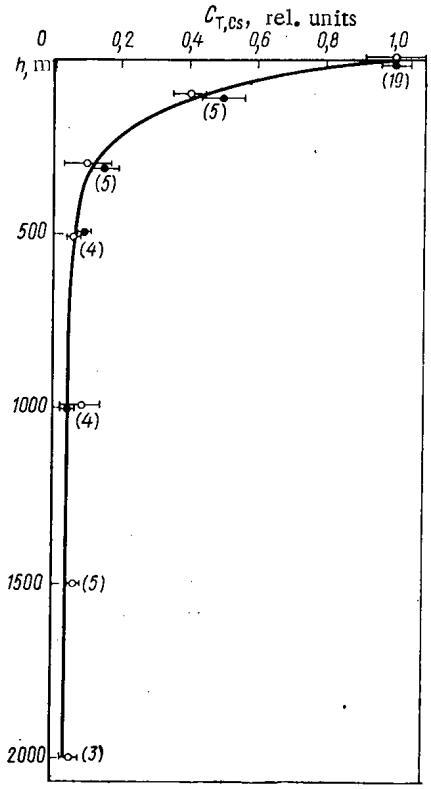

Fig. 2. Averaged vertical profile of concentration of ^{3}H (open circles) and ^{137}Cs (solid circles). The number of averaged values is given in parentheses (for convenience in reading the figure, the experimental points are somewhat shifted vertically).

were normalized to the surface concentration and can be satisfactorily approximated by an exponential relationship:

$$C_h = 0.96 \exp(-0.693\ h/h_{1/2}) + 0.04,$$

where C_h is the ^{3}H or ^{137}Cs concentration at depth h, relative units, h, sampling depth, m; and $h_{1/2}$, depth (82 m) at which the concentration of the radionuclide decreases by a factor of 2.

It should be pointed out, however, that the depth distribution of ^{3}H in the region adjacent to the Bosphorus differs from that in the central and eastern portions of the sea. This is clearly manifest in the depth distribution of ^{3}H on the Bosphorus-Sevastopol section (Fig. 3). The differences at points 5, 4, 3, and 2 may be explained by penetration

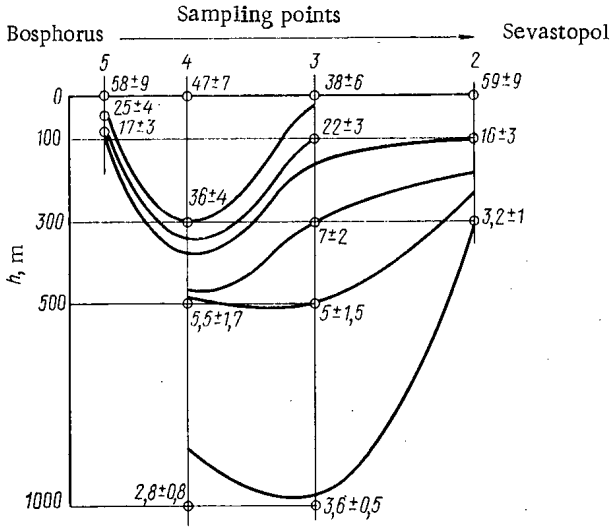

Fig. 3. Isolines of tritium concentration (tu) on the Bosphorus-Sevastopol section in September-October 1977.

TABLE 1. Reserve of ^{3}H and ^{137}Cs in Black Sea in September-October 1977

Layer, m	Volume of water in layer, 10^3 km^3 [11]	Mean conc.*		Reserve, Ci		Fraction of total reserve, %	
		^{3}H, tu	^{137}Cs, pCi/liter	^{3}H, 10^6	^{137}Cs, 10^3	^{3}H	^{137}Cs
0—100	37	35,5±3,7	0,45±0,04	4,3±0,5	16,6±1,5	35	45
100—300	62	12,8±3,2	0,18±0,04	2,6±0,7	11,2±2,5	21	30
300—500	60	5,0±2,5	0,05±0,02	1,0±0,5	3,0±1,2	8	8
500—1000	141	4,2±2,0	0,02±0,006	1,9±0,7	2,8±0,8	15	7,5
1000—1500	127	3,5±1,6	0,015±0,007	1,4±0,7	1,9±0,9	12	5
1500—2000	114	2,7±0,7	0,015±0,007	1,0±0,3	1,7±0,8	9	4,5
Total	541	—	—	12±3	37±8	100	100

*The mean concentration in the layer was taken to be equal to the half-sum of the mean concentrations on the boundaries of the layer.

of the denser surface water of the Sea of Marmora into the deep layers of the Black Sea. The data obtained on the distribution of ^{3}H and ^{137}Cs in surface and deep water enabled us to calculate the reserve of these radionuclides in the sea (see Table 1).

The layer-by-layer reserve of ^{3}H and ^{137}Cs was determined by multiplying the (layer-average) concentration by the volume of water in the layer. The mean ^{137}Cs concentration in the layer at a depth of 1-2 km was obtained by combining four samples taken in this layer on different sections, and by subsequent measurement of the combined sample. The reserves as thus computed in the water of the Black Sea amounted to (12 ± 3) MCi of ^{3}H and (37 ± 8) kCi of ^{137}Cs. Around 65% of the ^{3}H reserve, and more than 80% of the ^{137}Cs reserve, is found in a layer ≤ 500 m. The ratio of the ^{3}H and ^{137}Cs reserves is around 330.

To obtain the total ^{137}Cs reserve it is also necessary to determine the reserve in bottom sediments, which are good absorbers of cesium [12]. The ^{137}Cs content in samples taken at depths to 150 m varied from 80 to 30 mCi/km^2 with a mean value of 47 mCi/km^2. The content of ^{137}Cs in deep-water bottoms is much less than that in shallow water bottoms. For example, the value 0.4 mCi/km^2 was obtained for a sample from a depth of 660 m. Assuming the ^{137}Cs content to be 47 mCi/km^2 for depths to 150 m and 0.4 mCi/km^2 for the remaining part of the sea, we can determine the ^{137}Cs reserve in bottom sediments to be $5.2 \cdot 10^3$ Ci, or around 14% of the seawater reserve. Thus, the total reserve of ^{137}Cs in the sea is (42 ± 8) kCi, or 98 mCi/km^2, this agreeing with the ^{137}Cs reserve in soils for the given latitude band (100 mCi/km^2 [13]).

It is of interest to estimate the ^{3}H and ^{137}Cs reserve in the Black Sea on the basis of individual constituents of the balance. Such an estimate was first made for ^{137}Cs in [4]. In the present study, we computed the ^{3}H and ^{137}Cs reserve under the following assumptions:

there are no local sources of ^{3}H and ^{137}Cs input into the sea;

input of ^{3}H as a result of molecular exchange with the surface of the sea is equal to twice the input with atmospheric precipitation, by analogy with [14, 15];

^{3}H concentration in river water is equal to its concentration in precipitation of the given region [9].

Loss of ^{3}H through evaporation from the water area was not taken into account for the following reason. If we assume that the ^{3}H concentrations in evaporating moisture and in the surface water are the same, and assume that all the incoming ^{3}H is concentrated in a layer ≤ 50 m, then the annual evaporation loss will not exceed 1.7% — on the basis of the ratio of the volume of water evaporated per year to the volume of water in a layer ≤ 50 m. Since ^{3}H does in fact penetrate to layers more than 50 m in depth, the evaporation losses are even smaller and can be disregarded. For the same reason, outflow of ^{3}H to the Sea of Marmora and Sea of Azov as well as intake via the Bosphorus, was not allowed for (the annual volume of water exchanged amounts to 1.8, 0.3, and 0.9% respectively of the volume of water in a layer ≤ 50 m). We also disregarded the intake of ^{137}Cs with river drainage, because of its low concentration in river water.

Data on ^{3}H fallout with precipitation during 1953-1970 were taken from [16], while for 1970-1977 we employed the averaged results of our measurements for Odessa, Rostov-on-Don, and Tbilisi. Intake from the Sea of Azov was computed by multiplying the ^{3}H reserve in the Sea of Azov by the fraction of water entering the Black Sea via the Strait of Kerch. The ^{3}H reserve in the Sea of Azov was estimated in the same way as for the Black Sea. Data on ^{137}Cs fallout along with global atmospheric fallout were taken from [13], data on ^{137}Cs and ^{90}Sr concentration were taken from [3, 17-19] in computing the exchange with the Sea of Marmora and Sea of Azov. The ^{3}H margin in the Black Sea for 1977 as thus computed amounted to around 13 MCi (around 50% coming from molecular exchange, around 25% from precipitation, and 25% from continental drainage).

Estimates of the equilibrium reserve of ^{3}H of natural orgin based on the data of [20, 21] regarding the concentration of tritium in precipitation, equal to 8-10 tu, amount to 0.5 MCi, or around 4% of the reserve as determined from the measurement results. This implies that virtually all the ^{3}H in the Black Sea is of artificial orgin. Thus, the data on ^{3}H and ^{137}Cs reserves as obtained experimentally and as computed under the above assumptions regarding the intake of radionuclides into the sea are in good agreement. The difference is 10% for both radionuclides. This is evidence that contamination of Black Sea water by ^{3}H and ^{137}Cs stems from global sources.

LITERATURE CITED

1. V. P. Shvedov et al., Radioactive Contamination of Seas and Oceans [in Russian], Nauka, Moscow (1964), p. 76.
2. L. I. Belyaev, L. I. Gedeonov, and G. V. Yakovleva, Okeanologiya, 6, No. 4, 641 (1966).
3. L. I. Gedeonov et al., in: Disposal of Radioactive Wastes into Seas, Oceans, and Surface Waters, IAEA, Vienna (1966), p. 373.
4. V. P. Barannik et al., Okeanologiya, 14, No. 2, 274 (1974).
5. S. M. Vakulovskii et al., Trudy IÉM, No. 6(64), Gidrometeoizdat, Moscow (1977), p. 73.
6. H. Ostlund and E. Werner, in: Tritium in the Physical and Biological Sciences, IAEA, Vienna, Vol. 1 (1965), p. 95.
7. N. V. Brevnova et al., Byull. Izobret., No. 34, 72 (1972).
8. World Water Balance and Water Resources of the Earth [in Russian], Gidrometeoizdat, Leningrad (1974), p. 153.
9. S. M. Vakulovskii et al., At. Energ., 44, No. 5, 432 (1978).
10. V. B. Strodomskii, in: Problems of Radioecology of Water Organisms [in Russian], Ural Science Center, Academy of Sciences of the USSR, Sverdlovsk (1971), p. 53.

11. B. A. Skopintsev, Formation of Contemporary Chemical Composition of Black Sea Water [in Russian], Gidrometeoizdat, Leningrad (1975).
12. D. D. Baranova and G. G. Polikarpov, Okeanologiya, 5, No. 4, 646 (1965).
13. A. A. Moiseev and P. V. Ramzaev, Cesium-137 in the Biosphere [in Russian], Atomizdat, Moscow (1975).
14. R. Michel and H. Suess, J. Geophys. Res., 80, No. 30, 4139 (1975).
15. H. Dorsey and W. Peterson, Earth Planet. Lett., 32, No. 2, 342 (1976).
16. Environmental Isotope Data, IAEA, Vienna, Nos. 1-4 (1969-1973).
17. S. A. Patin and A. A. Petrov, Meteorol. Gidrol., No. 7, 105 (1976).
18. O. M. Aleksan'yan, in: Radioecology of Water Organisms [in Russian], Vol. 2, Zinatne, Riga (1973), p. 225.
19. G. G. Polikarpov et al., Stontium-90 in Brackish- and Fresh-water Reservoirs [in Russian], Atomizdat, Moscow (1966).
20. W. Schell, Q. Sayzay, and B. Payne, in: The Physical Behaviour of Radioactivie Contaminants in the Atmosphere, IAEA, Vienna (1973), p. 1.
21. Š. Šaro and A. Duka-Zoluomi, Yad. Energi., 22, No. 9, 338 (1976).

USE OF PERSONNEL NEUTRON FILM MONITORING TO DETERMINE EQUIVALENT RADIATION DOSE BEHIND PROTON ACCELERATOR SHIELDING

E. K. Gel'fand, M. M. Komochkov, B. V. Man'ko, M. M. Salatskaya, and B. S. Sychev

UDC 539.1.06.7:539.12.175

Attempts have been made [1, 2] to increase the reliability with which the neutron dose can be determined behind the shielding of high-energy accelerators by means of personnel neutron film monitoring (PNFM). To this end, it was proposed in [1] to take account of either the density of stars or the fraction of tracks which begin or end in the emulsion. In [2], besides type-K emulsion use was also made of N-3 emulsion with a lowered upper energy threshold of detection.

The results of studies of spectra in the rooms of accelerators and behind their shielding [3-5] allow two main groups to be distinguished: spectra of neutrons which have experienced multiple reflection from the inner wall surfaces of the room (spectra of slowing-down neutrons) and spectra formed when high-energy neutrons pass through shielding without apertures. In spectra of the first group high-energy neutrons are present in extremely small numbers since their albedo is small [6]. In spectra of the second group slowing-down neutrons are present only in the form of "concomitant" to the leading group of high-energy neutrons. In a paper [7] on the experimental investigation of neutron spectra in the JINR accelerators Aleinikov et al. call the spectra of the first group "soft" and those of the second, "hard."

In the present paper it is shown how the total equivalent dose of radiation can be determined more accurately than previously from the tracks formed in the emulsion of a personnel neutron film badge [1]. The basis for the solution of this problem was the circumstance that tracks in an emulsion have different grain densities, depending on the energy of the protons which form them. In [8] it was proposed to visually divide tracks in a type-K emulsion into "black" and "gray." We used the adjective black to describe tracks in which the fraction of length occupied by grains is greater than the fraction occupied by gaps. All other tracks were called gray. From the experimental data of [8], it can be concluded that the boundary between gray and black tracks corresponds to a proton energy of 40 MeV. The existence of gray tracks indicates the presence of high-energy protons. Fast neutrons ($E < 20$ MeV) can form only dark tracks.

Calculations were carried out to find the number of black and gray tracks formed in the emulsion of a PNFM bdge. The separation into gray and black concerned the projection of tracks onto the plane of the emulsion. A study was made of the reaction of the badge in radiation fields behind flat shields of ordinary concrete of varius thicknesses, irradiated with a broad beam of neutrons of various energy spectra: neutrons of direct nuclear reactions, emitted from targets bombarded with protons possessing an energy $E < 10$ GeV at an angle $\theta = 70°$ (I); neutrons with an energy spectrum uniformly distributed ores the range 3.68-480 MeV (II); neurons with an energy spectrum uniformly distributed over the range 3.68-660 MeV (III); neutrons with a 1/E spectrum uniformly distributed with respect to a logarithmic variable in the energy range 3.68 MeV-10 GeV (IV). Besides the variation of the neutron spectrum and the shielding thickness we studied the reaction of the film badge as a function of the upper sensitivity limit of the emulsion, which varied from 150 to 175 MeV. The boundary between the gray and black tracks was varied within the limits 30-50 MeV. The calculation of track formation by neutrons was carried out in accordance with [9]. The maximum value of the values of the equivalent dose in the tissue-equivalent plate (TEP) was associated with the density of the tracks produced. The energy spectra of neutrons and protons in the range $0.1 \text{ MeV} < E < E_0$ are shown in Fig. 1.

Translated from Atomnaya Énergiya, Vol. 49, No. 2, pp. 108-112, August, 1980. Original article submitted July 23, 1979; revision submitted March 7, 1980.

0038-531X/80/4902-0550$07.50

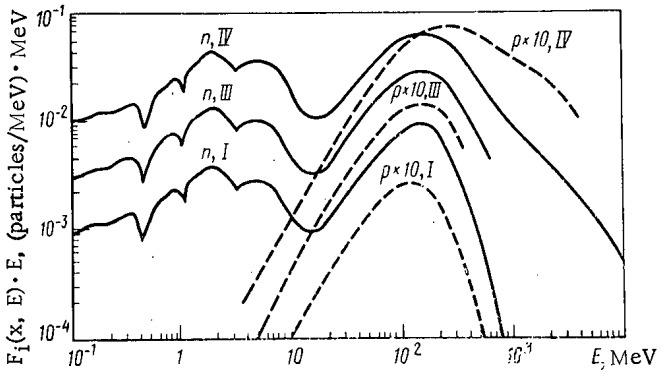

Fig. 1. Energy spectra of nucleons behind concrete layer with thickness of 500 g/cm², whose surface is bombarded by broad beam of neutrons with initial spectra I, III, IV.

TABLE 1. Composition of Hadron Field behind 500-g/cm² Concrete Layer with Various Primary Neutron Spectra*

Spectrum		Neutrons					Protons	$\pi^{\pm}$ mesons
		E, MeV						
		$4 \cdot 10^{-7}$–0,1	0,1–0,5	0,5–2	2–20	> 20	> 3,7	> 3,7
Calculation	I	0,36	0,11	0,23	0,29	0,97	0,031	0,001
	II	0,36	0,11	0,23	0,28	0,96	0,033	0,001
	III	0,34	0,11	0,23	0,29	0,95	0,048	0,003
	IV	0,36	0,12	0,24	0,35	0,82	0,125	0,051
Experiment	350 MeV†	0,40		0,91		1,0		
	480 MeV†	0,36		0,63		1,0		
	660 MeV†	0,16		0,39		1,0		

*Normalization to one hadron of energy higher than 20 MeV.
†The proton energy given is for synchrocyclotron operation with external target.

Calculated data characterizing the hadron field studied according to energy groups are presented in Table 1. For all of the initial spectra the fraction of cascade neutrons in the 2–20-MeV group is 10% of their number in the group above 20 MeV. Therefore, the 2–20-MeV group is represented on average by 70% slowing-down neutrons and 30% cascade neutrons. The calculated data are compared in Table 1 with experimental results [10] characterizing the neutron field behind the 2-m shielding of the JINR synchrocylotron. It is seen that the calculated composition of the neutron field corresponds to the experimental data, although there are some appreciable differences which can be explained by the difference in the conditions of the calculation and the experiment.

Table 2 gives the results of calculations of the density of track formation and the maximum equivalent dose H_{max} in TEP. The following notation is used here: x, thickness of the concrete layer (g/cm²); F_n and F_p, fluences of the cascade neutrons and protons (particles/cm²); N_n, N_p and N_n^b, N_p^b, densities of all the tracks and the black tracks, respectively, formed by the neutrons and protons of the radiation field (tracks/cm²); and N, total density of all tracks (tracks/cm²).

Analysis of Table 2 reveals a relatively weak dependence of the given functionals on the form of the primary spectrum and the shielding thickness. The number of tracks formed in PNFM badges by protons of the radiation field is roughly 7–20 times the number of tracks which are caused by recoil protons formed under the action of neutrons of the radiation field. At the same time, as is seen from Fig. 2, the maximum equivalent dose of fast neutrons (E < 20 MeV) is smaller than H_{max} by a factor of roughly 3. It thus follows that if the number of tracks is interpreted in terms of equivalent dose of fast neutrons, then it

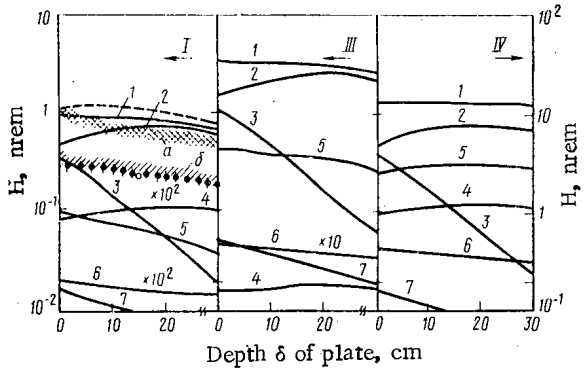

Fig. 2. Depth distributions of dose and its components in TEP behind 500-g/cm concrete layer (primary neutrons with spectra I, III, IV bombard the concrete surface): ———) equivalent dose (our calculation for monodirectional irradiation of TEP); 1) sum; 2) neutrons (E > 20 MeV); 3) neutrons (E < 20 MeV); 4) $\pi^{\pm}$ mesons; 5) protons; 6) π^{0} mesons; 7) γ rays; - - -) total equivalent dose (calculation [15]); a, b) total equivalent dose and absorbed dose (our calculation for "real" conditions of irradiation of TEP); ●, ○) total absorbed dose in TEP and without TEP (experiment [13]).

TABLE 2. Relation between Track Formation and Equivalent Radiation Dose (range of detection of gray tracks 40-150 MeV)

Spectrum	x, g/cm²	$\frac{F_n}{F_p}$	$\frac{N_p}{N_n}$	N_p^b/N_n^b	$N^b/N^g = k$	H_{max}/N^g, μrem·cm²/track	H_{max}/N_n, μrem·cm²/track
I	200	29,4	8,5	5,1	0,72	8,1	4,7
	500	33,5	7,8	4,9	0,75	8,6	4,9
	1100	39,1	7,1	4,6	0,78	9,2	5,2
	1550	41,9	6,8	4,4	0,80	9,5	5,3
	2000	43,9	6,5	4,3	0,81	9,8	5,4
II	200	20,6	12,2	6,8	0,62	6,3	3,9
	500	27,0	9,4	5,5	0,68	7,5	4,4
	1100	33,4	7,9	4,9	0,74	8,5	4,9
	1550	36,2	7,4	4,6	0,75	8,9	5,1
	2000	38,4	7,1	4,5	0,77	9,0	5,1
III	200	14,9	14,7	7,9	0,58	6,0	3,8
	500	21,1	10,8	6,2	0,65	7,0	4,2
	1100	28,1	8,7	5,2	0,70	8,0	4,7
	1500	31,6	8,0	4,9	0,73	8,5	4,9
	2000	35,0	7,6	4,7	0,75	8,8	5,0
IV	200	5,5	20,9	10,2	0,55	7,9	5,1
	500	7,3	16,4	8,4	0,59	7,7	4,9
	1000	9,8	13,6	7,3	0,62	7,9	4,9
	1550	11,1	12.6	6,9	0,63	7,9	4,9
	2000	12,3	11,9	6,6	0,65	8,0	4,9

is expected that the "true" value is overestimated by a factor of 20-60 and this was indeed established experimentally in [1].

The depth distribution of the radiation dose was calculated for conditions of normal incidence on the TEP surface. The data of [11] were taken as the initial data. We also estimated how sensitive the depth distribution is to the angular distribution of the radiation incident on the TEP surface. Figure 2 shows the depth distributions of the components of the equivalent dose for conditions of normal incidence with allowance for the angular distribution ("real" irradiation conditions). The indeterminacy in the results of the calculations for irradiation of TEP with allowance for the angular distribution is due mainly to the statistical fluctuations of the initial data which we used for the depth distributions of the dose [12]. In Fig. 2 the results of the calculations are compared with the experimental data [13] obtained behind the side shielding of the IFVÉ (Institute of High-Energy Physics) proton synchrotron. The distributions under comparison were normalized according to the adsorbed dose without a TEP; in the calculations this was the thickness of the TEP (0.5 cm) for conditions of normal incidence of radiation.

As is seen from Table 2 in the radiation fields under consideration the ratio between the track density and the maximum equivalent dose is quite stable. With this ratio, H_{max} for unknown fields with a "hard" spectrum can be determined from the track density. In real situations irradiation behind the shielding of accelerators can occur under conditions characterized by the superposition of "hard" and "soft" spectra. In this case as well H_{max} can be determined. Allowance must be made for the fact that only black tracks are formed in a "soft" spectrum while the black and gray tracks in a "hard" spectrum are in a ratio which is determined by coefficient R (see Table 2).

Taking the values of the numerical parameters into consideration, we get the following expression for determining the equivalent dose of a mixed field of radiation:

$$H_{\max} = (6.0 \pm 0.9)\, N - (9.8 \pm 1.8)\, N^{g}_{\text{rem}}, \tag{1}$$

where N and Ng pertain to scanning over a traverse of area 0.0225 cm^2.

For a clearly "hard" spectrum Eq. (1) is of the form

$$H_{\max} = (0.27 \pm 0.07)\, N \ \text{mrem}. \tag{2}$$

In the experimental determination of the track density in the emulsion there may be subjective errors owing to the indeterminacy of the grain density which in the scanning is adopted as the boundary between black and gray tracks as well as the minimum grain density when an ordered group of grains is perceived as a track. The latter is particularly important for tracks which intersect the emulsion at large angles to its surface. Both sources of error are taken into account partially when we vary the pertinent initial data. However, this variation is relatively small and apparently reflects the least error which should be expected when films are scanned by experienced laboratory assistants. As will be seen from experimental data given below the spread in the results of scanning of one emulsion by different laboratory assistants is greater than follows from our estimates, although on average we can speak of agreement between experiment and calculation within the limits of the expected error.

The experimental data are the results of scans of emulsions irradiated behind the shielding of the JINR and CERN proton accelerators. The scanning was done by two experienced laboratory assistants according to the proposed scheme of dividing tracks into black and gray. Using the scan results and Eqs. (1) and (2), we found the equivalent radiation dose H_i which we then compared with the value H_0 obtained by the most reliable methods of dose measurement. Table 3 presents the results of scans of 13 emulsions irradiated at six points behind the shielding of the JINR synchrocyclotron and synchrophasotron [1] and in the "hard" spectrum of the CERN synchrotron [14].

It must be borne in mind that points 1 and 3 (Fig. 1 [1]) were behind shielding without apertures and channels; therefore, the irradiation conditions at these points are close to the conditions of the calculation of the dose behind blind shielding, the results of which are given in the present paper. The radiation dose at points 1 and 2 (Fig. 2 [1]) is also due mainly to "hard" spectra. At point 4 (Fig. 2 [1]) the dose is due to a superposition of "hard" and "soft" spectra. At point 9 (Fig. 3 [1]) in the synchro-

TABLE 3. Results of Scanning of Emulsions Irradiated in Different Accelerators

Device	Point of meas.	No. of tracks on transv. N^b	No. of tracks on transv. N^g	$h = \frac{N^b}{N^g}$	Equiv. dose, mrem H_1	Equiv. dose, mrem H_0	$\frac{H_1}{H_0}$
JINR synchrocyclotron, E_p = 660 MeV, Fig. 1 [1]	1	340±50	560±120	0,60±0,15	240±70	210±70	1,1±0,5
	1	270±40	400±40	0,66±0,08	180±50	210±70	0,8±0,3
	3	420±50	740±90	0,56±0,15	310±80	310±110	1,0±0,5
	3	210±50	250±40	0,85±0,22	120±40	100±40	1,2±0,5
JINR synchrocyclotron, E_p = 660 MeV, Fig. 2 [1]	1	210±30	600±140	0,34±0,10	220±60	190±20	1,2±0,4
	1	270±60	670±170	0,41±0,20	250±70	190±20	1,3±0,4
	2	210±20	470±100	0,45±0,11	190±50	140±10	1,3±0,4
	2	180±20	450±160	0,40±0,20	170±60	140±10	1,2±0,4
	4	16±2	38±7	0,41±0,10	15±4	28±4	0,5±0,2
	4	20±6	64±9	0,31±0,15	23±4	28±4	0,8±0,2
JINR synchrophasotron, E_p = 10 GeV, Fig. 3 [1]	9	350±40	820±180	0,43±0,15	320±90	420±50	0,8±0,2
	9	110±10	490±30	0,23±0,02	160±40	190±20	0,8±0,2
CERN proton synchrotron, E_p = 28 GeV [14], "hard" spectrum		590±100	1550±340	0,38±0,16	580±160	600±90	1,0±0,3

TABLE 4. Results of Scan of Emulsion Irradiated in "Hard" Spectrum Behind Shielding of JINR Synchrocyclotron

No. of scan	No. of tracks on transverse N^b	No. of tracks on transverse N^g	No. of tracks on transverse N	h
1	340±30	390±30	730±40	0,87±0,09
2	430±30	320±30	750±40	1,3±0,1
3	290±20	300±20	590±30	0,96±0,08
4	400±40	230±30	630±50	1,7±0,3
5	340±30	560±50	900±60	0,60±0,08
6	210±20	480±30	690±40	0,45±0,06
7	270±20	340±30	610±30	0,79±0,09

phasotron tracks in the emulsion could also have been formed by secondary protons arising when the primary proton beam passed through a channel close to point 9. The mean value of the ratio H_1/H_0 according to the results of Table 3 is 1.0 ± 0.2, which confirms that the calculations are correct.

In order to evaluate the subjective errors, one of the emulsions irradiated in a "hard" spectrum was scanned by seven laboratory assistants. As is seen from the data of Table 4, the results obtained by different laboratory assistants differ substantially. Averaging the data of Table 4, we get: $\bar{N}^b$ = 330 ± 60 tracks/traverse, $\bar{N}^g$ = 370 ± 90 tracks/traverse, $k = \bar{N}^b/\bar{N}^g = 0.89 \pm 0.25$, and $\bar{N}$ = 700 ± 90 tracks/traverse. The mean deviation of the results of the scans exceed the statistical errors given in Table 4.

The equivalent dose found in this case according to Eq. (2) is 191 mrem. The value of the equivalent dose found with the most reliable measuring methods, in 210 mrem, is 15-20%. This permits the conclusion that the calculations are in agreement with the experiment. It must be pointed out that the results given here were obtained by laboratory assistants without prior training. The subjective error can be reduced significantly as the assistants master the new scanning technique.

On the basis of the data obtained, we propose the following technique for determining the equivalent dose. In scanning the emulsion count the number of black and gray tracks and then find $k = N^b/N^g$. If $0.4 \leq k \leq 1.1$, then determine the dose from Eq. (2) (the values 0.4 and 1.1 correspond to the limiting values $k = 0.71 \pm 0.16$ which was obtained by averaging the data of Table 1 with allowance for the subjective errors in dividing the tracks into black and gray). If $k < 1.1$, find the dose from Eq. (1). When $k < 0.4$, the irradiation conditions differ markedly from those considered in the present paper (e.g., irradiation inside the accelerator room), and further studies are called for.

Conclusions. Calculations have been made of the laws governing the formation of the radiation dose behind the shielding of proton accelerators. Numerical data have been ob-

tained on the indications of a personnel neutron film badge in the radiation fields studied. It has been demonstrated that it is possible in principle to determine the total equivalent dose of the radiation field behind the shielding of a proton accelerator by the PNFM method if division of tracks into black and gray is introduced into the emulsion scanning procedure. The reliability of the measurements of the equivalent dose in fields with a "hard" spectrum is higher in this case than when the method proposed in [1] is used; the reliability of the two methods is apparently the same in the case of superposition of "soft" and "ard" spectra. Comparison of the experimental and calculated values revealed that the computational method employed is applicable to modeling the dose characteristic of radiation behind the shielding of proton accelerators.

The authors express their gratitude to the workers of the personnel monitoring group of the Radiation Safety Department at the Joint Institute for Nuclear Research (JINR) for scanning the emulsions.

LITERATURE CITED

1. M. M. Komochkov and M. I. Salatskaya, JINR Preprint, R16-8175, Dubna (1974).
2. A. V. Antipov et al., Preprint IFVÉ LRI 77-10, Serpukhov (1977).
3. L. P. Kimel' et al., JINR Preprint R16-3409, Dubna (1967).
4. B. S. Sychev, JINR Preprint R16-4304, Dubna (1969).
5. M. M. Komochkov and B. S. Sychev, in: Proc. Meeting on Dosimetry and Physics of Accelerator Shielding [in Russian], JINR 16-4888, Dubna (1970), p. 15.
6. L. R. Kimel' et al., JINR Preprint R16-3514, Dubna (1967).
7. V. E. Aleinikov, V. P. Gerdt, and M. M. Komochkov, JINR Preprint R16-9870, Dubna (1976), At. Energ., 42, No. 4, 305 (1977).
8. M. M. Komochkov et al., JINR Preprint 13-10188, Dubna (1976).
9. B. V. Man'ko, in: Strong-Current Accelerators and Storage Rings [in Russian], Proc. Radio Engineering Institute, Academy of Sciences of the USSR, No. 30, Moscow (1977), p. 86.
10. V. E. Aleinikov, M. M. Komochkov, and V. I. Tsovboon, in: Int. Congress on Protection Against Accelerator and Space Radiation, CERN 71-16, Geneva (1971), p. 282.
11. Atlas of Dose Characteristics of External Ionizing Radiation [in Russian], Atomizdat, Moscow (1978).
12. C. Zerby and W. Kinney, Nucl. Instrum. Methods, 36, No. 1, 125 (1965).
13. A. N. Antipov et al., Preprint IFVÉ ORI 78-15, Serpukhov (1978).
14. M. M. Komochkov and M. I. Satatskaya, JINR Preprint R16-9780, Dubna (1976).
15. E. K. Gel'fand et al., in: Accelerator Technique [in Russian], Proc. Radio Engineering Institute, Academy of Sciences of the USSR, No. 22, Moscow (1975), p. 242.

EXPERIMENTAL SIMULATION OF RECUPERATOR FOR NEGATIVE-ION INJECTORS

S. K. Dimitrov, A. V. Makhin,
S. V. Turkulets

UDC 621.039.6

Injectors of fast atoms obtained from both positive and negative ions are employed to produce and heat plasma in some thermonuclear devices [1, 2]. In both cases the coefficient of ion conversion to fast atoms is appreciably smaller than unity and, therefore, in order to raise the efficiency of the injector it is necessary to effect direct conversion (recuperation) of the kinetic energy of the unrecharged ions into electrical energy.

The objective of the present paper is to study a variant of a system for recuperation of the energy of monoenergetic beams of negative ions. The experiments were conducted with electron beams since electron sources are simpler as is also their operation and the evacuation requirements are less stringent. With electron beams it is possible to experimentally simulate the effect of some factors on the efficiency of energy recuperation [e.g., the effect of the geometry of the system, the space charge, and other beam parameters).

The problems of beam slowing-down, in which the kinetic energy of the electrons is transformed into electric energy of the field and is returned to the external circuit, also arise in the construction of electron-beam tubes, radio-frequency electron tubes, and electrokinetic electric transmission lines now in the research stage.

In our study, we made an experimental investigation of the problem of slowing-down and collection of particles in a recuperation system consisting of a collector with suppressor and a set of diaphragms setting up a retarding electric field (Fig. 1a). A similar system was described in [3]. The surface of the collector is a cone with an apex angle α. An aperture in the collector along the axis of the system is necessary so that the recuperator could be used in the injector channel without need to use any deflecting magnetic field ("right through") and so that pumping of gas out of the region of the collector could be facilitated. In order to block the stream of ions passing through this aperture, a special electrode producing an ion-scattering electric field is placed behind the collector.

In such a system secondary electrons are blocked by a suppressor whose potential is lower than that of the collector [3]. In front of the diaphragms is a secondary-electron collector (SEC), whose current provides an approximation of the number of electrons which are reflected by the electric field of the system and do not reach the collector as well as secondary electrons not blocked by the suppressor. The SEC current is part of the loss of recuperated power in the calculation of the efficiency of energy conversion in the given system (the recuperation efficiency is the ratio of the electrical power taken from the collector to the beam power at the entrance to the recuperator).

The apertures of the collector, suppressor, and diaphragms were chosen with allowance for the angular divergence of the electron beam and the divergence due to the influence of the space charge in the stream of particles. In order to take the beam to the region of the collector with minimum losses, we employed beam focusing over the entire retardation zone. To this end, some diaphragms were given a negative potential roughly equal to the accelerating potential of the electron gun (see Fig. 1b). Because of this, with this system it is possible to recuperate beams with a large angular divergence (in our case, $\theta = 8°$). The system was optimized in respect of the potential of the collector U_c, the suppressor U_s, and the auxiliary electrode U_a, as well as the apex angle α of the cone.

The dependence of the efficiency η on U_c with an optimal U_s for each U_c is shown in Fig. 2. The dependence was measured at $\alpha = 30°$ and optimal U_a. The dependence of η on U_s with the other parameters at optimal values and $\alpha = 30°$ is shown in Fig. 3. The maximum efficiency of recuperation at an electron energy of 200 eV was $\eta = 88 \pm 2\%$. The decrease in η as U_s deviates from the optimal value can be explained as follows. Since the suppressor

Translated from Atomnaya Énergiya, Vol. 49, No. 2, pp. 113-115, August, 1980.
Original article submitted September 28, 1979.

 0038-531X/80/4902-0556$07.50

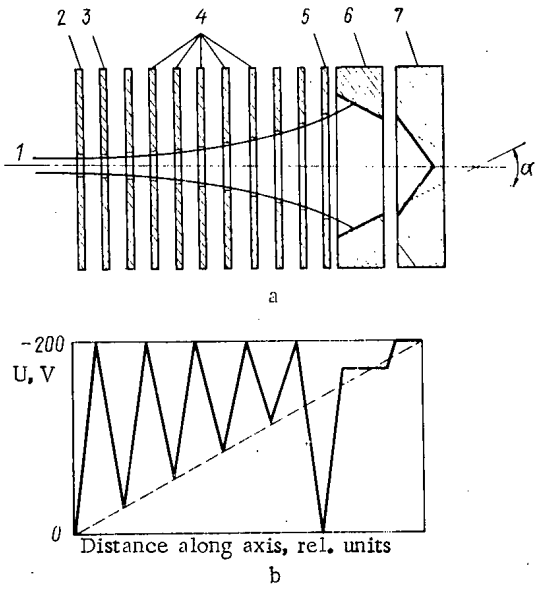

Fig. 1. a) Diagram of recuperator, and b) qualitative distribution of potential on electrodes: 1) beam; W_o = 200 eV; 2) collimating diaphragm; 3) secondary-electron collector; 4) retarding-field electrodes; 5) suppressor; 6) collector; 8) auxiliary electrode of scattering field.

serves to form a potential well in the near-collector region, thus stopping secondary electrons from reaching the collector, an increase in U_s reduces the ability of the suppressor to block electrons. When U_s falls below $U_{s\ opt}$ the region of the potential well grows so much that it covers the region in which the electron beam passes and prevents it from reaching the collector, reflecting the electrons backwards.

The efficiency of the system with a solid collector (without an aperture and auxiliary electrode, i.e., without beam scattering at the end of the retardation) proved to be lower since the potential well set up by the suppressor does not cover the central regions of the collector and does not stop secondary electrons, as indicated by the growth of the current from the SEC.

The experiments allowed it to be shown that in order to have maximum conversion efficiency, 90-95% of the beam should be retarded. The influence of the space charge in the beam, according to [4], is characterized by the dimensional parameter d/r_d, where d is the beam diameter and r_d is a parameter with the dimension of length and is calculated from the current density and beam energy. It was shown experimentally that within the limits of variation of d/r_d from 0.06 to 0.11 the efficiency remains constant. This is explained by the fact that the slight beam divergence owing to the space charge, which exerts an influence on the conversion efficiency, is compensated by the negative potential of the focusing diaphragms (Fig. 4).

The conversion efficiency also depends on the angle which the collector surface makes to the axis of the system. For maximum slowing-down of the particles this surface should be orthogonal to the electron trajectories. From the curves obtained (Fig. 5) it is seen that the efficiency of such a system reaches its maximum value of 89 ± 2% at a collector slope of 5° (other parameters remaining optimal).

As was ascertained, an appreciable influence on the electron trajectory (and, hence, on the efficiency) is exerted by the potential of the electrode forming the scattering field. The optimal potential U_a at which maximum efficiency is observed also depends on the geometry of that electrode. Figure 6 shows the dependence of the efficiency η on U_a for an electrode in the form of a solid cone (see Fig. 1a). With operation according to the

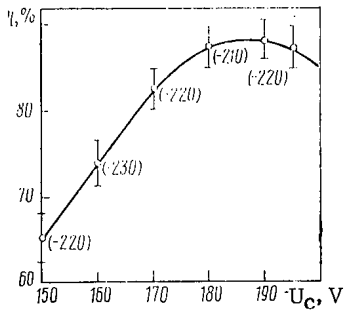

Fig. 2

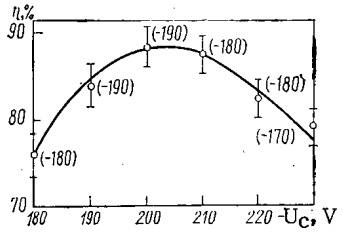

Fig. 3

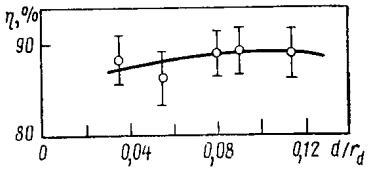

Fig. 4

Fig. 2. Dependence of efficiency η on U_c (the numbers in parentheses are the optimal values of U_s).

Fig. 3. Dependence of efficiency η on U_s (the numbers in parentheses are the optimal values of U_c).

Fig. 4. Dependence of efficiency on d/r_d.

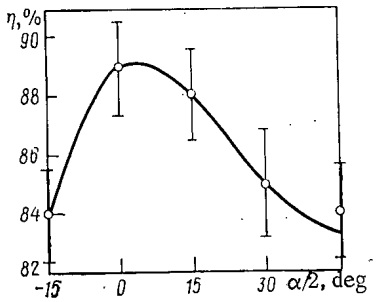

Fig. 5. Dependence of efficiency on $\alpha/2$.

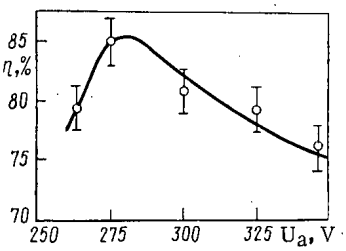

Fig. 6. Dependence of efficiency on potential U_a of scattering-field electrode for $\alpha/2 = 30°$.

straight-through scheme, the electrode should be made in the form of a ring. In this case the potential applied to it must be twice that applied to the solid design studied.

The process of retardation of a 500-keV ion beam in the given system with $d/r_d = 0.08$ was simulated by computer by the "large-particle" method. Figure 7 shows the position of the beam in the region of retardation and the picture of the equipotential lines. The role of the scattering electrode (made in the form of a ring) is illustrated. In the given case there is no necessity to have periodic focusing of the field since the beam emerging from the ion source has practically no angular spread. The length of the entire system is less than the distance over which a virtual cathode is formed (of the order of r_d).

The variant of the position of the recuperator in the injector system of a tokamak is shown in Fig. 8. The recuperator for D^+ ions formed as the result of the processes $D^\circ \rightarrow D^+$ and $D^- \rightarrow D^+$ may consist, e.g., of a system of skewed diaphragms [4] which, at D^+-beam parameters of $d/r_d = 0.08$, has a 90% efficiency (for a monoenergetic beam).

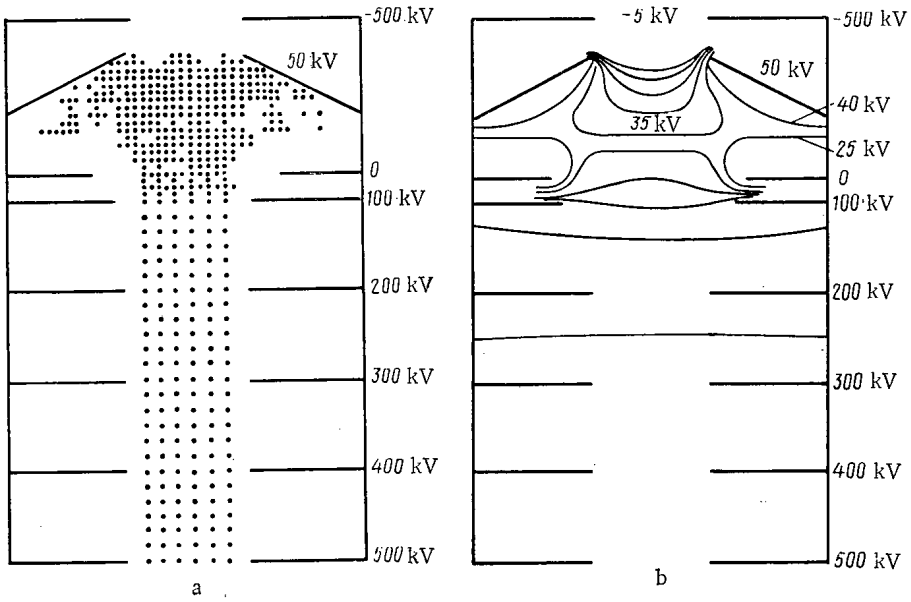

Fig. 7. Position of beam in retardation region (a) and picture of equipotential lines at the same parameters (b) when $t = 0.6$ μsec, $j = 55$ A/m^2, $W_o = 500$ keV.

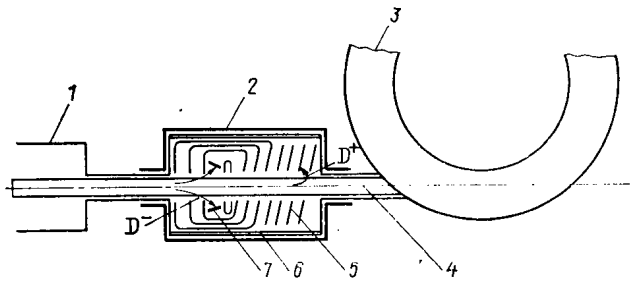

Fig. 8. Variant of position of recuperators in injector system of tokamak: 1) charge-exchange chamber; 2) magnetic shield; 3) tokamak; 4) atoms; 5) recuperator of D^+-ion energy (system of skewed diaphragms; 6) cryopanels; 7) recuperator of D^--ion energy.

Thus, the recuperation efficiency in the system studied, with $d/r_d = 0.08$–0.1, can be $\sim$ 90%, which is roughly 10% higher than in the system of skewed diaphragms for the same D^- beam parameters [5].

LITERATURE CITED

1. V. N. Pistunovich, Preprint IAÉ-2209, Moscow (1972).
2. Yu. V. Gribov, V. A. Chuyanov, and G. E. Shatalov, in: Proc. Second Soviet–American "Fusion–Fission" Seminar [in Russian], Atomizdat, Moscow (1978), p. 192.
3. E. A. Abramyan and A. N. Sharapa, Prib. Tekh. Eksp., No. 2, 30 (1971).
4. O. A. Vinogradova et al., At. Energ., 35, No. 1, 15 (1973).
5. S. K. Dimitrov and A. V. Makhin, At. Energ., 46, No. 4, 245 (1979).

MEASUREMENT OF TOTAL NEUTRON CROSS SECTIONS OF ^{168}Yb and ^{169}Yb

V. A. Anufriev, S. I. Babich,
A. G. Kolesov, V. N. Nefedov,
and V. A. Poruchikov

UDC 621.039.556

In this paper we present data on the total neutron cross sections and resonance parameters of ^{168,169}Yb ($T_{1/2}$ = 31 days). Measurements were made using the transit-time method and a neutron spectrometer mounted on the horizontal channel of an SM-2 reactor. The measurement procedure was described in [1].

To determine the total neutron cross section and resonance parameters of ^{168}Yb we measured the transmission of two specimens enriched with (15.6%). The characteristics of these specimens are given in Table 1.

Specimen No. 1 was made of Yb_2O_3 powder poured into a sealed aluminum ampule with an inner diameter of 1.8 mm. Specimen No. 2 was prepared in order to make a more precise determination of the resonance parameters of the "strong" level of ^{168}Yb with E_0 = 0.590 eV. A target with ^{169}Yb was obtained by exposure of a specimen analogous to specimen No. 1 in the SM-2 reactor to a flux of $3.2 \cdot 10^{20}$ neutrons/cm^2. Several measurements of the transmission of the irradiated specimen were made over a 175-day period in order to identify the levels and to determine the amount of ^{169}Yb.

The amount of ^{169}Yb was determined from the accumulation of ^{169}Tm upon β^+ decay of ^{169}Yb from the following expression:

$$N^{t_i}_{^{169}\mathrm{Yb}} = \frac{N^{t_{i+1}}_{^{169}\mathrm{Tm}} - N^{t_i}_{^{169}\mathrm{Tm}}}{1 - \exp\left[-\lambda_{^{169}\mathrm{Yb}}(t_{i+1} - t_i)\right]},$$

where t_i is the time of the i-th transmission measurement, days, $N^{t_i}_{^{169}\mathrm{Tm}}$, number of ^{169}Tm nuclei for the i-th transmission measurement, $\lambda_{^{169}\mathrm{Yb}}$ rate of ^{169}Yb decay, days^{-1}. In computing the amount of ^{169}Tm we employed the resonance parameters of the E_0 = 3.9 eV level, recommended in [2]. Figure 1 shows the transmission of an irradiated specimen of ytterbium in the region of the E_0 = 3.9 eV level for two measurements with a time interval of 24 days. It was determined that at the instant irradiation was terminated, there were $1.14 \cdot 10^{-4}$ nuclei/b ^{169}Yb, $1.9 \cdot 10^{-4}$ nuclei/b ^{168}Yb and $0.22 \cdot 10^{-4}$ nuclei/b ^{169}Tm in the specimen.

In the energy range 0.014-46 eV we discovered four levels of ^{168}Yb and 21 levels of ^{169}Yb. The form method, using the Bright–Wigner formula, was employed to compute the resonance parameters. Table 2 gives the neutron-resonance parameters of ^{168}Yb, which are compared with the data published in [3-5]. The 3.925 and 8.17 eV energy levels given in [4] were not observed by us.

The measured transmission was used to calculate the behavior of the total neutron cross section of ^{168}Yb in the range of neutron energies 0.014-1 eV (Fig. 2). The behavior of the total neutron cross section of ^{168}Yb in this range is described by the positive level parameter.

The resultant value σ_γ^{2200} = (2200 + 170)b (capture cross section of ^{168}Yb at thermal point) is much less than that recommended in [2]. This difference can be accounted for by the fact that the value σ_γ^{2200} = 3470 b of [2] is based on integral measurements employing either the cadmium difference method or measurements in the thermal Maxwellian neutron spectrum. The presence of a "strong" neutron level with E_0 = 0.590 eV near the cadmium boundary causes the cross section at the thermal point as obtained by the integral method to be too high.

The resultant parameter values were used to compute the resonance capture integral of ^{168}Yb, equal to I_γ = (24700 + 3000) b. The value of I_γ is less than that recommended in [2].

Translated from Atomnaya Énergiya, Vol. 49, No. 2, pp. 116-118, August, 1980.
Original article submitted October 22, 1979.

 0038-531X/80/4902-0560$07.50

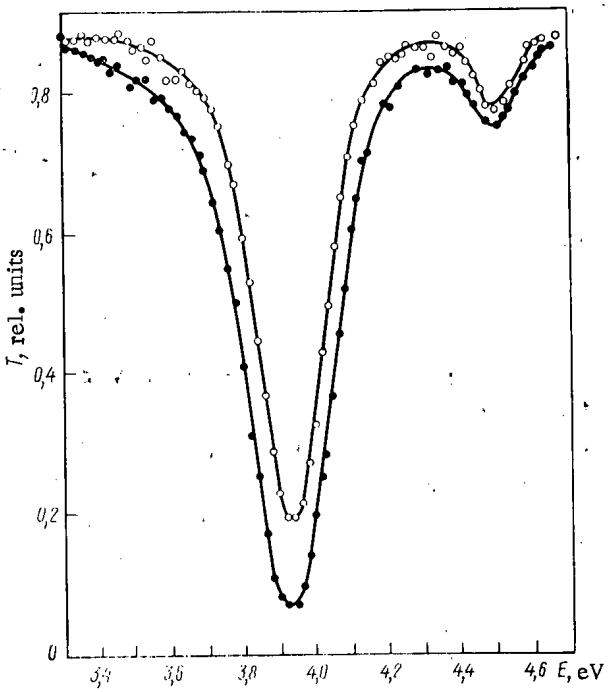

Fig. 1. Transmission of irradiated specimen of ytterbium in energy range 3.4-4.6 eV, 30 days (solid circles) and 6 days (open circles) after irradiation.

TABLE 1. Composition of Ytterbium Specimens, Nuclei/b*

Specimen number	Isotope of Yb, [×10⁵]						
	168	170	171	172	173	174	175
1	36,6	17,5	44,3	46,9	27,2	43,7	13,2
2	0,74	0,36	0,90	0,96	0,55	0,89	0,27

* 1 b = 10^{-28} m^2.

TABLE 2. Neutron-Resonance Parameters of ^{168}Yb

E_0, eV	Γ, eV	Γ_n, MeV	
		this paper	published data
0,590±0,005	66±3	2,2±0,1	3,1±0,3 [3] 2,1±0,2 [4]
9,71±0,01	(90)	0,08±0,01	0,16±0,06 [4]
22,44±0,05	172±9	24,6±1,0	50±5 [4] 29±2 [5]
27,17±0,06	(90)	2,45±0,20	5,2±2,0 [4]

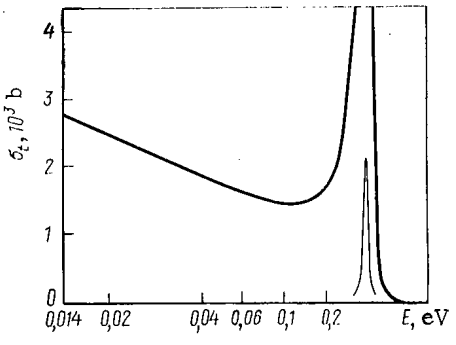

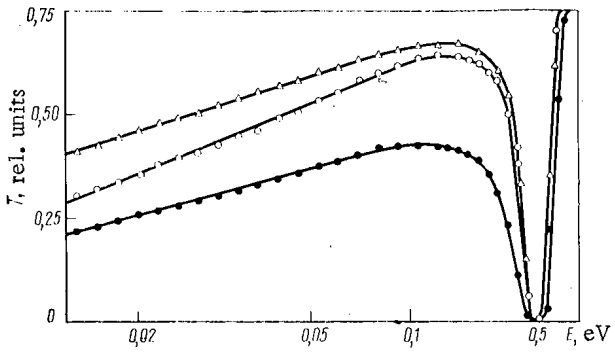

Fig. 2. Total neutron cross section of ^{168}Yb in energy range 0.014-1 eV. The peaks are reduced by a factor of 50.

Fig. 3. Transmission of unirradiated specimen and two transmissions of irradiated specimens in energy range 0.014-1 eV. Solid circles: prior to irradiation; open circles: 6 days after irradiation; triangles: 80 days after irradiation.

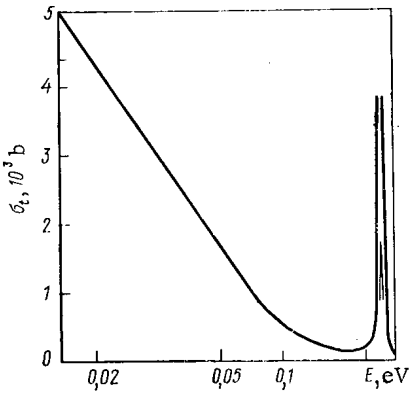

Fig. 4. Total neutron cross section of ^{169}Yb in energy range 0.014-1 eV. The peaks are reduced by a factor of 5.

TABLE 3. Parameters of Neutron Resonances of ^{169}Yb

E_0, eV	Γ^*, MeV	$2g\Gamma_n$, MeV	E_0, eV	Γ^*, MeV	$2g\Gamma_n$, MeV
0,807±0,005	(80)	0,42±0,03	23,3±0,1	(80)	2,9±0,5
1,32±0,01	(80)	0,046±0,08	24,1±0,1	(80)	1,0±0,5
2,19±0,02	72±9	0,42±0,04	25,1±0,1	(80)	2,9±0,5
6,90±0,04	(80)	0,35±0,05	28,3±0,1	(80)	10,2±1,5
8,57±0,06	(80)	0,55±0,08	33,5±0,2	(80)	14,7±7,0
9,20±0,06	75±11	2,7±0,2	33,9±0,2	(80)	9,3±5,0
12,31±0,07	93±12	2,4±0,2	37,4±0,2	(80)	2,6±1,6
12,53±0,07	(80)	1,6±0,2	41,6±0,2	(80)	11,2±2,6
13,46±0,08	(80)	1,1±0,4	43,2±0,2	(80)	5,7±2,3
14,66±0,08	103±26	6,2±0,6	45,4±0,2	(80)	20±10
21,8±0,1	(80)	5,5±0,6			

*Γ = 80 MeV was taken as the mean of the measured values for levels with E_0 = 2.19; 9.20; 12.30 and 14.66 eV..

Table 3 gives the neutron resonance parameters of ^{169}Yb, while Fig. 3 offers the results of two measurements of the transmission of an irradiated specimen and one measurement of that of an unirradiated specimen in the thermal range of neutron energies. The measurement interval for the irradiated specimen was 70 days. The differences in the transmission for the irradiated specimen can be accounted for by changes in the amount of ^{169}Yb and ^{169}Tm.

The total neutron cross section of ^{169}Yb in the thermal range of neutron energies is shown in Figs. 4. The behavior of the total neutron cross section of ^{169}Yb in the thermal range cannot be described by the resonance parameters of the positive levels. For ^{169}Yb we have $\sigma_\gamma^{2200} = (3600 + 300)$ b. The calculated value of $I_\gamma = (3800 + 500)$ b. The error in the measurement results is determined primarily by the contribution of the error in determining the amount of ^{168}Yb (5%) and ^{169}Yb (8%).

Our results enabled us to estimate for ^{168}Yb the mean distance between levels: $\overline{D} = 9$ eV and the force function: $S_0 = 2.4 \cdot 10^{-4}$. For ^{169}Yb the calculated values are $\overline{D} = 2.2 \pm 0.5$ eV and $S_0 = (2.1 \pm 0.7) \cdot 10^{-4}$.

LITERATURE CITED

1. T. S. Belanova et al., Preprint NIIAR, P-6(272), Dmitrovgrad (1976).
2. Neutron Cross Sections (3rd ed.), Vol. 1, BNL-325 (1973).
3. V. Sailor et al., Phys. Rev., 96, 1014 (1954).
4. V. P. Vertebnyi et al., in: Neutron Physics [in Russian], Part 1, Naukova Dumka, Kiev (1972), p. 181.
5. H. Liou, Phys. Rev., C7, No. 2, 823 (1973).

LETTERS

CHOICE OF OPTIMAL CONDITIONS OF EXPERIMENT TO FIND STOPPING POWER OF A SUBSTANCE BY STREAMING OF RADIATION THROUGH ABSORBERS OF ANY ARBITRARY THICKNESS

G. N. Potetyunko

UDC 539.12.04

In two earlier papers [1, 2] the present author proposed a new method of finding the stopping power of a substance from the results of experiments on radiation streaming through absorbers and developed the mathematics of the method. The application of the proposed [2] method of processing the experimental data was not related to any limitations on the absorber thickness; this permitted use of thicker absorbers than employed hitherto, thus reducing the error of determination of dE/dx introduced by the error in the value of the thickness. This circumstance is especially important when finding dE/dx in the region of the maximum of the dE/dx curve or before it where the standard method of finding dE/dx ($\Delta E/\Delta x$) gives overly large statistical and methodological errors [1]. Let us point out that apparently this is precisely why in the region of the maximum the error of reproduciblity, caused by the spread between the results of different authors, is substantially higher than at a higher energy [3] and greatly exceeds the statistical error of the experiments.

With an increase in the thickness of the absorber, however, the energy straggling also grows and, along with it, so do the attendant errors. Accordingly, there arises the question of the necessity of choosing the optimal conditions for the experiment. This conclusion is also confirmed by the results of numerical experiment [2] from which it follows that the experimental conditions affect the accuracy of the determination of dE/dx.

The gist of the problem is: on the basis of the published data obtained under different experimental conditions find how these conditions affect the accuracy of determination of dE/dx and, to the extent possible, to make particular tentative conclusions as to the optimal conditions.

The choice of experimental conditions boils down to the choice of the energy range in which dE/dx is determined and to the choice of the initial values of the beam energy and absorber thickness. The choice of the energy range is usually determined by the conditions of the problem. On the other hand, the choice of the values of the initial beam energy and absorber thickness can be made in various ways.

1. The initial beam energy is fixed and the abworber thickness is increased so that at maximum thickness the beam energy after the absorber would correspond to the minimum energy of the chosen energy range.

2. The absorber thickness is fixed and the beam energy is varied within the limits of the range chosen.

3. At several values of absorber thickness the beam energy is varied in more or less small steps or, conversely, at several beam energies the absorber thickness is varied within certain limits.

The results of experiments on streaming radiation through absorbers, allowing the technique of [2] to be employed, were given in [4,5]. The conditions of the experiments in these papers were different and it is therefore possible to reveal the effect of the experimental conditions on the accuracy of dE/dx.

Al-Bedri et al. [4] presented the results for protons in the energy range 0.3-1.6 MeV and the following media: melinex, aluminum, copper, and gold. The scheme of the experiment in the main corresponded to variant 1 formulated above: the number of values of the initial beam energy for each medium was two or three and for each value of beam energy the absorber thickness was varied within quite wide limits. The energy loss in this case ranged from 5 to 95-100% of the energy range.

Translated from Atomnaya Énergiya, Vol. 49, No. 2, pp. 119-121, August, 1980. Original article submitted January 24, 1979.

 0038-531X/80/4902-0564$07.50

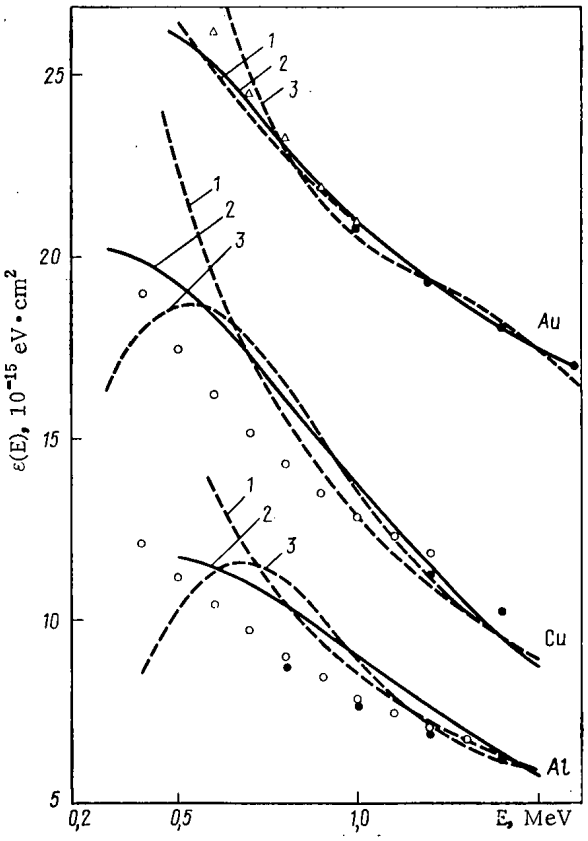

Fig. 1. Values of cross sections for proton stopping in aluminum, copper, and gold, obtained by processing the experimental data of [4] by the technique of [2]: ○) data of [6]; Δ) data of [7]; ●) data of [8].

Bourland et al. [5] gave the results for α particles in the energy range from 0.3 to 2.0 MeV. The medium was oxygen. The scheme of the experiment corresponded to variant 2: the target thickness was practically constant while the energy of the beam was varied. The energy loss was 5-20% of the energy range. The values of the initial beam energy and the particle energy after the absorber were distributed quite uniformly over the range.

The results of the processing of the experimental data of [4] are given in Figs. 1 and 2. The numbers next to the curves in these figures denote the degree of the polynomial in the energy used to approximate $(dE/dx)^{-1}$.

For gold, first and second-degree polynomials give results which practically coincide and are in fair agreement with the experimental data (see Fig. 1). We should only note the weakly expressed irregular bend in the curve in the low-energy range in the case of the second-degree polynomial. The third-degree polynomial makes the dE/dx curve begin to "wander" around the truve curve, deviating from it slightly only in the low-energy range. The wandering of the curve is explained by the fact that the degree of the polynomial is commensurate with the number of experimental points so that the statistical spread of the experimental data is affected. For aluminum and copper, polynomials of all three degrees yield results which are in poor agreement with the experimental data, with the third degree giving altogether absurd results.

For melinex (see Fig. 2), the first- and second-degree polynomials yield results which Practically coincide with each other while the third degree gives appreciably different results.

Thus, if the experiment is in accord with variant 1 formulated above, the results for dE/dx are unstable: along with correct results (gold) incorrect results are also obtained (aluminum, copper). More over, there is no stability of results in relation to an increase in the degree of the polynomial for $(dE/dx)^{-1}$.

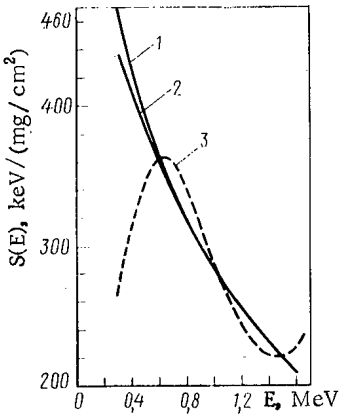

Fig. 2

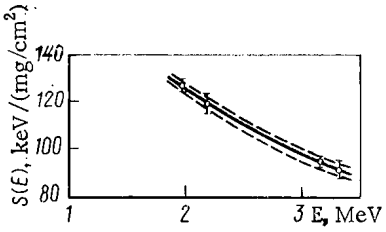

Fig. 3

Fig. 2. Values of mass stopping power of melinex for protons, obtained by processing the experimental data of [4] by the technique of [2].

Fig. 3. Values of mass stopping power of kovar for deuterons, taken from [9] (○) and obtained in the present paper by the technique of [2] with the use of the experimental data of [9] (——); - - -) "corridor of error."

TABLE 1. Stopping Cross Section for α-particles in Oxygen

E, keV	ε(E), 10^{-15} eV·cm²/mol.			E, keV	ε(E), 10^{-15} eV·cm²/mol.		
	results of [5], $\varepsilon_1(E)$	results of present paper, $\varepsilon_2(E)$	$\frac{\varepsilon_2-\varepsilon_1}{\varepsilon_1}$, %		results of [5], $\varepsilon_1(E)$	results of present paper, $\varepsilon_2(E)$	$\frac{\varepsilon_2-\varepsilon_1}{\varepsilon_1}$, %
300	81,8	81,9	0,1	1200	90,2	90,6	0,4
400	89,0	89,5	0,6	1300	87,8	87,9	0,1
500	93,4	94,3	1,0	1400	85,3	85,1	—0,2
600	96,0	96,9	0,9	1500	82,8	82,4	—0,4
700	97,0	97,9	0,9	1600	80,4	79,8	—0,7
800	96,9	97,7	0,8	1700	78,2	77,6	—0,8
900	96,0	96,7	0,7	1800	76,2	75,7	—0,7
1000	94,4	95,1	0,7	1900	74,0	74,2	—0,2
1100	92,4	93,0	0,6	2000	72,0	72,7	0,9

When α-particles pass through oxygen the polynomials for $(dE/dx)^{-1}$ up to the sixth degree give results which are in good agreement with [5]. Table 1 gives values of the stopping cross section taken from [5] and those which we obtained by using sixth-degree polynomials for $(dE/dx)^{-1}$. A further increase in the degree leads to wandering of the dE/dx curve.

Thus, experiments formulated in accordance with variant 2 give quite reliable results which are stable under an increase in the degree of the polynomial for $(dE/dx)^{-1}$.

Therefore, the results of our paper along with the results of [2] permit the first tentative conclusions to be drawn about the optimal conditions of experiments on determining dE/dx by the method of [2]. It is desirable to conduct the experiment according to the scheme in which, at several values of absorber thickness, the initial energy beam is changed in quite small steps. The absorber thickness is preferably taken so that the energy loss in it amounts to ∿ 5-20% of the energy range. The initial values of the beam energy must be distributed approximately uniformly over the energy range.

Along with the choice of optimal conditions of the experiment to determine dE/dx it is of interest to develop a technique for finding the corresponding variances. Comparative

analysis of the various methods of finding the variances can be conducted according to the results of [9]. That paper, in particular, gives the results of measurements of the mass stopping power of Kovar for deuterons by the $\Delta E/\Delta x$ method (under conditions when this method gives reliable results), the corresponding errors, and the experimental material necessary for processing by the technique of [2]. The analysis showed that the method of finding the errors [2], based on the classical theory of the transfer of the latter, gives results which are underestimated by a factor of 1.5-2 in comparison with the results of [9]. More exact results are obtained by using the following technique. Suppose that y_p is some experimental value of the ratio of the absorber thickness to the energy loss in it and $s(y_p)$ is the variance of that value. We process the experimental material according to the technique of [2] at values of the ratio of absorber thickness to energy loss in it equal to y_p and $y_p \pm s(y_p)$ and we take the difference of the corresponding values of dE/dx to be their variance. Figure 3 gives the results of such processing of the experimental data of [9]. It is seen that our results are in good agreement with the results of that paper.

LITERATURE CITED

1. G. N. Potetyunko, At. Energ., 41, No. 2, 134 (1976).
2. G. N. Potetyunko, At. Energ., 43, No. 2, 118 (1977).
3. G. N. Potetyunko, Izv. Vyssh. Uchebn. Zaved., Fiz., No. 9, 123 (1979).
4. M. Al-Bedri, S. Harris, and H. Parish, Rad. Effects, 27, No. 3-4, 183 (1976).
5. P. Bourland, W. Chu, and D. Powers, Phys. Rev. B, 3, No. 11, 3625 (1971).
6. D. Kahn, Phys. Rev., 90, No. 4, 503 (1953).
7. D. Green, J. Cooper, and J. Harris, Phys. Rev., 98, No. 2, 446 (1955).
8. H. H. Andersen et al., Phys. Rev. A, 16, No. 5, 1929 (1977).
9. C. Shepard and L. Porter, Phys. Rev. B., 12, No. 5, 1649 (1975).

CRITERION OF IGNITION AND RESERVE AT IGNITION FOR THERMONUCLEAR TARGETS

Yu. S. Bakhrameev, V. N. Mokhov, and N. A. Popov

UDC 533.92

In comparing various types of thermonuclear targets compressed by the action of external energy sources (lasers, electron beams, magnetic fields, etc.), the relation of the thermonuclear energy obtained to that expended and to the demands placed on the energy source to ignite the target (the energy delivered and the character of its growth in time), we usually consider the quality of the target as the basic parameter. However, in order to obtain a real thermonuclear flash in compressing systems, it is necessary to have a certain reserve at the ignition in order to compensate for calculational inaccuracies and possible variation of real parameters from their calculated values. Therefore, it may be incorrect to compare targets without calculating their reserve at ignition.

At the present time sufficiently powerful external energy sources have not been created and we are lacking the possibility of experimentally checking the thermonuclear combustion of various types of targets. It is necessary to have an understanding of the reserve at ignition in order to unambiguously define the target characteristics, which is especially important, particularly for a more correct comparison of various targets. Below we will present one of the possible criterion of ignition and the corresponding definition of the reserve at ignition. This criterion is practically the generalized Lawson criterion [1] for a dynamic system.

We will examine a target of volume Ω, which has a mass M of thermonuclear fuel. In the process of compression, the target volume $\Omega(t)$ and the matter temperature $\theta(t)$ change with time t. The change of entrophy $S(\Omega, \theta)$ is defined by

Translated from Atomnaya Énergiya, Vol. 49, No. 2, pp. 121-122, August, 1980. Orginal article submitted April 23, 1979.

0038-531X/80/4902-0567$07.50

$$\frac{dS}{dt}=\frac{1}{0}Q_{\text{tn}}(\Omega, 0)-\frac{1}{0}Q_{\text{th}}\quad(\Omega, 0, t)\ \ldots, \tag{1}$$

where Q_{tn} is the thermonuclear energy generated and Q_{th} is the thermal loss.

If we consider nuclear fuel consisting of only tritium and deuterium, then

$$Q_{\text{tn}}=q_1(\sigma v)_{dd}\frac{N_d^2}{\Omega}+q_2(\sigma v)_{dt}\frac{N_dN_t}{\Omega},$$

where $(\sigma v)_{dd}$ is the thermonuclear reaction rate for deuterium into two approximately equal channels (producing ^{3}He or T) [1, 2], N_d and N_t are the number of deuterium and tritium atoms in the volume Ω, and q_1 and q_2 are energies which are released by the corresponding thermonuclear reactions in the volume Ω. In particular, if the neutrons remove their entire energy from ≈ and the charged particles are completely retained in it, then q_1 Ω 1.3 MeV and $q_2 \approx 3.6$ MeV. At the same time the possible reactions of neutrons and ^{3}He are not calculated.

We will assume that we know the solution to a complete system of equations describing the compression and initial heating of a target without calculating the thermonuclear reactions. From this solution we know the temporal change in the volume V(t) and the temperature T(t) of the above mass of matter M. These quantities conform to equation

$$\frac{dS(V, T)}{dt}=\frac{1}{-T}Q_{\text{th}}\quad\{V, T, t\}. \tag{2}$$

To determine the criterion of ignition, we will examine the very beginning of heating when (and also long before this) $\theta(t) \approx T(t)$, the significant difference between T(t) and θ(t) comes later. Concerning this, it is possible to neglect the depletion of nuclear fuel, i.e., suppose N_d = const and N_t = const, furthermore, we may consider that Ω(t) = V(t), because the rate of change dΩ/dt is weakly dependent on the temperature, and time is necessary for the difference to develop.

Equation (1) determines the temperature θ(t) from the values of V(t), which we assume to be well known. To obtain an approximate analytical expression for θ(t) we will isolate the basic dependence of $(\sigma v)_{dd}$ and $(\sigma v)_{dt}$ on θ in the range of temperatures where ignition occurs (θ ≈ 2-6 keV), as a power function:

$$(\sigma v)_{dd}=\theta^m f_1(0)\ \text{and}\ (\sigma v)_{dt}=\theta^m f_2(\theta),$$

where $m \approx 4$, and $f_1(\theta)$ and $f_2(\theta)$ in the selected interval θ are weakly dependent on the temperature.

Following this, in the weakly temperature-dependent functions, for θ we will substitute T, i.e., we put $f_1(\theta) \approx f_1(T)$ and $f_2(\theta) \approx f_2(T)$. In the same manner, we will put $\theta_{th}\{\Omega, \theta, t\}/\theta \approx \theta_{th}\{V, T, t\}/T$, as the temperature dependence of the heat flow, in the cases of interest, is moderate (bremstrahlung loses, electron thermal conductivity). By calculating all that stated above from expressions (1) and (2), we obtain an equation for the temperature in the form

$$\frac{d}{dt}[S(V, \theta)-S(V, T)]=\left(\frac{0}{T}\right)^{m-1}\frac{Q_{\text{tn}}(T, V)}{T}, \tag{3}$$

which, for the case of an ideal gas with an equation of state E = AMT, allows us to reach the following solution:

$$\theta(t)=T(t)/\left[1-(m-1)\int_{-\infty}^{t}\frac{Q_{\text{tn}}(T, V)}{AMT}\,dt\right]^{\frac{1}{m-1}}. \tag{4}$$

Let us call the moment of ignition that moment when θ(t), according to formula (4), becomes infinite. In reality, at a high temperature its growth ends due to dispersal and burnout of the target matter and weakening of the dependence of $(\sigma v)_{dd}$ and $(\sigma v)_{dt}$ on T. However, for the characteristics of ignition (we are not interested, in this work, in fuel energy release) this is irrelevant. Thus, ignition of a system is determined by the expression

$$W(t) = (m-1)\int_{-\infty}^{t} \frac{Q_{th}(T, V)}{AMT}\, dt. \qquad (5)$$

If we find such a volume V in the target, which has, at the moment t W > 1, that target will ignite. To characterize the reserve at ignition, we propose to use $W(t_m)$, the value of W at the moment of maximum compression, t_m of the region of the target considered. A limitation at this time is connected with the fact that after the maximum compression during the dispersal of the target matter, pertubations usually grow very quickly and turbulent mixing occurs. Therefore if the system does not ignite at time t_m then the probability of ignition is generally small.

The criterion for whether or not ignition is obtained in a system which during time has a constant density τ and temperature T, is expressed by the well-known Lawson criterion [1]:

$$n\tau > \frac{AMT}{Nq_2(\sigma v)_{dt}} \frac{4}{m-1}, \qquad (6)$$

where $n = 2n_d = 2n_t$ is the density of the nuclei, and N is the total number of nuclei in the D + T mixture. At the minimal value of the right-hand side of inequality (6) (at $T \approx 15$-20 keV), we get $n\tau > 10^{14}$ cm^{-3}· sec.

The criterion of ignition found and the subsequent understanding of the reserve at ignition $W(t_m)$ might be easily extended to more complex cases. For example, when the temperatures at various points in the volume Ω are unequal, or when the equation of state of the matter is not that of an ideal gas, a more exact calculation of the dependence of Q_{th} on temperature is required. Also to be considered are systems with admixtures of various chemical elements in the nuclear fuel or with other types of fuel. This article does not make a recommendation on the selection of the volume V, as this is intimately connected with the concrete construction of a target and the fulfillment of the approaches shown above.

For the majority of practically interesting systems the use of the proposed criterion does not cause difficulties and gives satisfactory accuracy. The authors understand, however, that systems are possible for which criteria of another type might be more expedient.

LITERATURE CITED

1. S. Yu. Luk'yanov, in: Hot Plasma and Controllable Nuclear Synthesis [in Russian], Nauka, Moscow (1973), p. 17.
2. B. N. Kozlov, At. Energ., 12, No. 3, 238 (1962).

NONDESTRUCTIVE METHOD FOR THE CONTROL OF NONIRRADIATED NUCLEAR REACTOR FUEL USING A PULSED NEUTRON SOURCE

S. B. Shikhov, V. L. Romodanov,
V. G. Nikolaev, V. A. Luppov,
and D. F. Rau

UDC 621.039.516.22

Significant progress in the area of experimental methods of nuclear physics has recently caused a wide circulation of nuclear-physical methods of analyzing the composition of expensive prepared products without their destruction [1, 2]. This is related to the definition of the contents of ^{235}U in the fuel elements of nuclear reactors.

The physical basis of the proposed method of control of the fissionable matter consists of the following. The pulsed neutron source irradiates the moderator block, after slowing down, the thermal neutrons enter the sample studied where fission of ^{235}U occurs. The fast neutrons from fission, slowed in another moderator block surrounded by a neutron absorbing screen, are recorded by thermal neutron counters. To calculate the shielding by the internal layers of the fuel, thermal neutron counters are used. There are arranged in such a way as to record the transmission of thermal neutrons through the sample (Fig. 1).

The temporal behavior of the neutron current in the detector of fission neutrons, which consists of moderator 3 and thermal neutron counter 6, for times after the pulse of the source, may be described by the following expression

$$\Phi(t) = A \exp(-\alpha t) + B \exp(-\beta t) + \Phi_0. \quad (1)$$

The first term characterizes the temporal decrease in moderator 3 of the thermal neutrons which are formed form the secondary neutrons arising as a result of the fission of ^{235}U nuclei by thermal neutrons. Here α is the time constant of thermal neutrons in moderator 1, as these neutrons, which cause fission of ^{235}U, will have a rate of decrease which is determined by the material and geometry of moderator 1. The coefficient A depends on the concentration of ^{235}U and is proportional to the power of the source. The second term reflects the temporal decrease of thermal neutrons which are formed as a result of the slowing down of the source neutrons in moderator 3, β is the time constant of thermal neutrons in moderator 3. The coefficient B is proportional only to the source power. The material and sizes of the moderators are selected to satisfy the condition $\beta > \alpha$, Φ_0 is determined by the delayed neutrons and is constant, if the repetition period of the pulsed source is much less than the minimum half-life of the delayed neutrons, Φ_0 is also proportional to the source strength.

We will designate by N_A, N_B, and N_0 the portions of each component of the flux $\Phi(t)$ of the total neutron number flux recorded in the interval of time (t_0, t_1), where t_0 and t_1 are the beginning and end of the analysis interval (e.g., $N_A = \int_{t_0}^{t_1} A \exp(-\alpha t)\, dt$).

We determined the functions:

$$F(\rho\gamma_5) = N_A/N_B; \quad (2)$$

$$\varphi(\gamma_5/\gamma_8) = N_0/N_A. \quad (3)$$

Here ρ is the fuel density, γ_5 and γ_8 are the concentrations of ^{235}U and ^{238}U in the sample. The functions $F(\rho\gamma_5)$ and $\phi(\gamma_5/\gamma_8)$ do not depend on the source strength, their value is measured in a single electronic channel and we thereby eliminate errors associated with instabilities of the apparatus. One may determine the content of ^{235}U in the sample if one compares the values of the functions $F(\rho\gamma_5)$ and $\phi(\gamma_5/\gamma_8)$ with their analogs on the calibragraph.

Translated from Atomnaya Énergiya, Vol. 49, No. 2, pp. 122-123, August, 1980.
Original article submitted August 6, 1979.

 0038-531X/80/4902-0570$07.50

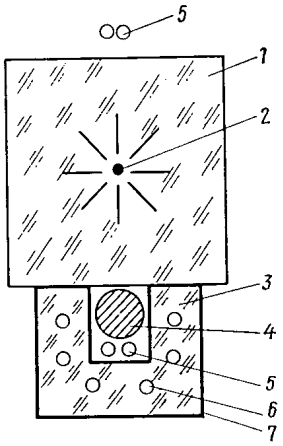

Fig. 1

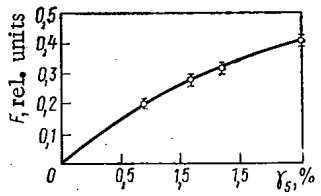

Fig. 2

Fig. 1. The experimental arrangement: 1) Moderator block for source neutrons, 2) pulsed neutron source, 3) moderator block for fission neutrons, 4) sample studied, 5) thermal neutron counter measuring transmission through the sample, 6) thermal neutron counter, 7) cadmium shield.

Fig. 2. Dependence of the function F on the concentration of ^{235}U (ρ = 18.7 g/cm^3).

A constructed and optimized arrangement was used for experimentally checking the method. It seems that the accuracy of determining the concentration is essentially dependent on the ratio of the time constants β and α. By optimally measuring the arrangement we get the following values for the time constants: $\beta = (31920 + 100)$ sec^{-1}, $\alpha = (5890 + 5890 + 56)$ sec^{-1}. Organic glass served as the material for the moderators. The characteristic dependence of function F on the concentration of ^{235}U is shown in Fig. 2. The temporal range of analysis of $\Phi(t)$ was the following: t_0 = 250 μsec, t_1 = 2000 μsec. The neutron source was a neutron generator with a frequency of neutron pulses equal to 450 Hz and the mean strength was $\sim 10^8$ neutrons/sec. The accuracy of determining the concentration here was equal to 5%. The value is not limiting and can be improved in the future.

LITERATURE CITED

1. V. V. Frolov, Nuclear-Physical Methods of Controlling Fissionable Materials, [in Russian], Atomizdat, Moscow (1976).
2. T. Dragnev, At. Energy Rev., 11, 341 (1973).

STUDY OF THE FIELD OF SECONDARY RADIATION BEYOND LEAD ABSORBERS IRRADIATED BY 640-MeV PROTONS

A. Ya. Serov, B. S. Sychev,
S. I. Ushakov, and E. P. Cherevatenko

UDC 539.12.175

This work, an extension of [1], measures the space—energy and radial distribution of secondary radiation which exits when a lead absorber is under bombardment by a beam of 640-MeV protons. The thickness of the absorber along the beam direction is d = 60 cm (680 g/cm^2); the cross-section is 70 × 40 cm. The proton beam diameter at the forward end of the absorber (from the beam side) is 2.5 cm (Fig. 1).

The beam is monitored with an ionization chamber calibrated by way of measuring the absolute yield of products of the reactions ^{27}Al(p, 3pn)^{24}Na, ^{27}Al(p, spall) ^{18}F and ^{12}C (p, pn)^{11}C in aluminum foil and graphite plates. During this work, data from [2] concerning the cross sections of these reactions were used. The estimated calibration error was ∿10%. The energy spectra were measured by a spectrometer along with the time of flight with time resolution 2 τ = 1 nsec and with a proton detection threshold of 60 MeV. A more detailed description of the spectrometer is given in [3].

The spectra of protons were measured at a constant distance of 1 m from the absorber end to the first counter and a distance L = 2.36 m between base counters (spectrometer base). The angular resolution was $5.7 \cdot 10^{-4}$ Sr. The cross section of the spot "viewed" by the spectrometer on the end of the absorber was 9.8 × 9.8 cm^2. The systematic error (∿ 12%) of the measured spectra of protons was determined by the error of monitoring (10%), by the inaccuracy of the alignment of the spectrometer (6%), and also by the portion in the spectra of charged $\pi^{\pm}$ mesons and protons which occur during the interaction of neutrons with the material of the scintillator in the first counter (∿4%). The background level, which is determined with experimental samples, does not exceed 1%.

The measured distribution of the secondary yield is seen in Fig. 2. The cross-hatched region of indeterminancy is caused by the statistical error, energy resolution of the spectrometer, and in the region of energy below 150 MeV, by the indeterminancy of the correction for multiple coulomb scattering. The systematic error is not calculated.

This work will present a calculation of fields of secondary radiation which are formed during the development of an internuclear cascade in the given lead absorber with the help of program CASC-2 [4], which realized the method of successive collision, applied to calculating an internuclear cascade in the axisymmetric geometry [5]. The system of constants D2N1 [4, 6] was used as the input information. This work also experimentally determined the radial distribution of the fluence of secondary particles and absorbed doses. Carbon detectors, nuclear emulsion of type K, and x-ray film were used for measurements. The absolute yield of the reaction ^{12}C(x, xn)^{11}C in the irradiated carbon detectors was measured using the scintillation γ spectrometer. The cross section of this reaction for secondary nucleons of energy E > 20 MeV was equal to 21 mb (1 b = 10^{-28} m^2) [2]. From the data in [7] it follows that the effective region of the registration of protons in nuclear emulsion of type K corresponds to the energy interval 0.5-150 MeV. X-ray films, intended for measuring the exposed dose of γ radiation, were used for measuring the absorbed dose in this work. The response of the x-ray films was interpreted in terms of an absorbed dose, considering the data relative to its sensitivity to the protons [8]. Experimental and calculated data on the radial distribution of detector readings are seen in Fig. 3.

The fraction of protons and $\pi^{\pm}$ mesons in the fluence of hadrons beyond the lead absorber of such a thickness is 2-3%. Figure 4 shows the angle integrated energy spectra of protons and neutrons for various distances r. The data from this diagram (originally for

Translated from Atomnaya Énergiya, Vol. 49, No. 2, pp. 123-124, August, 1980.
Original article submitted September 28, 1979, revision submitted March 26, 1980.

0038-531X/80/4902-0572$07.50

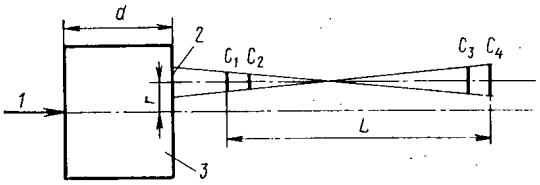

Fig. 1. Geometry of the experiment: 1) incident protons; 2) "spot"; 3) lead.

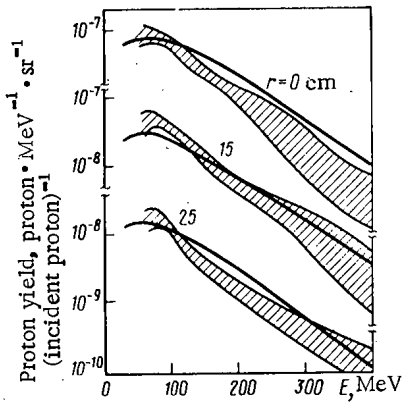

Fig. 2. Energy spectra of protons emitted from the surface of the lead absorber at various distances r from the beam axis at angle $\theta = 0°$: the cross-hatched section is the experiment; ——) calculation.

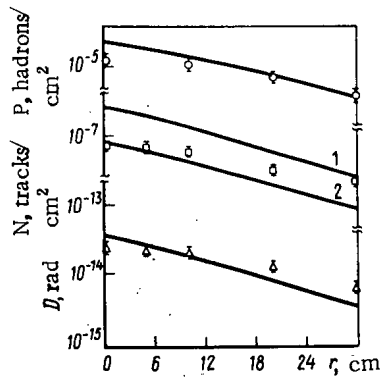

Fig. 3

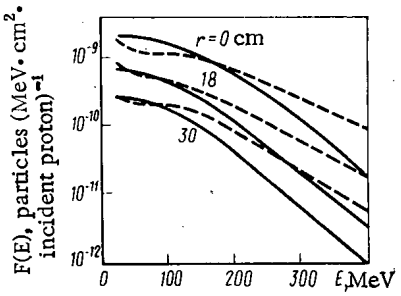

Fig. 4

Fig. 3. Experimental (○, □, Δ) and calculated (——) data on the radial distribution of detector readings beyond the lead absorber, ○) F, fluence of hadrons with energy E > 20 MeV, □) N, density of tracks in nuclear emulsion, Δ) D, absorbed dose (measured by the blackening of the x-ray films), calculation of N: 1 and 2) E_{thr} = 150 and 50 MeV.

Fig. 4. Calculated energy spectra of protons and neutrons at the surface of a lead absorber at various distances from the axis of the beam: ——) protons, - - -) neutrons (the calculated data have been multiplied by 0.01).

calculating the fluence of hadrons) clearly illustrates the small fraction of protons in the field of nucleons.

Since we cannot reliably determine the effective correct threshold of the response of the emulsion K, the experimentally measured number of tracks will be compared with the calculated data in Fig. 3, which corresponds to the values of the threshold 50 and 150 MeV. A comparison of the experiment and the calculation show their fully satisfactory agreement.

In conclusion, the authors wish to express their thanks to V. P. Dzhelepov for support of the work, Yu. M. Kazarinov and V. S. Kiselev for assistance in its execution. We are grateful to M. M. Komochkom, M. I. Salatskoi, and G. N. Timoshenko for showing methodical help. Throughout the entire work we were constantly helped by our colleagues E. K. Gel'fand, A. A. Dem'yanov, and Yu. A. Razumov, to whom we are deeply grateful.

LITERATURE CITED

1. A. Ya. Serov and B. S. Sychev, At. Energ., 45, No. 3, 235 (1978).
2. E. Bruninx, CERN-61-1, Geneva (1961).
3. A. Ya. Serov and B. S. Sychev, in: Methods of Controlling Accelerators [in Russian], Proceedings of the Radiotechnical Institute, No. 25, Academy of Sciences of the USSR, Moscow (1976), p. 176.
4. E. K. Gel'fand et al., in: Questions of Dosimetry and Radiation Shielding, [in Russian], No. 18, Atomizdat, Moscow (1979), p. 160.
5. A. Ya. Serov, E. K. Gel'fand, and B. S. Sychev, in: Thesis. Second All-Union Conference on the Shielding of Nuclear-Technical Arrangements from Ionizing Radiation, MIFI, Moscow (1978), p. 28.
6. A. Ya. Serov and B. S. Sychev, in: Charged Particle Accelerators [in Russian], Proceedings of the Radiotechnical Institute, No. 14, Academy of Sciences of the USSR Moscow (1973), p. 173.
7. M. M. Komochkov, et al., Report of the Joint Institute for Nuclear Research 13-10188, Dubna (1976).
8. A. Ya. Serov and B. S. Sychev, in: Proceedings of the Fifth All-Union Conference on Charged Particle Accelerators, [in Russian], Vol. 1, Nauka, Moscow (1977), p. 210.

FIELD EMISSION MICROSCOPE STUDY OF RADIATION DAMAGE IN TUNGSTEN CAUSED BY ^{252}Cf FISSION FRAGMENTS

V. M. Aleksandrov, I. A. Baranov,
R. I. Garber, Zh. I. Dranova,
A. S. Krivokhvatskii, I. M. Mikhailovskii,
and V. V. Obnorskii

UDC 537.534:539.16

The characteristics of radiation damage significantly depend on the type of material, its structure [1, 2], the energy and nature of the particles of the penetrating radiation [3], and also the radiation dose [4]. Radiation damage of tungsten by fission fragments was studied [5, 6] with the help of the field emission microscope. Irradiation was carried out in the core of a reactor using ^{235}U as the fissionable material. However, the interpretation of the results obtained caused definite difficulties due to the continuous energy spectra of fission fragments in the region up to 100 MeV, connected with the great thickness of the ^{235}U layer, which exceeded the range of the fission fragments. Therefore, this work used a thin layer of ^{252}Cf as the source of fission fragments, becasue the energy spectra of ^{252}Cf has two maxima. Since the tungsten needles arrange the perpendicular flow of fission fragments, we succeeded in exposing the deformation of the structure and other defects which had not been detected in previous studies [5, 6].

Translated from Atomnaya Énergiya, Vol. 49, No. 2, pp. 124-126, August, 1980.
Original article submitted October 4, 1979.

 0038-531X/80/4902-0574$07.50

Experimental Method. The irradiated samples presented their own point, which was formed by electrochemical etching from a tungsten wire of 99.95% purity and exposed subsequently to low-temperature evaporation in an electric field of high intensity ($\sim 5 \cdot 10^8$ V/cm) for the purpose of forming an atom-smooth surface. The irradiation was conducted in a vacuum chamber, here the point arranged the perpendicular flow of fission fragments at a distance of 6 mm from the layer of ^{252}Cf with thickness 10 $\mu g/cm^2$. The intensity of the current of fission fragments over 4π sr was $3.5 \cdot 10^6$ sec^{-1}. The fission fragments were collimated in angle by $\pm 25°$. The time of irradiation was chosen in order to provide the incidence of several fission fragments onto the peak of the point. To cut-off nuclear recoils of ^{248}Cm of energy 100 keV due to the α decay of ^{252}Cf, and also to prevent contamination of the vacuum chamber and samples, the layer of californium was covered by two thin films of nickel of a combined thickness of 200 $\mu g/cm^2$. The mean energy of heavy and light fission fragments is, accordingly, 69 and 96 MeV (Fig. 1). Since ^{252}Cf is simultaneously the source of α-particles of energy 6.1 MeV, and also of fission neutrons of mean energy 2 MeV, it is necessary to evaluate the additional fraction in the radiation damage of the tungsten needles. Having information [5] about the role of fission neutrons and the low value of the fluence of fast neutrons for the irradiated points (less than $1 \cdot 10^{12}$ neutrons/cm^2) allows us to neglect the influence of such a factor. The dose of α-particles which hit the point is $2 \cdot 10^{12}$ particles/cm^2. The control experiment of irradiating tungsten needles with an equivalent current of α-particles was carried out using a ^{238}Pu source. To cut-off the nuclear recoils of ^{234}U with energy 100 keV, which occur from the α-decay of ^{238}Pu, the layer of plutonium was covered by a thin film of nickel.

The irradiated samples were studied in a helium field emission microscope with cooling of the tungsten needles by liquid nitrogen. The image is registered using an electron-optical transformer with an amplification coefficient of 10,000. The microphotographs of the surface of the irradiated samples were studied by the distribution of the field-emission contrast and by its changes in the process of controlled evaporation of atomic layers (110) with a field .

Results of the Experiment and Discussion. The control samples, irradiated by α-particles from a plutonium source to a dose of $2 \cdot 10^{12}$ cm^{-2}, after the desorption by an electric field of two-four atomic layers, showed practically atomic layers, showed practically an atom-smooth surface. Evaporation of the material of the samples to a depth 10^2 nm did not show extended damage to the lattice. The characteristic atom-smooth surface of a tungsten point with a radius of curvature at the top of 21 nm irradiated by α-particles is seen in Fig. 2.

In the samples irradiated with fission fragments, we see surface damage as depressions with a mean diameter of up to 7 nm. Immediately after irradiation of samples with fission fragments and the removal from their surface of absorbed atoms, we can observe two depressions in the area of the faces (101) and (011) having a type of crater connected with bright contrast bands (Fig. 3). An analysis of a series of microphotographs obtained during laminar evaporation by the field shows that the craters are arranged on a line perpendicular to the axis of the sample, and, evidently, correspond to the point of entrance and exit of the fragment. Such a correlated arrangement of depressions is observed in all irradiated samples. In individual cases over the area of the passage of the fragment we see the damaged zones of width up to 9 nm (Fig. 4), indicating that the passage of the fission fragment in the surface layer essentially changes the topography of this surface region. In Fig. 4a, b the divergence of the axis of the fragment track from the surface reaches 12 nm, but similar distortions are detected even after the passage of the fragment to a depth of 15 nm. An analysis of a series of field emission microphotographs allows us to construct the dependence of the width of the damage zone on the depth of the axis of the fragment track (Fig. 5). During the increase of the intensity of the electric field ($> 4.5 \cdot 10^8$ V/cm), inside damage zones separate atoms appear; these zones are characterized by porous layers. Similar damage was not detected earlier [5, 6], possibly due to the use of samples arranged almost parallel to the current of fragments, many of which were slowed down inside the source. The appearance of big craters is connected [5] with the action of a return pulse which occurs in the case when the fragment does not exit the sample. It was also discovered in [6] that at complete passage of the fission fragment across the point, the surface remains almost undamaged, which is explained [6] by the absence of the return pulse. The experiments conducted show that at the complete passage of fission fragments of energy greater than 50 MeV through the tungsten needle, large craters form at the places of entrance and

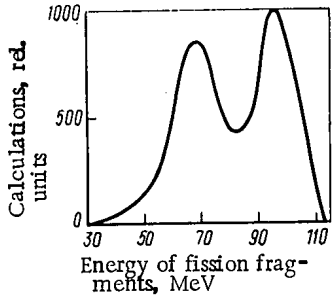

Fig. 1. Energy spectrum of fission fragments from ^{252}Cf.

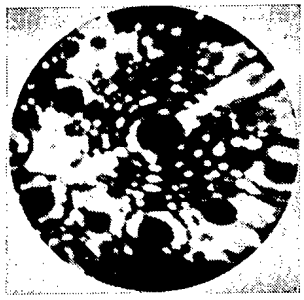

Fig. 2

Fig. 3

Fig. 2. Surface of a microcrystal of tungsten irradiated by α particles.

Fig. 3. Field-emission image of a tungsten sample irradiated by fission fragments. The damaged parts of the surface are marked by arrows.

Fig. 4. Erosion of part of the surface of tungsten by the tracks of fission fragments of ^{252}Cf immediately after irradiation (a) and after evaporation to a depth of 2.3 nm (b).

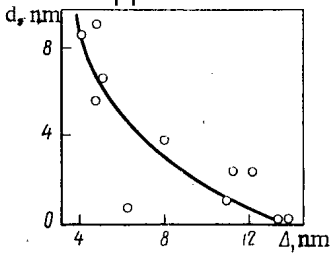

Fig. 5. Dependence of the width of the damage zone d on the distance from the fragment track, Δ.

exit of the fragment that were not detected earlier [6] with the radiation by slowed fission fragments. The size and form of the damage of tungsten needles by fragments of high energy may, evidently, be described as a result of the formation of a thermal spike around the track of the fragment.

A characteristic peculiarity of these experiments is a sufficiently close location of the tracks near the atom-smooth surface of the sample. Therefore, the surface atoms succeed in evaporating at the beginning of recrystallization. As a result, the formation of craters occurs, as does a porous layer of a certain part of the surface over the track of the fission fragment.

In conclusion, we should note that the presence of a band of contrast, analogous to that described earlier [8], will confirm the former conclusion about the possibility of the formation of a belt of contrast due to the formatio of saddle-shaped surfaces connected with localized depressions (e.g., craters).

The authors wish to extend their thanks to V. P. Éismont for discussing the results.

LITERATURE CITED

1. K. Izni, J. Phys. Soc. Jpn., 20, No. 6, 915 (1965).
2. B. M. Aleksandrov et al., At. Energ., 41, No. 6, 417 (1976).
3. B. M. Aleksandrov et al., At. Energ., 38, No. 1, 47 (1975).
4. J. Biersack and D. Fink, J. Nucl. Mater., 36, 193 (1974).
5. K. Bowkett et al., Phil. Mag., 11, No. 111, 651 (1965).
6. K. Bowkett, ibid., 15, No. 134, 415 (1967).
7. Van Byuren, Defects in Crystals, Publ. Abroad, Moscow (1962).
8. I. M. Mikhailovskii et al., Fiz. Tverd. Tela, 19, No. 4, 1116 (1977).

CALCULATION OF THE PERTUBATION OF FUNCTIONALS OF THE FLOW OF NEUTRONS BY A DIRECT MONTE CARLO METHOD USING CORRELATED SAMPLES

V. D. Kazaritskii

UDC 539.125.52:621.039.51.12

The definition of pertubations of reactivity by the direct method of diffusion of neutrons correct to second-order terms is seen in [1]. An analogous approach may be extended to arbitrary linear functionals of the neutron flux.

The Boltzmann equation in the integral form in the context of the density of collisions is

$$\Psi(x) = \int K_s(x/x')\,\Psi(x')\,dx' + \int K_f(x/x')\,\Psi(x')\,dx'. \tag{1}$$

Here x is the point of phase space $X = \{r, E, \Omega\}$, and K_s (x/x') and K_f(x'x') are accordingly the kernels of scattering and fission. The search for a solution to Eq. (1) proceeds by iteration. For this purpose, it may be split into the system of coupled equations

$$\Psi_i(x) = \int K_s(x/x')\Psi_i(x')\,dx' + S_i(x); \tag{2}$$

$$S_i(x) = \int K_f(x/x')\,\Psi_{i-1}(x')\,dx',\ i = 2, 3\ \ldots, \tag{3}$$

$S_1(x)=S(x)$. The system of equations (2), (3) is itself solved by the Monte Carlo method for the successive generations of neutrons. Subscripts i-1 and i indicate the i-1 and i-th generation of neutrons. We will introduce a linear functional of the flow of neutrons

$$R_i = \int \varphi(x)\,\Psi_i(x)\,dx \Big/ \int S_i(x)\,dx, \tag{4}$$

where $\varphi(x)$ is a bounded function, and R_i is normalized per fission neutron. In a physical sense this is the reaction rate. The variation of the functional is equal to

$$\delta R_i = \Big\{ \int \delta\varphi(x)\,\Psi_i(x)\,dx + \int \varphi(x)\,\delta\Psi_i(x)\,dx - R_i \int \delta S_i(x)\,dx \Big\} \Big/ \int S_i(x)\,dx. \tag{5}$$

The function $\psi_i(x)$ is the solution to Eq. (2) and is given by the Neumann series [2]:

$$\Psi_i(x) = S_i(x) + \int K_s(x/x_0)\,S_i(x_0)\,dx_0 + \int\int K_s(x/x_1)\,K_s(x_1/x_0)\,S_i(x_0)\,dx_1 dx_0 + \ldots . \tag{6}$$

The collision density in the perturbed system $\psi^p_i(x)$ is given analogously. We will now introduce the function

$$\Psi^p_{1i}(x) = S_i(x) + \int K^p_s(x/x_0)\,S_i(x_0)\,dx_0 + \int\int K^p_s(x/x_1)\,K^p_s(x_1/x_0)\,S_i(x_0)\,dx_1 dx_0 + \ldots . \tag{7}$$

Series (6), (7) converge and corresponding solutions exist; this follows from the properties of the operator $K_s(x/x')$ and the function $S_i(x)$:

$$0 < S_i(x),\ 0 < \int K_s(x/x')\,dx' < 1. \tag{8}$$

Translated from Atomnaya Énergiya, Vol. 49, No. 2, pp. 126-127, August, 1980. Original article submitted October 22, 1979.

0038-531X/80/4902-0578$07.50

TABLE 1. Results of Calculating the Basic Reaction Rates and Their Pertubation as a Consequence of Neutron Loss for Homogeneous Uranium–Water Lattices

Type of reaction	Program MK6			Data [5]	
	R	δR	δR_1	R	δR
Epithermal:					
absorption by ^{238}U	0,2047 ±0,0018	−0,0222 ±0,0018	−0,0191 ±0,0006	0,2048 ±0.0010	−0,0253
fission of ^{238}U	0,0405 ±0,0010	−0,0029 ±0,0008	−0,0018 ±0,0002	0,0363 ±0,0003	−0,0033
fission of ^{235}U	0,0394 ±0,0010	−0,0046 ±0,0008	−0,0044 ±0,0003	0,0396 ±0,0002	−0,0051
Thermal:					
absorption ^{238}U	0,1458 ±0,0018	−0,0232 ±0,0015	−0,0202 ±0,0007	0,1490 ±0,0003	−0,0228
fission of ^{235}U	0,3893 ±0,0023	−0,0614 ±0,0024	−0,0526 ±0,0010	0,3948 ±0,0008	−0,0603
K_∞	1,152 ±0,006	−0,167 ±0,006	−0,142 ±0,003	1,155 ±0,003	−0,1681

The function $\Psi^p_{1i}(x)$ may be viewed as the first approximation to the density of collisions in the perturbed system $\Psi^p_i(x)$. Now let us write the perturbed collision density $\delta\Psi_i(x)$ in the form

$$\delta\Psi_i(x) = \Psi^p_{1i}(x) - \Psi_i(x) + \Psi^p_i(x) - \Psi^p_{1i}(x). \tag{9}$$

The formula obtained presents the possibility of successively evaluating the perturbation. If, as a result of the i-1 iteration in the unpertubated system, we produce as the steady distribution $S_i(x)$, one may, modeling the trajectory alternately in both systems, obtain in (5) for the perturbation of the functional for the value of the first integral, and for the value of the second integral equal to

$$\int \varphi(x)\,(\Psi^p_{1i}(x) - \Psi_i(x))\,dx. \tag{10}$$

We will designate the sum of the valuation, correct to the first order, as δR_{1i}. The trajectories, not reaching the perturbed volume, do not contribute to integral (10), therefore, there is no need to model them in the perturbed system. The remaining trajectories should begin from the point of the first entry in that volume. Such a correlated sample was already used in [3]. For evaluating the portion of the second difference term in Eq. (9), it is necessary to evaluate $S^p(x)$. If we assume that the distribution of the source is established during one generation, then

$$S^p_i(x) = \int K^p_f(x/x')\Psi^p_{1i}(x')\,dx'. \tag{11}$$

Now, for the separated trajectories, one may calculate the source for the iteration according to formulas (3) and (11) and then evaluate the term in δR_i from the last difference term in Eq. (9). Simultaneously, the integral of the difference $\delta S_i(x) = S^p_i(x) - S_i(x)$ is calculated for the last term in formula (5), which enters as the difference in coefficients of mutliplication of the two systems. By the repetition of the described procedure for each generation of neutrons of the nonperturbed system, one may evaluate the functional R_i, and the pertubation δR_i or simultaneously several functionals and their pertubations and also their statistical errors.

This method is the basis for modifications to the program for the universal calculation of a reactor by the Monte Carlo method, MK6 [6]. By using this program we can calculate the pertubation of the neutron multiplication coefficient and the reaction rate in the

lattice-type fuel elements which were used in [5] for checking nuclear-physical constants of thermal reactors. The information necessary for the calculations is presented in [5].

In our work we will evaluate a pertubation to the lattice with a ratio of moderator volume to fuel equal to 2.35. We approximately propose that the reactor has a finite height with upper-level material parameters equal to their experimental values (B^2 = 57.0 m^{-2}). The results of the calculation of the reaction rate for an infinite lattice (B^2 = 0) are given in Table 1 together with the neutron loss corrections. The calculation required 3 h of machine time on the high-speed electronic computer BESM-6, 2 h of this time was required for the model trajectories in an unperturbed system (44250 histories), and 40 min was required for the first iteration in the perturbed system. Twenty minutes was required for the second iteration.

The data from [5] are seen on the right side of Table 1; here the reaction rate is evaluated by the Monte Carlo method, and the corrections are evaluated by using a simultaneous homogeneous calculation. The disagreement in the reaction rates can be explained by differences in the original neutron data. As far as evaluating the perturbation is concerned, they are practically in agreement. Only for absorption by ^{238}U in the epithermel region does the difference exceed the statistical error. However, as the major part of the absorption in this case is from resonance neutrons, this may be related to the uncertainty which occurs in the transition from the heterogeneous calculation to the homogeneous one.

LITERATURE CITED

1. M. Nakagawa and T. Asoaka, J. Nucl. Sic. Technol., 15, 400 (1978).
2. G. A. Mikhailov, Several Questions Concerning the Theory of the Monte Carlo Method [in Russian], Nauka, Novosibirsk (1974).
3. H. Takahashi, Nucl. Sci. Eng., 41, 259 (1970).
4. V. D. Kazaritskii, ITÉF-137, Moscow (1978).
5. J. Hardy in: Proceedings of the Seminar on Uranium-238 Resonance Capture, BNL-NCS-50451, Brookhaven National Lab. (1975), p. 18.

INFLUENCE OF A SMALL CHANGE OF THE FORM OF A REACTOR ON ITS CRITICALITY

Yu. V. Petrov and É. G. Sakhnovskii

IDC 621.039.51

We will consider the influence of a pertubation of the form of the boundary of a cylindrical reactor on its criticality. If the pertubation is limited to the sides of a right-circular cylinder, then the equation of the boundary in polar coordinated (r, φ) can always be written as

$$R^2/r^2 = 1 + \delta(\varphi), \quad \delta(\varphi) = \sum_{n=1}^{\infty} (a_n \cos n\varphi + b_n \sin n\varphi), \tag{1}$$

where $\delta(\varphi)$ is the deflection of the side from the circle of radius R. We will write the kinetic transfer equation for the distribution function of the neutron flux $f(r, \varphi, z, v)$ in the reactor as

$$(k_{\text{eff}}^{-1}F + G) f(r, \varphi, z, \mathbf{v}) = 0, \tag{2}$$

where F is the fission operator, and G is the moderator operator and loss of neutrons from the element of phase space. The coordinate transformation

$$r' = r\sqrt{1+\delta(\varphi)}; \quad \varphi' = \varphi \tag{3}$$

Translated from Atomnaya Énergiya, Vol. 49, No. 2, pp. 127-129, August, 1980. Original article submitted October 22, 1979.

 0038-531X/80/4902-0580$07.50

TABLE 1. Values of the Geometric Parameter of Reactors of Various

Geometry of the cross section of the reactor	B^2/B_0^2		
	second approximation	exact value	error %
Square,	1,094	1,086	0,8
Hexagon,	1,028	1,026	0,2
Ellipse:			
$\varepsilon=0{,}152$	1,011	1,011	0,0
$\varepsilon=0{,}473$	1,128	1,127	0,1
$\varepsilon=0{,}801$	1,641	1,616	1,6

changes the equation of boundary (1) into the equation of a circle in the plane (r', φ'), and Eq. (2) into a perturbed form with the operator $G' = G + \Delta G$. This method [1] allows us to apply the perturbation theory below in its traditional form. Following [2], we will construct an algorithm of successive approximations to the solution of the problem, assuming that the perturbation is equal to $\varepsilon\delta(\varphi)$. Having obtained the desired values of k_{eff}^{-1} and $f(r', \varphi, z, v)$ as a power series in ε, we can obtain, as the zeroth approximation ($\varepsilon = 0$), the critical unperturbed axisymmetric reactor, for which $k_{eff}^{(0)} = 1$, and $f_{eff}^{(0)} = F_0(r', z, w)$, which, because of the symmetry, does not depend on the polar angle φ. The adjoint function $f_0^+(r', z, v)$ has a similar property, so that from the expression for correcting the reactivity in the first approximation [2] it follows that

$$k_{eff}^{(1)} \sim \langle f^{(0)+} | \Delta G | f^{(0)} \rangle \sim \left\langle f_0^+ \middle| \sin\theta \sin\chi \left[(\sigma(\varphi) \operatorname{ctg}\chi - \frac{d\sigma}{d\varphi}) \frac{\partial}{\partial r'} + \frac{1}{r'} \delta(\varphi) \left(\frac{\partial}{\partial\varphi} - \frac{\partial}{\partial\chi} \right) \right] \middle| f_0 \right\rangle = 0, \tag{4}$$

as the integration over φ is reduced to the integration over the full period of the functions $\delta(\varphi)$ and $d\delta/d\varphi$, which gives zero. In Eq. (4) θ is the angle between the direction of the neutron velocity $\mathbf{v}$ and the z axis, and χ is the angle between the projection of the velocity v on the xy plane and the polar axis r.

Thus, one may formulate the following theorem: the first-order correction to the reaction multiplication coefficient for a perturbed axisymmetric cylindrical reactor is zero. In other words, the correction should be proportional to the square of the deviation of the square of its derivatives.

Let us find this correction for a homogeneous symmetrical, relatively Cartesian axis of a cylindrical reactor, without a reflector, with an equation of the sides (1) having $b_n \equiv 0$. Then, instead of expression (2) for the flux of neutrons we have a wave equation

$$L_0\psi(r, \varphi) + B^2\psi(r, \varphi) = 0 \tag{5}$$

with the Laplacian L_0 in the polar system of coordinates. The coordinate transformation (3) changes the boundary (1) to a circle of radius R, and Eq. (5) into the perturbed equation (relative to $\varepsilon\delta(\varphi)$):

$$[L_0 + \varepsilon\Delta_1 L + \varepsilon^2 (1 + \varepsilon\delta(\varphi))^{-1} \Delta_2 L] \Phi(\rho, \varphi) + \xi^2 \Phi(\rho, \varphi) = 0, \tag{6}$$

where the dimensionless flow $\Phi = \psi/\Phi_0^{(0)}$ is introduced, as are the polar radius $\rho = r'/R$ and the geometric parameter $\xi^2 = B^2R^2$. The pertubation of the operator L_0 is $\Delta L = \varepsilon\Delta_1 L + \varepsilon^2\Delta_2 L$, where

$$\Delta_1 L = \sigma(\varphi) L_0 + \frac{1}{\rho} \left(\frac{d\delta}{d\varphi} \frac{\partial^2}{\partial\rho\,\partial\varphi} + \frac{1}{2} \frac{d^2\delta}{d\varphi^2} \frac{\partial}{\partial\rho} \right);$$
$$\Delta_2 L = \frac{1}{4} \left(\frac{d\delta}{d\varphi} \right)^2 \left(L_0 - \frac{2}{\rho} \frac{\partial}{\partial\rho} - \frac{1}{\rho^2} \frac{\partial^2}{\partial\varphi^2} \right). \tag{7}$$

Let us write the basic solution to Eq. (6) in the series

$$\xi_{min}^2 = \xi_0^2 = \xi_0^{(0)2} + \sum_{m=1}^{\infty} \varepsilon^m \xi_0^{(m)2}; \quad \Phi = \Phi_0 = \Phi_0^{(0)} + \sum_{m=1}^{\infty} \varepsilon^m \Phi_0^{(m)}, \tag{8}$$

where the zeroth approximation $\Phi_0^{(0)}$ is the unperturbed ($\varepsilon = 0$) solution of the wave equation, which is zero on the extrapolated boundary $\rho = 1$, and $\xi_0^{(0)2}$ is the corresponding eigenvalue. Inserting expression (8) into Eq. (6), we obtain a system of equations defining $\Phi_0^{(m)}(\rho, \varphi)$

$$L_0\Phi_0^{(m)} + \xi_1^{(0)2}\Phi_0^{(m)} = -\Delta_1 L\Phi_0^{(m-1)} - \Delta_2 L\Phi_0^{(m-2)} - \sum_{n=1}^{m} \xi_0^{(n)2}\Phi_0^{(m-n)}, \quad m = 1, 2, 3, \ldots \tag{9}$$

with boundary conditions $(\Phi_0^{(m)})_{\rho=1} = 0$. From the conditions for the existence of a solution to the inhomogeneous equation (9) together with the normalization conditions $(\Phi_0^{(0)}, \Phi_0^{(n)}) = \delta_{n,0}$ ($n = 0, 1, 2, 3, \ldots$), for the required correction to $\xi_0^{(0)2}$ we obtain*

$$\xi_0^{(m)2} = -(\Phi_0^{(0)}, \Delta_1 L\Phi_0^{(m-1)} + \Delta_2 L\Phi_0^{(m-2)}), \quad m = 1, 2, 3, \ldots . \tag{10}$$

The complete set of eigenfunctions of the operator L_0 which are symmetrical in φ are the functions v_{nm} ($n = 0, 1, 2, \ldots$, $m = 1, 2, 3, \ldots$):

$$v_{nm}(\rho, \varphi) = \| v_{nm} \|^{-1} J_n(\nu_{nm}\rho)\cos n\varphi;$$
$$\| v_{nm} \|^2 = \frac{\pi}{2}(1 + \delta_{n,0}) J_{n-1}^2(\nu_{nm}), \tag{11}$$

where the eigenvalues ν_{nm} are the roots of the Bessel function $J_n(x)$, so that $\xi_0^{(0)} = \nu_{01} = \min \nu_{0m} \approx 2.405$, and $\nu_{0m}(\rho)$ are the eigenfunctions with axial symmetry. From Eq. (10), in accordance with the theorem, it follows that

$$\xi_0^{(1)2} = \langle v_{01} | \Delta_1 L | v_{01} \rangle = \left\langle 01 \left| \delta(\varphi)\xi_0^{(0)2} - \frac{1}{2\rho}\frac{d^2\delta}{d\varphi^2}\frac{\partial}{\partial\rho} \right| 01 \right\rangle = 0. \tag{12}$$

From expression (9) it is not difficult to obtain

$$\Phi_0^{(1)}(\rho, \varphi) = \sum_{n,m=1}^{\infty} \frac{c_{nm}}{\nu_{nm}^2 - \nu_{01}^2} v_{nm}, \tag{13}$$

where the matrix element is

$$c_{nm} = \langle nm | \Delta_1 L | 01 \rangle = \frac{\pi\nu_{01}a_n n^2}{2\| v_{01} \| \| v_{nm} \|}\int_0^1 J_n(\nu_{nm}\rho)\left[J_1(\nu_{01}\rho) - \frac{2\nu_{01}\rho}{n^2} J_0(\nu_{01}\rho) \right] d\rho. \tag{14}$$

Having inserted Eq. (13) into (10) for the second apprxoimation to the lowest eigenvalue $\xi_0^{(0)2}$, we get

$$\xi_0^{(2)2} = \frac{1}{2}\nu_{01}^2 \sum_{n=1}^{\infty} a_n^2 \left(\frac{n^2}{4} - 1 \right) - \sum_{n,m=1}^{\infty} \frac{c_{nm}^2}{\nu_{nm}^2 - \nu_{01}^2}. \tag{15}$$

Here the first sum, conditioned by the action of the operators Δ_1, L and $\Delta_2 L$ on v_{01}, corresponds to the first order of pertubation theory in the operator ΔL, but is second order in $\delta(\varphi)$. The second sum corresponds to the second-order correction from the operator ΔL, and, as is well know, is always negative.

As an example, we obtain the value of the geometric parameter for an ellipse with a semiaxis $a = R/\sqrt{1-\varepsilon}$, $b = R/\sqrt{1+\varepsilon}$ and eccentricity $e^2 = 2\varepsilon/(1+\varepsilon)$. Such an equation is $R^2/r^2 = 1 - \varepsilon\cos 2\varphi$ and, consequently, in formula (1) $n = 2$, $a_2 = -\varepsilon$. from which Eq. (15) becomes

$$B^2 = \frac{\nu_{01}^2}{R^2}\left[1 - 8\varepsilon^2 \sum_{m=1}^{\infty} \frac{\nu_{2m}^2}{(\nu_{2m}^2 - \nu_{01}^2)^3} \right] \approx \frac{\nu_{01}^2}{R_0^2\sqrt{1-\varepsilon^2}}(1 - 0.027\varepsilon^2). \tag{16}$$

where R_0 is the radius of the circle having the same area as the examined ellipse.

The equation for the regular polygon with 2k sides and with apothem p can be expressed in the Fourier cosine series on the space $[0, 2\pi]$ as in (1)

$$\delta(\varphi) \sum_{m=1}^{\infty} \frac{2\gamma}{1 - k^2m^2}\cos 2km\varphi, \tag{17}$$

$$R^2 = 2p^2/\alpha, \quad \gamma = (\alpha - 1)/\alpha, \quad \alpha = 1 + \frac{k}{\pi}\sin\frac{\pi}{k}.$$

*The round brackets denote scalar products; $\delta_{n,0}$ is the Kronecker symbol.

Upon inserting Eq. (17) into formula (15), for a right prism with 2k sides we obtain

$$\xi_0^{(2)2} = \nu_{01}^2 \left(1 - \frac{\pi}{k} \operatorname{ctg} \frac{\pi}{k}\right) \gamma^2 - \sum_{n,\, m=1}^{\infty} \frac{c_{2kn,\, m}^2}{\nu_{2kn,\, m}^2 - \nu_{01}^2} \left\langle \nu_{01}^2 \left(1 - \frac{\pi}{k} \operatorname{ctg} \frac{\varphi}{k}\right) \gamma^2 \right. \tag{18}$$

and

$$B^2 = \zeta (\nu_{01}^2 + \xi_0^{(2)2})/R_0^2, \quad \zeta = \alpha \frac{k}{\pi} \operatorname{tg} \frac{\pi}{2k}. \tag{19}$$

The results for the value of the second approximation to the geometric parameters of the examined figures relative to those of the equivalent circles of radius R_0, $B_0^2 = \nu_{01}^2/R_0^2$ for a calculation through m = 10 in formula (19) are seen in Table 1. The exact values, B^2/B_0^2, in Table 1 for the hexagon are obtained in [3] by the Ritz method, and those for the ellipse are given in [4] using the expansion of the exact solution (Mathieu functions) in a series of Bessel functions. As is evident from Table 1, the second order of the pertubation theory has sufficient accuracy for practical purposes and the simple formula (16) describes very well the entire tabulation in [4] of the values of the geometric parameters of the ellipse.

In conclusion, we will note that the analogous method can be used to investigate the criticality of a reactor for small deflection of its form from spherical or cubical.

The authors thank G. A. Bate, A. D. Galanin, and V. A. Ruban for a fruitful discussion of the present note; and S. A. Artamonov and I. A. Shlyakhter for hlep with the calculations.

LITERATURE CITED

1. A. B. Migdal and V. P. Krainov, Approximation Methods of Quantum Mechanics, [in Russian], Nauka, Moscow (1966).
2. É. A. Stumbur, Use of Pertubation Theory in the Physics of Nuclear Reactors [in Russian], Atomizdat, Moscow (1976).
3. G. I. Plindov, in: Physics of Nuclear Reactors [in Russian], Vol. 1, ONTI FÉI, Obinsk (1966), p. 374.
4. P. Gast and A. Bournia, Nucleonics, 14, No. 4, 109 (1956).

ELECTRICAL CONDUCTIVITY OF BINARY ALLOYS OF THORIUM TETRAFLUORIDE WITH LITHIUM AND SODIUM FLUORIDES

V. N. Desyatnik, A. P. Koverda, N. N. Kurbatov, and V. V. Bystrov

UDC 621.3.035.45:537.311.3:546.16'33'34'841

The problem of developing a fused-salt nuclear reactor is closely bound up with investigations on the thermophysical properties of possible fuel compositions, especially fusions of the fluorides of alkali metals and fluorides of uranium, thorium, and plutonium since these fusions have a relatively low melting point, low vapor pressure, and low viscosity.

The practically unlimited solubility of thorium fluoride in fusions of the fluorides of alkali metals allows fuel breeding to be accomplished with slow neutrons [1]. A certain inadequacy of data on the electrical conductivity of fluoride fusions with a relatively high thorium concentration is apparently explained by the complexity of the selection of structural elements of the measuring cell because of the high corrosivity of these fusions [2].

The electrical conductivity of fluoride fusions was measured in a stainless steel retort. The molybdenum-lined retort was placed in a resistance furnace. The high-temperature zone of the retort was separated from the cold part by a system of nickel screens. The capillaries were MgO tubes with an internal diameter of 2.0 mm. The electrodes, the crucible containing the fusion under study, and the sheath of the thermocouple were made of nickel. The

Translated from Atomnaya Énergiya, Vol. 49, No. 2, pp. 129-130, August, 1980. Original article submitted October 22, 1979.

0038-531X/80/4902-0583$07.50

TABLE 1. Coefficients of the Equation of Temperature Dependence of Conductivity of Fused Salt Systems

ThF_4 content, mole%	Coefficient of equation			SD, S	Temp. range, °K
	$-a$	$b \cdot 10^2$	$-c \cdot 10^6$		
		$LiF-ThF_4$			
0	8,4086	2,1400	6,0606	0,0034	1140—1300
20	6,3708	1,3095	3,0219	0,0018	860—1340
30	8,6232	1,3713	2,9674	0,0044	900—1400
40	6,2508	0,8504	0,8802	0,0041	980—1400
45	3,5151	0,4244	—0,5796	0,0029	1060—1400
55	6,8017	0,7696	—0,5598	0,0027	1120—1400
70	1,2523	—0,0837	—2,3639	0,0034	1240—1480
85	9,8144	1,0680	1,6071	0,0018	1340—1480
100	1,8653	—0,1064	—2,6339	0,0033	1380—1480
		$NaF-ThF_4$			
0	—0,7451	0,3900	0,3842	0,0025	1280—1440
15	5,5903	1,0517	2,6080	0,0021	1180—1400
30	4,9297	0,8530	2,0095	0,0027	960—1420
45	4,3189	0,6498	1,1118	0,0030	1020—1440
53	6,3829	0,8751	1,7888	0,0031	1080—1440
60	6,8455	0,8409	1,3858	0,0018	1140—1480
75	7,4516	0,8201	1,0664	0,0034	1280—1480
90	7,1091	0,5845	0,1191	0,0041	1360—1480

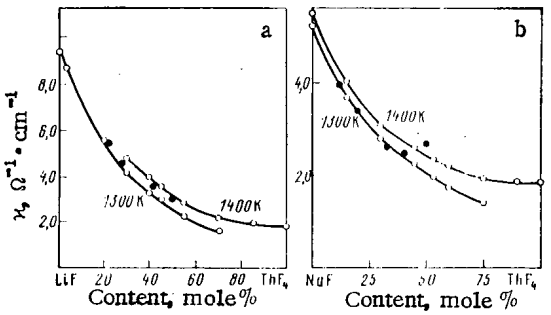

Fig. 1. Isotherms of conductivity of fused systems: a) $LiF-ThF_4$ and b) $NaF-THF_4$, ○) present paper, ●) data of [2].

resistance was measured with a R568 ac bridge at 50 kHz. The voltage applied to the electrodes did not exceed 30 mV. The capillary constant was determined in experiments with a KCl fusion at 1070-1225°K, in which use was made of published KCl electrical conductivity values [3]. Extrapolation was employed at higher and lower temperatures and the validity of the extrapolation was verified by calibrating the capillary with a 1 N NaCl solution at room temperature. The maximum error in the determination of the capillary constant was 1%, according to estimates. The maximum calculating error in the measurement of the electrical conductivity is 2%.

In the experiment much attention was paid to the preparation of anhydrous salts. Thorium tetrafluoride was prepared from ThO_2, which was dissolved in fuming nitric acid. Tetrafluoride in the form of $ThF_4 \cdot nH_2O$ was deposited from the solution with hydrofluoric acid. The deposit was rinsed on a filter with distilled water, dried in a nickel dish at 100°C for days, and then calcined in a vacuum furnace and then gradually heated to the melting point. Chemical analysis of the thorium tetrafluoride showed it to contain no more than 1 wt.% impurities.

Lithium and sodium fluorides of spectrally very pure grade were dried for 3-4 h at 300°C under a vacuum and then remelted and crystallized in an argon atmosphere. In order to homogenize the fusions of a mixture of salts of the required composition, we held them for 3-4 h at a temperature above the melting point by 50-80°C, after which the temperature was raised to the necessary value and the electrical conductivity was measured as the melt was cooled at the rate of 2-2.5 deg/min. Upon completion of the experiment, the individual melts were analyzed for thorium content in order to monitor the variability of the composition.

The electrical conductivity of the fused lithium and thorium fluorides, containing 20, 30, 40, 45, 55, 70, 85, and 100 mole % ThF_4 and sodium and thorium fluorides containing 15, 30, 45, 53, 60, 75, and 90 mole % ThF_4, as well as pure lithium, sodium, and thorium fluorides was measured in an environment of argon purified from traces of water and oxygen. The results of the conductivity measurements of the salt fusions were processed by the least-squares method in the form of the equation

$$\varkappa = a + bT + cT^2,$$

where $\varkappa$ is the conductivity ($\Omega^{-1}\cdot cm^{-1}$), T, temperature (°K), and a, b, and c, coefficients of the equation. As an indicator of the accuracy of the description of the experimental results by an equation of the given form we calculated the standard deviation S (see Table 1)

Figure 1 gives the isotherms of the electrical conductivity of the salt fusions studied as well as the published [2] values of the conductivity at a ThF_4 concentration of up to 40 mole % are in good agreement with known values [2] but as the ThF_4 concentration increases there is a growing discrepancy between the values. The experiments show that the conductivity of these fusions decreases monotonically as the ThF_4 content rises.

LITERATURE CITED

1. V. Ya. Blinkin and V. M. Novikov, Liquid-Salt Nuclear Reactors [in Russian], Atomizdat, Moscow (1978), p. 111.
2. G. Janz et al., Phys. Chem. Ref. Data, 3, No. 1, 1 (1974).
3. Handbook of Fused Salts [in Russian], Vol. 1, Khimiya, Leningrad (1971), p. 24.

EFFECT OF HEAT TREATMENT ON BLISTERING OF TsM-6 MOLYBDENUM ALLOY

D. M. Skorov, M. I. Guseva,
B. A. Kalin, and V. L. Yakushin

UDC 621.039.531

High-melting metals (molybdenum, vanadium, niobium) and alloys based on them are considered to be promising structural materials for the first wall of the discharge chamber fusion power reactors [1]. With the interaction of plasma with the wall material erosion of the wall due to sputtering and blistering is observed.

It was shown in [2] that the initial structure of the target has a substantial influence on the parameters of blistering and erosion on the materials. Thus, cold-rolled vanadium and niobium specimens irradiated at room temperature with 500-keV helium ions have much smaller blisters and erosion coefficients as a result of their destruction in comparison with recrystallized specimens. It is known that heat treatment is one way of altering the structure and properties of metals and alloys. Accordingly, for the practical use of materials in a thermonuclear reactor it is important to know how heat treatment effects their erosion under ion bombardment.

In the present paper we study the helium blistering of the molybdenum alloy TsM-6 (Mo-0.13 wt.% Zr-0.002 wt.% C-0.0015 wt.% B) depending on the heat treatment of the specimens. We studied materials in the following states: initial state (hot rolled), recrystallized, quenched, and aged. The specimens were quenched in liquid gallium after soaking in a vacuum of $2.6\cdot10^{-3}$ Pa at 2000°C for 1 h. According to [3] quenching in liquid gallium ensures that the material cools at a rapid rate and this results in the most complete fixation of the supersaturated solution. The quenched specimens were recrystallized and aged in a TVV-4 furnace in a vacuum of $6.6\cdot10^{-3}$ Pa at 1600°C and soaking for 1 h. This annealing regime fixes the maximum aging of alloys of the molybdenum–zirconium–carbon system [4]. After heat treatment the specimens were polished, at first mechanically and then electrolytically. The ready specimens were bombarded in an ILU-3 accelerator with a horizontally scanning ion beam

Translated from Atomnaya Énergiya, Vol. 49, No. 2, pp. 130-132, August, 1980. Original article submitted October 29, 1979.

0038-531X/80/4902-0585$07.50

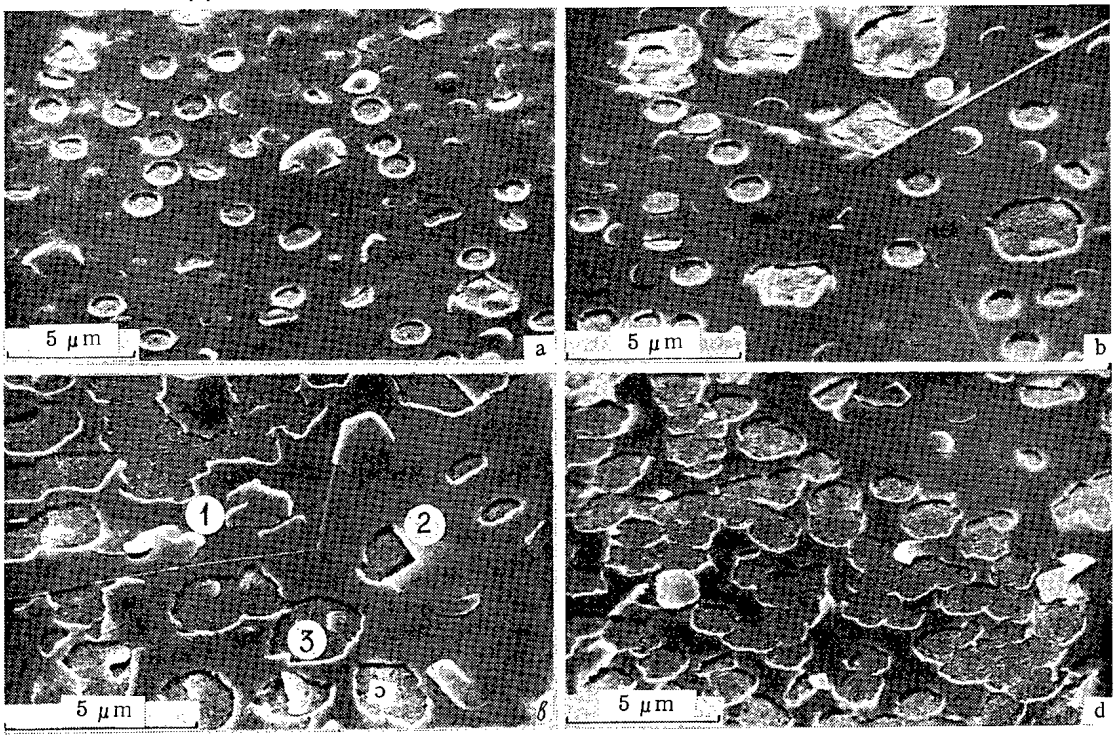

Fig. 1. Electron-microscope photographs of surface of TsM-6 alloy bombarded with 40-keV helium ions at 120°C with a dose of $2 \cdot 10^{18}$ ions/cm^2: a) initial state, b) quenched, c) aged, d) recrystallized.

normal to the surface of the target. After, the ion bombardment the surface was examined in a Quickscan electron microscope. From the electron-microscope photographs we calculated the erosion coefficients of the material by determining the geometric dimensions of the damaged portions and calculating the number of atoms in them.

In analyzing the electron-microscope photographs of the surface of the bombarded specimens we noticed that heat treatment has a marked effect on the character of the damage of the alloy and the erosion coefficients (see Fig. 1). It is seen that all materials, regardless of their initial treatment, were subject to radiation erosion but the character and degree of the erosion depends essentially on the form of the heat treatment of the alloy prior to bombardment. If the erosion of the original rolled alloy occurs mainly as the result of the destruction of individual blisters (see Fig. 1a), then both blistering and scaling (see Fig. 1b) or mainly scaling of one layer (see Fig. 1d) are observed in heat-treated specimens while scaling of one layer and damaged second-generation blisters can be seen on quenched and aged specimens (see Figs. 1b, c). The erosion coefficients, calculated from the electron-microscope photographs, were $(5.5 \pm 1.6) \cdot 10^{-2}$, $(7.6 \pm 2.3) \cdot 10^{-2}$, (0.16 ± 0.05), and (0.18 ± 0.05) atom/ion for the initial, quenched, aged, and recrystallized states, respectively. Therefore, the highest radiation stability under ion bombardment is possessed by the initial strained and quenched specimens while the alloy is subject to maximum erosion in the recrystallized state.

Such differences in the behavior of the molybdenum alloy under ion bombardment, depending on the heat treatment, may be due to a number of factor. First, strained and quenched specimens of low-carbon TsM-6 alloy have higher strength characteristics than do the recrystallized and aged materials. This results in a reduction in the number of blisters with damaged caps and a decrease in the erosion of the surface. Moreover, a large number of dislocations and broken boundaries of grains and subgrains are formed in the original strained material in the rolling process. The increased density of dislocations and boundaries may be an effective sink for vacancies and helium interstitial atoms which is conducive to retardation of the formation of small helium bubbles in the metal under bombardment. This makes it difficult for bubbles in the metal under bombardment. This makes it difficult for bubbles to coalesce into gas cavities, constituting blister nuclei, and obstructs blistering.

It is also known that a rolling texture is formed in sheet molybdenum as in other metals with a bcc lattice, with {001}<001> being the dominant texture, [4], i.e., most of the crystallites in the rolled alloy parallel to the surface have a plane with a {001} orientation. The mechanical properties of molybdenum depend on the direction of the crystallographic orientation, the bonds in the [100] direction being the strongest [4]. Thus, the rolling texture is conducive to most crystallites growing so that the strongest bonds are perpendicular to the target surface, which also leads to an increase in the radiation stability of the strained alloy under ion bombardment. The effect of the crystallographic orientation of the surface of single crystals on the degree of blistering and the erosion of the material was noted, e.g., in [2, 5]. Anisotropy of the radiation erosion of grains with various crystallographic orientation is also observed upon analysis of the microstructure of the irradiated surface at the triple point (see Figs. 1b and c). It is clear that the character of the damage and erosion change significantly in the passage from one grain to another. The calculated erosion coefficients are (0.31 ± 0.09), (0.07 ± 0.02), and (0.24 ± 0.07) atom/ion for grains 1, 2, and 3, respectively (see Fig. 1c).

Thus, the investigations reported in this paper show that, from the practical point of view, in order to prepare structural elements for the discharge chamber of a thermonuclear reactor it is advisable to use TsM-6 molybdenum alloy in the strained state (after hot rolling) with the dominant texture in the {001} plane.

The authors thank A. F. Sorokin for his assistance in the electron-microscopic examination of the specimens.

LITERATURE CITED

1. J. Davis and G. Kulcinsky, Nucl. Fusion, 16, No. 2, 355 (1976).
2. S. Das and M. Kaminsky, Adv. Chem., No. 158, 112 (1976).
3. A. I. Evstyukhin et al., Fiz. Khim. Obrab. Mater., No. 3, 149 (1976).
4. N. N. Morgunova et al., Molybdenum Alloys [in Russian], Metallurgiya, Moscow (1975).
5. V. M. Gusev et al., Fiz. Khim. Obrab. Mater., No. 3, 9 (1978).

BLISTERING OF MATERIALS UNDER CYCLICAL BOMBARDMENT WITH IONS IN A WIDE SPECTRUM OF ANGLES OF INCIDENCE

B. A. Kalin, S. N. Korshunov,
D. M. Skorov, and V. L. Yakhushin

UDC 621.039.531

The first wall of the discharge chamber and other elements of the thermonuclear reactor during operation will be subjected to intense bombardment with ions of hydrogen and helium isotopes with a wide spectrum of angles of incidence and energies. The interaction of the plasma with the structural materials results in their erosion and contamination of the plasma with heavy impurities as the result of cathode sputtering and blistering. Considerable investigations are being conducted on the blistering of prospective materials for use in such a reactor. Most of the investigations, however, have been carried out with the targets being bombarded by monoenergetic beams at normal incidence. Only in [1] and [2] has a study been made of blistering with a simulation of the energy spectrum of helium ions similar to that expected in the thermonuclear reactor. The objective of the present paper is to study blistering under cyclical bombardment of the targets in a wide spectrum of angles of ion incidence, ranging from the normal to the surface to glancing angles.

In order to obtain a wide spectrum of angles of ion incidence, a device was built for the collector of a mass monochromator to allow the target to be rotated at constant velocity around an axis perpendicular to the incident ion beam (Fig. 1) during bombardment. The de-

Translated from Atomnaya Énergiya, Vol. 49, No. 2, pp. 132-134, August, 1980. Original article submitted October 29, 1979.

0038-531X/80/4902-0587$07.50

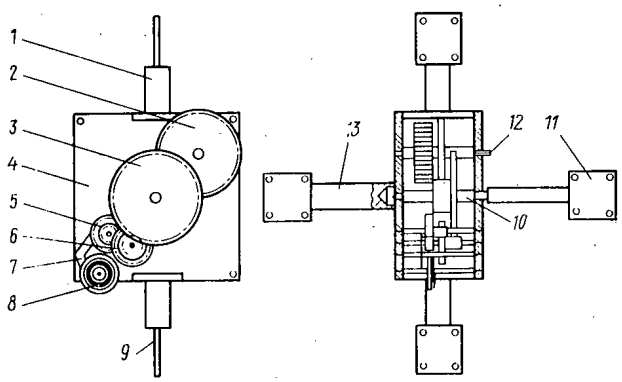

Fig. 1. Device for cyclical bombardment of specimens in wide spectrum of angles of ion incidence.

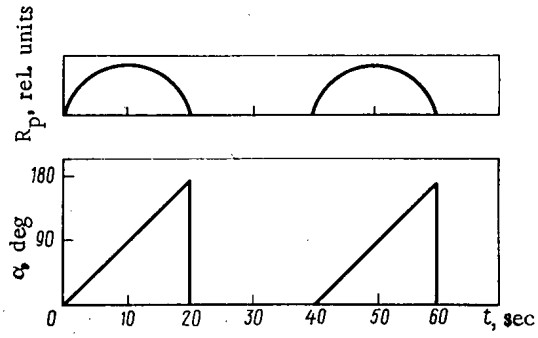

Fig. 2. Character and parameters of ion bombardment cycles.

vice consists of a housing 4, lugs 1 and 13 with holders for specimens 9 and 11, motor 12, a system of gears 2, 3, 5, and 6, and a system ensuring that the shaft 10 rotates uniformly and in a given way. Through gear 2 the spring motor transmits rotation to the main shaft, whose uniform rotation is effected through the pair of gears 5 and 6 and limiter 7 which conveys in inverse order the oscillations of the spiral-shaped pendulum 8. The entire mechanism is mounted inside a housing attached to the rotation feed of the mass-monochromator collector, thus making it possible for specimens fastened in the holders to be put under the beam successively.

With the targets rotating continuously the materials are bombarded in a cyclical regime over a wide range of angles of ion incidence, thus ensuring a smooth variation of the projection of the ion mean free path R_p in the target from zero to a maximum value corresponding to the depth of penetration of the ions at the given energy. During the first half-period of the cycle (T = 40 sec) the specimen mounted on one side of the rotating holder 9 is bombarded while during the second half-period the target on the other side of the holder is bombarded. In one half-period the angle of ion incidence α (the angle between the plane of the specimen and the incident beam) varies from 0 to 180°. Figure 2 gives a diagram illustrating the character and parameters of cyclical bombardment. The angular distribution of the bombarding helium ions can be expressed as

$$\Phi = \Phi_0 \sin \alpha.$$

In our experiment we studied the blistering of vacuum-melted MChCP molybdenum and electron-beam-melted VÉL-2 vanadium. The materials were bombarded with 20-keV helium ions at a dose of $2 \cdot 10^{18}$ ions/cm^2 with the target at near room temperature. The conditions of ion bombardment are described in greater detail in [3]. The surface of the specimens after ion implantation was studied in an ÉVM-100L electron microscope with the aid of carbon replicas shadow-cast with chromium. From the results of the electron-microscopic examination we determined the parameters of the blisters and the coefficients of erosion owing to their destruction.

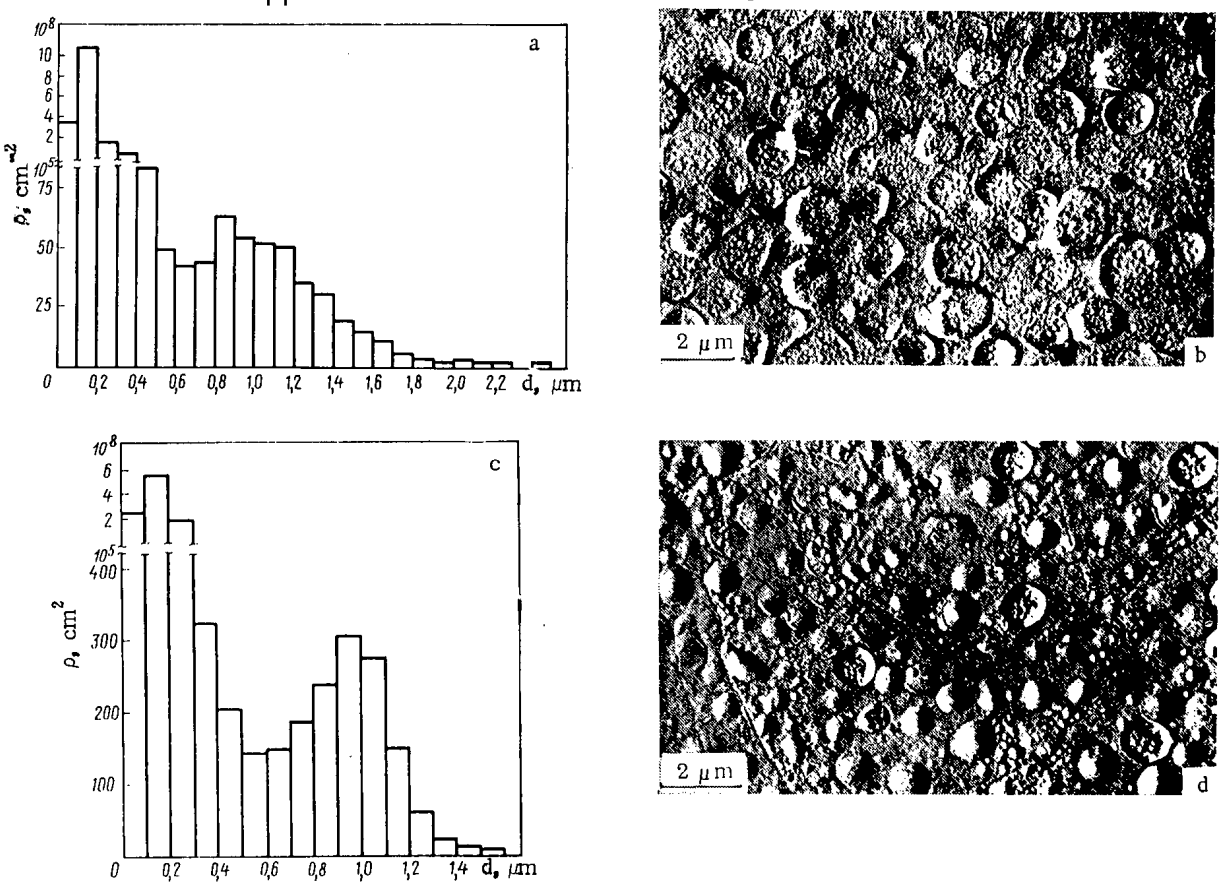

Fig. 3. Histograms of blister distribution according to size and electron micrographs of surface of MChVP molybdenum: a, b) stationary position of target, c, d) rotating target.

The results of studies of the surface of materials bombarded with helium ions in a stationary position (bombardment with an ion beam normal to the surface) and with rotation of the target showed that under identical conditions of ion bombardment rotation of the targets results in a change in the parameters of the blisters and the coefficients of radiation erosion in comparison with the stationary position of the target.

Figure 3 shows typical electron micrographs of irradiated surface and histograms of the blister distribution according to size for MChVP molybdenum after irradiation in a stationary position and with rotation of the target. As shown in Figs. 3a and c, regardless of the fact that in both cases the shape of the blister distribution according to size is the same with two distinct maxima, the corresponding mean sizes being d ≈ 0.1-0.2 and 0.8-1.1 μm, some peculiarities are observed when rotating specimens are bombarded. First, if the mean size of the blisters of the first peak remains practically constant, then for large bulging blisters the mean size decreases from 1.1 to 0.85 μm. Second, the density of small blisters decreases from $10.8 \cdot 10^8$ to $5.6 \cdot 10^8$ blisters/cm² and the density of bulging blisters with a mean size of 0.3-1.3 μm increases noticeably, thus leading to an increase in the area of the surface occupied by blisters, from 68 to 95%. Third, in specimens bombarded with a wide specrtum on angles of ion incidence there is no "tail" in the distribution of bulging blisters according to size (see Fig. 3c). Thus, whereas the blister size reaches 2.6 μm in the case of a stationary target, in the case of rotating targets we observed blisters with a maximum size of 1.6 μm.

Such changes in the blister distribution according to size is probably due to the fact that when a rotating target is bombarded the implanted gas is distributed closer to the bombarded surface and more symmetrically about the mean value of the projection of the ion path. This is confirmed well by the histograms (Figs. 3a and c) as well as by the fact that the thickness of the caps of the destroyed blisters during bombardment of materials in a wide spectrum of angles of ion incidence decreases from $0.96 \cdot 10^{-7}$ to $0.52 \cdot 10^{-7}$ m and from $1.13 \cdot 10^{-7}$ to $0.64 \cdot 10^{-7}$ m for MChVP molybdenum and VEL-2 vanadium, respectively.

In addition to changes in the blister distribution according to size and density, we also found that when a rotating target is bombarded there is a decrease in the coefficient of radiation erosion of the surface owing to the destruction of blisters. Thus, for molybdenum bombarded with a dose of $2 \cdot 10^{18}$ ions/cm^2 the area of blister caps scaled off falls from 9.3 to 3.2% and the erosion coefficient drops from $3 \cdot 10^{-2}$ to $0.6 \cdot 10^{-2}$ atom/ion. The reduction of radiation erosion is probably due to the fact that, as was demonstrated, with rotation of the targets the mean blister size is reduced and the thickness of the blister caps is almost halved.

Thus, the investigations reported on here have shown that bombardment of materials in a cyclical regime in a wide spectrum of angles of ion incidence leads to a decrease in the surface erosion of the materials as the result of the destruction of blisters and to a change in the blistering parameters.

LITERATURE CITED

1. M. I. Guseva et al., J. Nucl. Mater., 63, No. 1, 245 (1976).
2. S. K. Das et al., in: Proc. All-Union Conf. on Engineering Problems of Thermonuclear Reactors [in Russian], Vol. 3, Izd. NIIÉFA, Leningrad (1977), p. 256.
3. D. M. Skorov, in: Proc. All-Union Conf. on Engineering Problems of Thermonuclear Reactors [in Russian], Vol. 3, Izd. NIIÉFA, Leningrad (1977), p. 226.

EXPERIENCE IN THE OPERATION OF THE KOLA NUCLEAR POWER STATION AT INCREASED POWER

A. P. Volkov, B. A. Trofimov,
Yu. I. Savchuk, V. V. Zverkov,
E. I. Ignatenko, and A. N. Litvinov

UDC 621.039.5.56

The first stage (two units) of the Kola nuclear power station was commissioned in 1974. Analysis of the basic parameters and conditions of operation of this station during the operations process itself showed that some margin in plant power existed throughout the process scheme of the station as a whole, which showed during 1976-1977 that some experimental uprating of both units would be possible. This was carried out in line with a resolution of the controlling authorities.

The power of the units was uprated by stages to a level of 2-4, 6, and 7% above rated. The first unit operated at a power of 2-4% above rated during the period October-December 1976 for 50 effective days during its second fuel charge. The unit had run for 220 effective days prior to the commensement of the uprating. The unit had operated continuously at rated power in its original state. The variation factor of the cassette did not exceed 1.3 under these conditions (with the regulating roup standing H_6 = 130 cm from the base of the reactor core). At that particular moment in the operating period, a close agreement between the calculated variation factors in cassette power and the operating data was observed. The variation factor of the neutron field throughout the reactor core was 1.35 at H_0 = 147 cm. When the height of the regulating group was increased, these variation factors fell to 1.27 and 1.19, respectively, wit' :he reactor operating on rated power.

With the unit operating at 104% rated, the thermal power reached 1430 MW while the electrical power rose to 460 MW. The power variation factor of the cassette comprised 1.32 at H_6 = 220 cm. This value subsequently fell away during the process of fuel burnup. The neutron field variation factor with respect to height within the core was 1.23 at H_6 = 184 cm and with a boric acid concentration of 0.3 g/kg in the coolant. The temperature rise of the coolant in the reactor core did not exceed 29.8°C, the temperature at entrance to the reactor was 266-267°C and 295-296°C at exit. The maximum temperature of the coolant at exit from the most highly stressed cassette did not exceed 304°C.

Translated from Atomynaya Énergiya, Vol. 49, No. 2, pp. 134-135, August, 1980. Original article submitted November 12, 1979.

0038-531X/80/4902-0590$07.50

The flow rate of feed water and steam in the steam generators was 2800 tons/h (105% of rated). This was not limited by the flow characteristic of the secondary coolant circuit. The main regulators of the unit functioned satisfactorily at the increased load, the automatic power regulator (ARM-4) the primary circuit pressure regulator, the steam generator feed regulators, the steam generator level regulators, the high and low pressure superheaters and 0.6 MPa deaerators. Heat runs were carried out on the main generators No. 1 and 2 while the unit was operating on increased power. The active load on the generators was 455 MW. The results of the test show that all the parameters lie within permissible limits.

From Jan. 15 to July 2, 1977, the second unit of the Kola nuclear power station operated at 106% rated power. Prior to this, the unit had been run for 83 effective days from the start of the fuel cycle, while directly prior to the uprating it had operated for 1 month at full rated power. The maximum coolant temperature at the outlet from the cassette when running at full rated power level was 301°C (coordinate 17-32), the maximum variation factor in cassette power was 1.28, while the maximum variation factor in neutron field throughout the height of the core was 1.25. Before the unit was uprated, the results of measurements of the most important parameters, which could prevent the increase in power from taking place, were analyzed. It was observed that the minimum flow rate of coolant through the cassettes exceeded the minimum value by 6-7% and did not appear to be a limiting factor. Separation tests in the steam generator showed there to be a margin in steam moisture content, which would allow of an increase of not less than 10% in load. During the tests and the analysis of the rating data, it was established that turbine type K-220-44, generator type TVV-220-2A, and transformer type TDTsG-250000-330 could operate at powers that were 10% greater than their rated levels.

The reactor achieved a level of 1460 MW while the unit was operating at 106% of rated thermal power, and the electrical side developed 470 MW, the mean coolant temperature was 280-281°C under these conditions, the inlet temperature being 265-266°C and the outlet temperature being 295-296°C. The temperature rise in the coolant in the core did not exceed 30°C. The temperature setting at the output of the cassette corresponded to 100% power, and these settings never once operated during the time the reactor was running at 106% load. This is clear evidence of the margins that exist in coolant temperature rise in the cassettes. The maximum temperature at the outlet from the cassette did not exceed 304°C. The maximum variation factor was 1.30 during the initial period, it then fell to 1.27 at H_6 = 200 cm. The maximum variation factor in the neutron field throughout the height of the reactor core was practically constant during operation at the increased power level, and constituted 1.20-1.25.

The activity of the primary-circuit coolant was one-thirtieth of the permissible level when the reactor was operating at 106% load. Emissions of radioactive gases in the ventilation stacks were 1/400th of the lower permissible level. The radiation situation on the power station corresponded to the radiation safety standards and did not differ significantly form the radiation field that existed when the unit was operating at rated load. During measurements of the vibration on the main plant, it was observed that the levels on this plant (turbogenerators, feed pumps, and condensate and drainage pumps) were within their permitted limits and practically the same as when the unit was running at rated load.

The flow rates of feed water and steam from the steam generator did not exceed 2800 tons/h. When the total thermal load was uprated to 106%, the thermal load on an individual steam generator on maximum load was 109% (250 MW). The flow rate of the steam from the individual steam generators was 490 tons/h. The opening of the regulators feeding the steam generators represented 45-50% of the fully open state of the valve. The opening of the condensate regulator in the separator of the steam generator did not exceed 78%. After the power was uprated to 106%, heat runs were carried out over a 24 h period on the main plant of the turbine and generator houses, which consisted in determining an extended number of the unit parameters. The tests showed that all the parameters of the main plant were within the permitted limits.

It proved possible to determine certain statistical data for analyzing fault situations at increased loads during the adequate time that the units operated at increased power. A turbogenerator (TG-4) was twice tripped out by the automatic control system at a load of 460 MW and the first-generation fault protection on the reactor operated twice when the turbogenerator tripped out. Under these circumstances, the pressure safety equipment (BRU-K) operated successfully, reducing the pressure in the main steam manifold from 5.1 to 4.4 MPa,

at this point, the ARM-4 system reduced the thermal power of the reactor to the necessary level. In May 1977 the second unit was tripped by the unit circuit breakers. The turbogenerators were unloaded by means of the automatic control systems to a power level of 15-20 MW, the pressure safety equipment operated, the primary load on the reactor being maintained by the ARM-4 (50% of the original load), but the ARM-4 was then tripped out and further load shedding was carried out manually.

Consequently, a fault reduction in the load from the increased level has been successfully carried out. The main parameters are maintained automatically and the unit protection systems remain within permitted bounds.

Between June 4 and Aug. 1, 1978, the second unit at the Kola nuclear power station operated at increased power (up to 106%). The unit had been running for 236.1 effective days from the start of the fuel cycle prior to this. The maximum temperature of the coolant at the outlet of the cassette was 303°C (coordinate 20-41). The maximum variation factor in cassette power did not exceed 1.27, while the maximum variation factor in the neutron field throughout the height of the core was 1.18. The electrical load was maintained at 475 MW during the time that the unit was operating on increased power. The mean coolant temperature at this power level was 278°C, the temperature at the inlet being 263°C, while that of the outlet was 293°C. The temperature rise of the coolant in the core did not exceed 20.8°C. The flow rate of water and steam in the steam generators was 2870 tons/h.

From Dec. 1, 1978, both units at the Kola power station operated at a load of 107% rated. The thermal power of the reactors constituted 1470 MW, while the electrical power was 470 MW. The temperature settings at the outlet of the cassette corresponded to 100% power on both units and these were not exceeded during the time the units were running at 107% of rated power. The mean temperature of the coolant at this power level was 282°C (first unit) and 283-284°C (second unit), the temperatures at the inlet to the reactor being 267-269°C on both the first and second units. The temperature rise of the coolant in the reactor core was 31.5°C in the first unit and 30.7°C in the second unit. The maximum temperature of the coolant at the outlet of the cassette did not exceed 306°C (first unit) and 305°C (second unit). The maximum variation factor in cassette power did not exceed 1.26 for the first unit and 1.27 for the second unit, which were in close agreement with calculated data. The variation factor in the neutron field throughout the height of the core comprised 1.2 (first unit) and 1.22 (second unit). The activity of the coolant in the primary circuit was one hundredth of the permitted level during the time the sets were running at increased power.

COLORIMETRIC γ-RAY DOSIMETER

I. Kh. Abdukadyrova

UDC 535.342:666.1

Work has recently been undertaken to perfect dosimeters based on glass which has a varying transparency or luminescence [1-3]. Their disadvantages are substantial fading, the influence of impurities and the dose rate, complexity, and the limited measuring range. The aim of the present paper is to make a detailed study of the dosimetric characteristics of KI quartz glasses under irradiation with ^{60}Co γ rays with doses of 10^4-10^9 rad (1 rad - 0.01 g-R).

Absorption spectra have been measured in the wavelength region from 200 to 700 nm and changes in them under irradiation have been studied. It is known [3] that irradiated specimens exhibit a number of additional bands, among which a wide band with a maximum at 540 nm in the visible region is of particular interest.

The relative change in the optical density at the band maximum for various specimens with an increase in dose is shown in Fig. 1. It is seen that dependence obtained is almost linear within the limits under consideration (10^4-10^8 rad). The character of the curves testifies to a monotonic increase in the rate of color-center accumulation with the growth of the specimen thickness from 0.7 to 10 mm, which makes it possible to vary the sensitivity of the system. According to the calculated values of the relative change in the optical density for a dosimeter, the optimal thickness in the region under study is 2-3 mm.

One of the main parameters of the dosimeter is its stability under storage. Quartz glasses irradiated with a dose of $2 \cdot 10^7$ rad were held at room temperature for various lengths of time and were then measured in a spectrophotometer. The data obtained are listed in Table 1 from which it follows that after storage for almost 2000 h in the dark the glass discolor. The good stability of the induced color allows the optical density to be measured repeatedly under various holding conditions.

The influence of the irradiation conditions was traced in plates with a thickness of a millimeter for a dose rate varied from 80 to 4000 R/sec (1 R = $2.58 \cdot 10^{-4}$ C/kg). Measurements of the intensity of the source did not reveal any noticeable influence on the readings of the system.

The dependence of the intensity of the color on the temperature was studied in the range from 30 to 200°C. It was established (Fig. 2) that within the limits studied the transformation rate is practically independent of the temperature in the irradiation zone. Such a property is very valuable for a dosimeter since it makes the instrument suitable for use at elevated temperatures.

Specimens were heated step by step, with a holding time of 0.25 h at each value of the temperature. The temperature in the furnace was varied from 20 to 500°C (see Fig. 2). The high color stability in the first stage (up to 250°C) must be pointed out. The stage of effective annealing occupies the region from 350 to 480°C, i.e., the induced color of the glass can be "removed" by heating above 400-500°C.

From the slope of the temperature dependence of the color-center destruction we estimated the activation energy of the process. According to preliminary results, this energy is equal to ∿0.6 eV in the segment of intense discoloration. This, as well as the kinetic laws of coloration, apparently indicate that a radiation-induced center is due to a structure defect interconnected with an impurity ion.

After thermal annealing the previously irradiated glass was once again subjected to irradiation with one particular dose or to step-by-step accumulation of the limiting dose (Table 2). Repeated experiments according to a scheme of irradiation and color annealing

Translated from Atomnaya Énergiya, Vol. 49, No. 2, pp. 135-136, August, 1980. Original article submitted November 28, 1979.

0038-531X/80/4902-0593$07.50

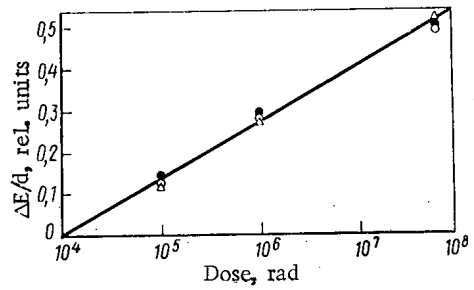

Fig. 1

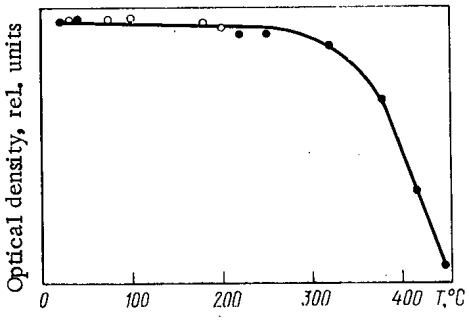

Fig. 2

Fig. 1. Dependence of relative change in optical density of KI quartz glass on γ-ray dose at wavelength of 540 nm and initial specimen thickness of 0.7 (●), 1 (○), and 3 (Δ) mm.

Fig. 2. Annealing of color centers at various temperatures of irradiating apparatus (○) and furnace (●). Radiation dose 16^6 rad, thickness 1 mm.

TABLE 1. Discoloration of Glass Irradiated with Dose of $2 \cdot 10^7$ rad at Room Temperature*

Specimen thickness, mm	Time after irradiation, h								Mean
	0,5	1	2	9	12	24	65	1900	
1,0	0,45	0,46	0,45	0,43	0,45	0,45	0,45	0,45	0,449
0,7	0,30	0,28	0,30	0,29	0,29	0,30	0,30	0,29	0,294
3,0	1,92	1,94	1,92	1,92	1,94	1,93	1,90	1,91	1,923

*The optical density was measured at a wavelength of 540 nm.

TABLE 2. Dependence of Optical Density of Glass 0.7 mm Thick on Specimen Prehistory

State of specimen	Irradiation dose, rad			
	10^6	10^7	$6 \cdot 10^7$	10^8
Initial	0,20	0,29	0,34	0,36
After 1st anneal	0,21	0,28	0,35	0,37
After 2nd anneal	0,20	0,30	0,35	0,37
After 3rd anneal	0,18	0,28	0,31	0,39
Mean	0,198	0,288	0,335	0,373
Error, %	1,01	0,69	2,98	0,54

showed convincingly that short heat treatment completely destroys the induced color centers and makes the system ready once again to accept the next bit of information. The sensitivity of the specimen to γ rays after annealing practically does not change and the relative error in this case does not exceed 3%.

Thus, comprehensive studies of various characteristics of KI quartz glass show that it satisfies most of the requirements made of absorption dosimeters and can be recommended for testing in the range of intermediate and high doses of γ rays (10^4–10^8 rad). In comparison with other systems, this glass has the advantage that while it is colorless at first, under irradiation it acquires a lilac color whose optical density increases with the dose, this makes it possible to carry out semiquantitative visual dosimetry.

LITERATURE CITED

1. K. Becker, Nucl. Instrum. Methods., 36, No. 2, 323 (1965).
2. E. Freydag, Health Phys., 20, No. 1, 93 (1971).
3. G. V. Byurganovskaya et al., Effect of Radiations on Inorganic Glasses [in Russian], Atomizdat, Moscow (1968).

EFFECT OF HEAT-CONDUCTING PROPERTIES OF SPACERS ON CURRENT–VOLTAGE CHARACTERISTICS AND TEMPERATURE FIELDS OF THERMIONIC FUEL CELLS

N. M. Rozhkova and V. V. Sinyavskii

UDC 621.362

The required interelectrode gap in thermionic electricity-generating cells (EGC) is ensured with a special system of spacers, specifically, in the form of belts of microspacers between the emitter and collector at the edges of the EGC [1].

The appearance of local heat transfer from the emitter to the collector as the result of heat conduction through the material of the spacers leads to a decrease in the temperature and electric fields of the EGC with deterioration of the output energy characteristics. A similar change in the characteristics was also observed in the course of testing of multiple-element assemblies [2].

In the present paper, using numerical experiments on a mathematical model of an EGE, we study the influence of the heat-conducting properties of the spacing system on the current–voltage (I–V) characteristics and temperature fields of EGC. The EGC model was an improvement on the model described earlier [3, 4] by the introduction of a differential equation for the heat conduction of the collector and terms taking account of heat conduction through the spacers. Moreover, in order to improve the agreement of the numerical solution of the system of differential equations and to increase the accuracy, the Newton method [3, 4] was replaced by the difference factorization method.

In the mathematical model the discrete spacers were replaced by a continuous belts of spacers of height $h = l_g$ with an effective thermal conductivity coefficient of $\lambda_g^* \approx \lambda_g n \delta'' 2\pi r$, where λ_g is the thermal conductivity coefficient of the spacer material, n is the number of spacers in contact with the emitter, δ_g is the width of the zone of contact ("indented" from the spacer into the body of the emitter), and $\bar{r} = (r_E + r_C)/2$ is the mean radius of the belt of spacer. Thus $\lambda_g^* = 0.002$ W/cm·deg corresponds to $\delta_g = 0.2$ mm. Such a value was observed in post-reactor studies of a six-element assembly which had operated in a reactor for 2670 h [2]. In view of the fact that the total emitter surface in contact with the spacers is small, in our calculations we took no account of the decrease in the emitting area of the emitter.

For the main object of study we chose an EGC with a tungsten emitter of diameter $2r_E$ = 1 cm, length l_E = 3 cm, and spacer system [1] with l_g = 0.3 cm. Our investigation showed that the static I–V curves (at constant thermal power q_V = const) depend on λ_g^*, i.e., on the degree of contact of spacers with emitter surface. The deterioration of the I–V curves as λ^*_g increases is due, first, to thermal losses through the spacers reducing the thermal power which can be converted into electrical energy (deterioration of the I–V curve equivalent to some reduction of the thermal power) and, second, to the lowering of the emitter temperature T_E^* in the vicinity of the contact with the spacers, which reduces the density of the electrical power generated by these segments (deterioration of the I–V curve equivalent to some reduction of l_E).

The reduction of the power W and efficiency η of the EGC with an increase in λ^*_g has a tendency to reach saturation for two reasons: first, the thermal losses $Q_g \sim \lambda^*_g \{T_E^*(\lambda^*) - T_C^*(\lambda^*_g)\}$ are not directly proportional to λ^*_g since with the growth of λ^*_g uniformly in the

Translated from Atomnaya Énergiya, Vol. 49, No. 2, pp. 137-139, August, 1980. Original article submitted December 11, 1979.

0038-531X/80/4902- 0595$07.50

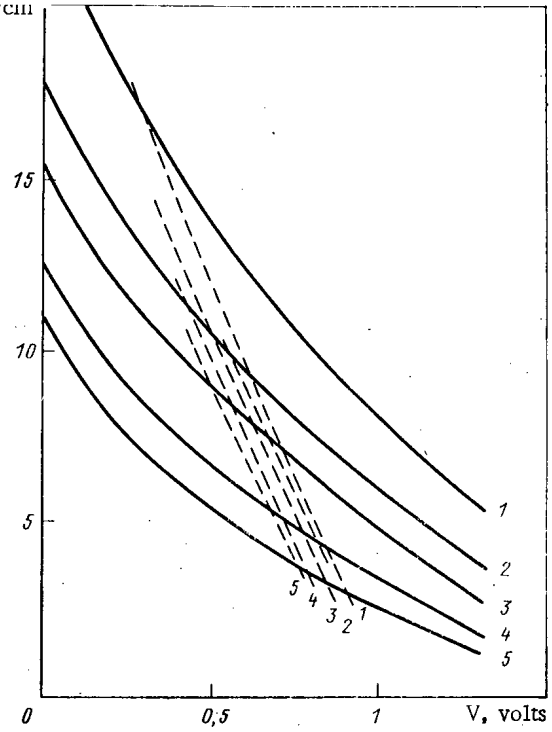

Fig. 1. Variation of static I–V curves of EGC for $\bar{q}_V$ = 400 W/cm³ (———) and isothermal I–V curves of EGC for $T_{E,max}$ = 2100°K (- - -) as effective λ_g^* increases: 1) 0; 2) 0.001; 3) 0.002; 4) 0.005; and 5) 0.01 W/cm·deg.

vicinity of a contact reduces the emitter–collector temperature difference $T_E^*(\lambda_g^*) - T_c^*(\lambda_g^*)$ and, second, from some λ_g^* because of a lowering of T_E^* segments in the vicinity of spacers practically cease to generate current ($j \approx \bar{j}$). A further reduction of W will occur only as a result of the expansion of the zone of influence of the spacers. The relative reduction in W and η is almost independent of the operating voltage of the EGC but depends slightly on the emission characteristics of thermionic fuel elements, $j(v, T_E, T_c)$.

The itothermal I–V curves T_E = const also deteriorate as λ_g^* increases, although their change is less pronounced than that of static I–V characteristics (Fig. 1). This is due to the change in the emitter temperature field $T_E(z)$; for short EGC the effect of the thermal losses through the spacers extends over the entire length of the emitter and with the growth of λ_g^* there is a lowering of $T_{E,max}$ as well as $\bar{T}_E$ while the nonisothermal character of the emitter ($T_{E,max} - T_E$) grows. With the spacers situated on either side at the edges of the EGC instead of a flat curve with a "steep drop" to the end from the side of the commutation connector the distribution $T_E(z)$ becomes bell-shaped (Fig. 2). With an increase in the emitter length l_E the influence of λ_g^* on the temperature field of the central part of the EGC decreases and with $l_E \geq 6$ cm the influence of the spacers no longer extends over the entire length of the emitter; however, the lowering of T_E and the rise in T_c in the zone of contact with spacers remains the same for any l_E. As a result, with an increase in l_E the influence of λ_g^* on the power and the efficiency of the EGC diminishes. Figure 3 shows the plot of the relative EGC electrical power $\bar{W} = W(\lambda_g^*)/W(\lambda_g^* = 0)$ for various EGC lengths.

As $T_E(z)$ changes so does the current-density distribution j(z) with a concomitant reduction of W. The absolute level of the thermal power $\bar{q}_V$ exerts an appreciable effect on the relative reduction in $\bar{W}(\lambda_g^*)$ (Fig. 4). When λ^*_g = const and the other parameters are constant, the relative decrease in W diminishes as $\bar{q}_V$ grows. This is due to the fact that with an increase in $\bar{q}_V$ and electronic cooling of the emitter, the relative fraction of losses through the spacers to the total thermal balance of the emitter diminishes. Accordingly, particular care should be taken in developing the spacer system in thermionic assemblies with a low electrical power density in which the influence of λ_g^* is very pronounced owing to the low values of q_V.

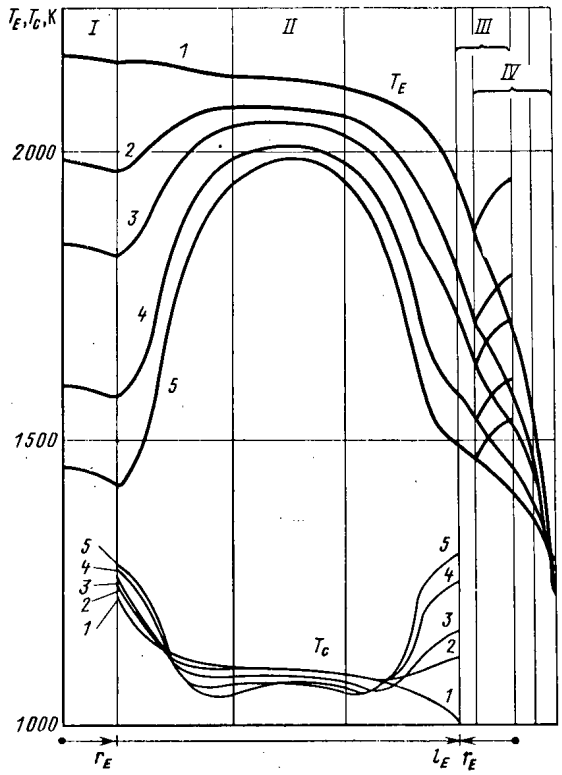

Fig. 2. Variation of temperature fields $T_E(z)$ of emitter sheath, including free end (I), emitter (II), end from connector side (III), connector (IV), and collector $T_c(z)$ (II) of EGC of length 3 cm at constant thermal power of 400 W/cm³, operating voltage of 0.5 V, and increase in λ_g^* (values of λ_g^*, in cm, in Fig. 1).

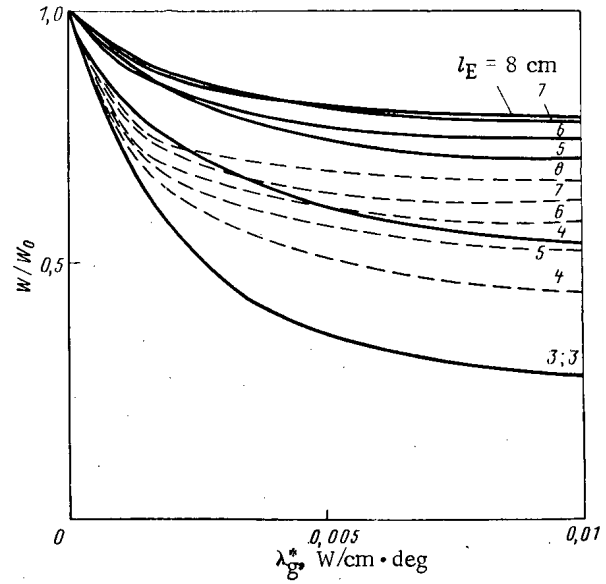

Fig. 3. Dependence of relative power of EGC on λ_g^* for various values of l_E: ——) l_g = 0.3 cm; - - -) l_g/l_E = 0.1.

In studying how the form of the distribution function of the density of the thermal flux from the heat-releasing core affects the emitter sheath, including the change in the relative amount of heat delivered to the end parts of the sheath, we found that the influence of spacers on the character and absolute values of the characteristics studied remained unchanged.

Particular attention should be paid to the influence of the thermal conductivity coefficient λ_E of the material of the emitter sheath or to be more exact, the product $\lambda_E\delta_E$, where δ_E is the thickness of the emitter sheath. With an increase in λ_E the static I-V characteristics at q_V = const deterioriate because of the expansion of the zone of influence of local sinks for heat from the emitter (through the commutation connector and the spacer), as a result of which the overall level of $T_E(z)$ is lowered, including the central part of the emitter. At the same time an increase in observed in the emitter temperature T_E^* in the region of spacers because of the increase in the supply of heat from the central part of the

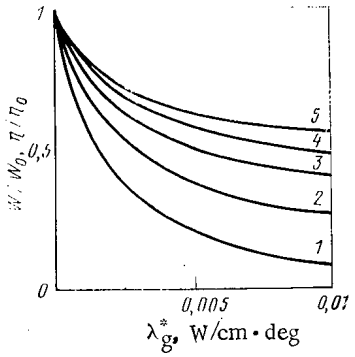

Fig. 4. Dependence of relative power and relative efficiency of EGC on λ_g^* for various values of thermal power: 1) q_V = 200 W/cm^3 (q_F = 46 W/cm^2) 2) 300 (68.5); 3) 400 (91.5); 4) 500 (114); and 5) 600 (137).

emitter which finally increase the total heat loss Q_g and worsens the energy characteristics of the EGC. However, a decrease in λ_E (or a thinning of the emitter sheath) leads heightens the nonisothermality of the emitter which, in a number of cases, may prove to be dangerous or undesirable. The influence of the thermal conductivity coefficient of the collector material is insignficant. The results of our investigations indicate the necessity of taking account of the local character of the effect of spacers on the characteristics of thermionic fuel cells, especially at low electrical power densities.

LITERATURE CITED

1. V. I. Berzhatyi et al., At. Energ., 34, No. 6, 585 (1971).
2. G. A. Batyrbekov et al., At. Energ., 40, No. 5, 382 (1976).
3. Yu. A. Broval'skii et al., in: Thermionic Energy Conversion. Papers of Soviet Scientists at Second Int. Conf. on Thermionic Fuel Cells [in Russian], VNIIT, Moscow (1973), p. 281.
4. Yu. A. Broval'skii et al., Teplofiz. Vys. Temp., 13, No. 1, 171 (1975).

ALLOWANCE FOR INDUCED ACTIVITY OF STRUCTURAL MATERIALS OF BOREHOLE NEUTRON GENERATORS TO ENSURE RADIATION SAFETY

D. F. Bespalov, A. A. Dyluk, and Yu. V. Seredin

UDC 621.039.58'68

In work on starting, adjusting, and repairing borehole neutron generators (BNG) used for pulsed neutron well logging, a serious factor of radiation danger to the personnel besides the intense (10^7-10^9 neutrons/sec) pulsed fluxes of 14-MeV neutrons [1, 2] is posed by the induced activity of the sturctural materials of the generators (especially their protective casings). Insufficient provision for this factor can result in excessive irradiation of personnel engaged in various work on the generator right after shut-down.

With a view to making a quantitative estimation of the γ-ray dose due to the induced activity of the structural materials of the BNG, theoretical and experimental investigations were conducted on the spectra and dynamics of the variation in the dose of γ rays from the induced activity of the BNG. It was established that the main contribution to the dose rate comes from the γ rays emitted by the steel protective casings of the BNG as the result of the reaction ^{56}Fe(n, p)^{56}Mn [3, 4].

The dose rate at a given point in space around the generator is defined as the sum of the dose rates from the individual segments of the protective casing of the BNG with quasi-uniform distribution of induced activity [5]. In order to identify such segments, studies were made of the activation of cylindrical specimens of the material of the protective casings of BNG with various forms of target in the neutron tube and the axial and radial distribution of the induced activity in the BNG protective casings was studied [6].

Translated from Atomnaya Énergiya, Vol. 49, No. 2, pp. 139-140, August, 1980. Original article submitted December 24, 1979.

 0038-531X/80/4902-0598$07.50

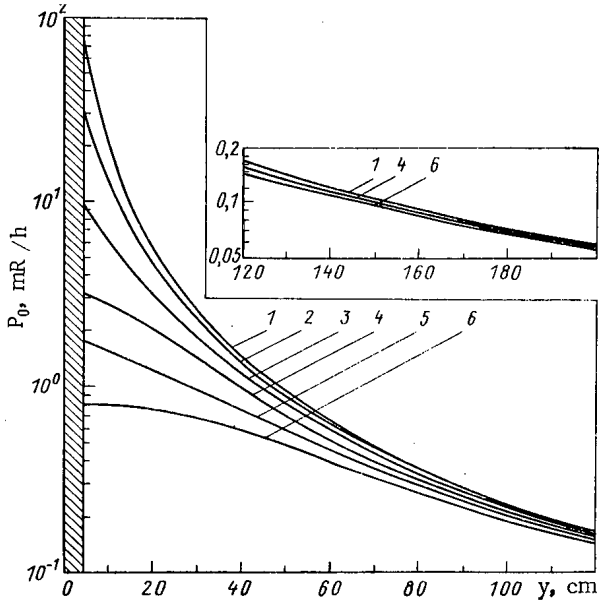

Fig. 1. Speatial distribution of γ-ray dose rate P_0 corresponding to saturation activity of steel protective casing of BNG of Gerakl-1M type: x, y) axial and radial coordinates of point of observation, 1) x = 0, 2) 10, 3) 20, 4) 30, 5) 40, and 6) 50 cm, neutron yield 10^9 neutrons/sec (the hatching indicates the overall dimensions of the borehold instrument).

Some formulas were derived for describing the γ-ray dose rate due to the induced activity of the BNG protective casings, with allowance for their material and dimensions, as well as the neutron yield and the transient operating conditions. The analytic expression for the exposure dose rate P_0, corresponding to the saturation activity, at a point in space lying on a normal to the BNG axis and passing through the center of the target is in the following form:

$$P_0 = \frac{1.35 \cdot 10^{-8} \Sigma \Phi K_\gamma}{y + R_{\text{eff}}} \left[\left(\frac{G_1}{H_1} - \frac{G_2}{H_2} \right) F(\varphi_1, \alpha) + \left(\frac{G_2}{H_2} - \frac{G_3}{H_3} \right) F(\varphi_2, \alpha) + \frac{G_3}{H_3} F(\varphi_3, \alpha) \right], \quad (1)$$

where Φ is the yield of 14-MeV neutrons (neutrons/sec), Σ, macroscopic cross section for the activation of the material of the BNG protective casing with 14-MeV neutrons (cm^{-1}), K_{γ_i}, γ dose-rate constant of the induced activity ($R \cdot cm^2/h \cdot mCi$, 1 R = $2.58 \cdot 10^{-4}$ Ci/kg, 1 Ci = $3.700 \cdot 10^{10}$ disintegrations/sec), y, distance from the center of the BNG target to the point of observation (cm), R_{eff}, effective radius of the BNG protective casing (cm) (equal to the radius of an infinite cylinder of the same activity producing at the point of observation the same dose rate as the real protective casing), G_1-G_3, geometric factors of the activation of segments 1-3 of the protective casing (reckoned from the activity) (cm), H_1-H_2, lengths of the protective casing with quasiuniform distribution of activity (cm), and $F(\varphi, \alpha)$ an elliptic interval of the first kind, where

$$\alpha = \operatorname{arctg} \frac{\sqrt{yR_{\text{eff}}}}{y + R_{\text{eff}}}; \quad \varphi_1 = \operatorname{arctg} \frac{H_1}{y - R_{\text{eff}}};$$

$$\varphi_2 = \operatorname{arctg} \frac{H_1 + H_2}{y - R_{\text{eff}}}; \quad \varphi_3 = \operatorname{arctg} \frac{H_1 + H_2 + H_3}{y - R_{\text{eff}}}.$$

The results of measruements and calculations of the dose rate at various distances from the surface of the protective casing of a switched-off BNG of the Gerakl-1M type [1] after operation at various neutron fluxes for different intervals of time [3, 4] showed satisfactory agreement. Thus, the dose rate measured by an SRP-2 radiometer at a distance of 35 cm from the axis of the BNG after the generator had operated continuously with an average yield of $2.8 \cdot 10^8$ neutrons/sec was 170 μR/h with the elapse of 34 min after shut-down of the BNG.

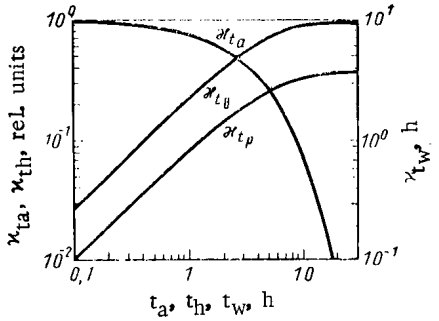

Fig. 2. Nomogram for determining corrections for activation time of BNG steel protective casing, the holding time, and the working time of the personnel.

TABLE 1. Relative Excess of γ-Ray Dose Rate from Induced Saturation Activity of Structural Materials of BNG of Gerakl-1M Type Over and Above Regulation Value (2.8 mR/h)

y, cm	x, cm					
	0	10	20	30	40	50
6,5	17,40	8,54	3,16	1,09	0,618	0,294
10	7,54	4,80	2,16	1,00	0,552	0,292
20	2,01	1,68	1,16	0,754	0,443	0,280
40	0,525	0,439	0,425	0,396	0,268	0,209
50	0,343	0,326	0,291	0,252	0,209	0,172

The calculated dose rate for these conditions, obtained from Eq. (1), was 155 μR/h. The discrepancy between the calculated and experimental values did not go beyond the limits due to the experimental error.

The analytic expression obtained for the exposure dose rate of γ rays due to the induced activity of the structural materials of the Gerakl-1M type of BNG was used to construct nomograms (Fig. 1, 2) which permit effective estimation of the dose under various operating conditions of the apparatus and the personnel by means of the expression

$$D = P_0 \varkappa_\Phi \varkappa_{t_a} \varkappa_{t_h} \varkappa_{t_w}, \qquad (2)$$

where P_0 is the dose rate corresponding to the induced activity and the nominal neutron flux (determined from Fig. 1), $\varkappa_\Phi$, correction for the real value of the neutron flux of the BNG during operation as found from $\varkappa_\Phi = \Phi/\Phi_{nom}$, $\varkappa_{t_a}$, correction for the real activation time of the structural materials of the BNG, i.e., for the time of continuous operation of the BNG (found from Fig. 2), $\varkappa_{t_h}$, correction for the nolding time after shut-down of the BNG, after which time the operating personnel appears in the zone affected by the γ rays from the induced activity of the NBG, calculated from $\varkappa_{t_h} = \exp(-\lambda t_h)$ (determined from Fig. 2), and $\varkappa_{t_w}$, correction for the working time of the personnel in the zone affected by the γ rays from the induced activity of the BNG, calculated from $\varkappa_{t_w} = [1 - \exp(\lambda_{t_w})]/\lambda$.

The excessive level of the γ-ray dose rate due to the induced activity of the BNG as found from the nomograms (see Table 1) attests to the necessity of taking this factor of radiation hazard into account when conducting start-up and ajustment, experimental, and other work with BNG during which the personnel may be near the BNG shortly after shut-down.

Existing health regulations [8] do not contain provisions concerning the length of time a generator must be kept after shut-down, so that its induced activity drops to a level which is safe for the operating personnel. The data presented here make it possible to establish the numerical values of these periods and to safely conduct repair and maintenance and other work with BNG after their shutdown.

LITERATURE CITED

1. D. F. Bespalov et al., in: Nuclear-Geophysical Well-Logging Apparatus with Controlled Radiation Sources [in Russian], ONTI VNIIYaGG, Moscow (1978), p. 5.
2. D. F. Bespalov, A. A. Dylyuk, and A. A. Starinskii, in: Nuclear-Geophysical Well-Logging Apparatus with Controlled Radiation Sources [in Russian], ONTI VNIIYaGG, Moscow (1978), p. 11.
3. D. F. Bespalov et al., in: Abstracts Third All-Union Scientific-Practical Conf. on Radiation Safety [in Russian], VTsNIIOT, Moscow (1976), p. 72.
4. A. A. Dylyuk, N. V. Sizikova, and M. S. Khozyainov, in: Nuclear-Geophysical Apparatus [in Russian], No. 26, ONTI VNIIYaGG, Moscow (1976), p. 60.
5. L. R. Kimel' and V. P. Mashkovich, Protection from Ionizing Radiation (Handbook) [in Russian], Atomizdat, Moscow (1972), p. 125.
6. D. F. Bespalov and A. A. Dylyuk, Geofizika, No. 8, Paper 8DZ07 (1977).
7. Radiation Safety Standards (NRB-76), [in Russian], Atomizdat, Moscow (1978), p. 55.
8. Health Regulations for Work with Borehole Neutron Generators [in Russian], ONTI VNIIYaGG, Moscow (1976), p. 17.

NEW RUSSIAN JOURNALS

IN ENGLISH TRANSLATION

BIOLOGY BULLETIN

Izvestiya Akademii Nauk SSSR, Seriya Biologicheskaya

The biological proceedings of the Academy of Sciences of the USSR, this prestigious new bimonthly presents the work of the leading academicians on every aspect of the life sciences—from micro- and molecular biology to zoology, physiology, and space medicine.

Volume 7, 1980 (6 issues) $195.00

SOVIET JOURNAL OF MARINE BIOLOGY

Biologiya Morya

Devoted solely to research on marine organisms and their activity, practical considerations for their preservation, and reproduction of the biological resources of the seas and oceans.

Volume 6, 1980 (6 issues) $115.00

WATER RESOURCES

Vodnye Resursy

Evaluates the water resources of specific geographical areas throughout the world and reviews regularities of water resources formation as well as scientific principles of their optimal use.

Volume 7, 1980 (6 issues) $215.00

HUMAN PHYSIOLOGY

Fiziologiya Cheloveka

A new, innovative journal concerned *exclusively* with theoretical and applied aspects of the expanding field of human physiology.

Volume 6, 1980 (6 issues) $195.00

SOVIET JOURNAL OF BIOORGANIC CHEMISTRY

Bioorganicheskaya Khimiya

Features articles on isolation and purification of naturally occurring, biologically active compounds; the establishment of their structure, methods of synthesis, and determination of the relation between structure and biological function.

Volume 6, 1980 (12 issues) $245.00

SOVIET JOURNAL OF COORDINATION CHEMISTRY

Koordinatsionnaya Khimiya

Describes the achievements of modern theoretical and applied coordination chemistry. Topics include the synthesis and properties of new coordination compounds; reactions involving intraspheral substitution and transformation of ligands; complexes with polyfunctional and macromolecular ligands; complexing in solutions; and kinetics and mechanisms of reactions involving the participation of coordination compounds.

Volume 6, 1980 (12 issues) $255.00

THE SOVIET JOURNAL OF GLASS PHYSICS AND CHEMISTRY

Fizika i Khimiya Stekla

Devoted to current theoretical and applied research on three interlinked problems in glass technology; the nature of the chemical bonds in a vitrifying melt and in glass; the structure-statistical principle; and the macroscopic properties of glass.

Volume 6, 1980 (6 issues) $145.00

LITHUANIAN MATHEMATICAL JOURNAL

Litovskii Matematicheskii Sbornik

An international medium for the rapid publication of the latest developments in mathematics, this quarterly keeps western scientists abreast of both practical and theoretical configurations. Among the many areas reported on in depth are the generalized Green's function, the Monte Carlo method, the "innovation theorem," and the Martingale problem.

Volume 20, 1980 (4 issues) $175.00

PROGRAMMING AND COMPUTER SOFTWARE

Programmirovanie

Reports on current progress in programming and the use of computers. Topics covered include logical problems of programming; applied theory of algorithms; control of computational processes; program organization; programming methods connected with the idiosyncracies of input languages, hardware, and problem classes; parallel programming; operating systems; programming systems; programmer aids; software systems; data-control systems; IO systems; and subroutine libraries.

Volume 6, 1980 (6 issues) $115.00

SOVIET MICROELECTRONICS

Mikroelektronika

Reports on the latest advances in solutions of fundamental problems of microelectronics. Discusses new physical principles, materials, and methods for creating components, especially in large systems.

Volume 9, 1980 (6 issues) $160.00

Send for Your Free Examination Copy

PLENUM PUBLISHING CORPORATION, 227 West 17th Street, New York, N.Y. 10011
In United Kingdom: 88/90 Middlesex Street, London E1 7EZ England
Prices slightly higher outside the U.S. Prices subject to change without notice.